Analiza utjecaja točkastog pridržanja na stanje naprezanja i deformacija u konstrukcijskom staklu

Ivanušić, Karlo

Master's thesis / Diplomski rad

2025

Degree Grantor / Ustanova koja je dodijelila akademski / stručni stupanj:
University of Split, Faculty of Civil Engineering, Architecture and Geodesy / Sveučilište u Splitu, Fakultet građevinarstva, arhitekture i geodezije

Permanent link / Trajna poveznica: https://urn.nsk.hr/urn:nbn:hr:123:847734

Rights / Prava: In copyright/Zaštićeno autorskim pravom.

Download date / Datum preuzimanja: **2025-03-22**

Repository / Repozitorij:

FCEAG Repository - Repository of the Faculty of Civil Engineering, Architecture and Geodesy, University of Split

SVEUČILIŠTE U SPLITU
FAKULTET GRAĐEVINARSTVA, ARHITEKTURE I GEODEZIJE

DIPLOMSKI RAD

Karlo Ivanušić

Split, 2025.

SVEUČILIŠTE U SPLITU

FAKULTET GRAĐEVINARSTVA, ARHITEKTURE I GEODEZIJE

Karlo Ivanušić

Analiza utjecaja točkastog pridržanja na stanje naprezanja i deformacija u konstrukcijskom staklu

Diplomski rad

Split, 2025.

SVEUČILIŠTE U SPLITU
FAKULTET GRAĐEVINARSTVA,
ARHITEKTURE I GEODEZIJE

UNIVERSITY OF SPLIT
FACULTY OF CIVIL ENGINEERING,
ARCHITECTURE AND GEODESY

STUDIJ: SVEUČILIŠNI DIPLOMSKI STUDIJ GRAĐEVINARSTVO
KANDIDAT: Karlo Ivanušić
MATIČNI BROJ: 0083223319
KATEDRA: Katedra za otpornost materijala i ispitivanje konstrukcija
KOLEGIJ: Mehanika materijala

ZADATAK ZA DIPLOMSKI RAD

Tema: Analiza utjecaja točkastog pridržanja na stanje naprezanja i deformacija u konstrukcijskom staklu

Opis zadatka: Potrebno je numerički modelirati i analizirati utjecaj točkastih pridržanja na stanje naprezanja i deformacija u konstrukcijskim staklenim elementima. Analize treba provesti na elementima fasade objekta *Karla Tower-a (Karlatornet)* u Gothenburgu. Dobivene rezultate usporediti s eksperimentalnim ispitivanjima provedenima u laboratoriju Građevinskog fakulteta Sveučilišta u Coimbri.

U Splitu, 08.02. 2024.g.

Mentor: Predsjednik Povjerenstva za završne i
Prof. dr. sc. Mirela Galić   diplomske ispite studija Građevinarstvo:
                                 izv. prof. dr. sc. Ivan Balić

SVEUČILIŠTE U SPLITU
FAKULTET GRAĐEVINARSTVA,
ARHITEKTURE I GEODEZIJE

UNIVERSITY OF SPLIT
FACULTY OF CIVIL ENGINEERING,
ARCHITECTURE AND GEODESY

IZJAVA O AKADEMSKOJ ČESTITOSTI

kojom ja, Karlo Ivanušić, JMBAG: 0083223319, student Fakulteta građevinarstva, arhitekture i geodezije Sveučilišta u Splitu, kao autor ovog diplomskog rada izjavljujem da sam ga izradio samostalno pod mentorstvom prof. dr. sc. Mirele Galić, te u suradnji s doc. dr.sc. Sandrom Jordao na Sveučilištu u Coimbri, gdje sam boravio u sklopu ERASMUS programa mobilnosti.

U radu sam primijenio metodologiju znanstvenoistraživačkog rada i koristio literaturu koja je navedena na kraju rada. Tuđe spoznaje, zaključke, teorije, formulacije i grafičke prikaze koje sam izravno ili parafrazirajući naveo u radu citirao sam i povezao s korištenim bibliografskim jedinicama.

_____
(vlastoručni potpis studenta)

Analiza utjecaja točkastog pridržanja na stanje naprezanja i deformacija u konstrukcijskom staklu

Sažetak:

Staklo ima veliki potencijal i postalo je vremenom često korišten materijal u građevinarstvu. Tehnološkim razvojem (toplinska obrada i laminacija) pretvoren je u konstrukcijski materijal te ima veliku primjenu u graditeljstvu, posebice u fasadama, ali i upečatljivim arhitektonskim elementima. Kako propisi za projektiranje konstrukcijskih staklenih elemenata nisu u potpunosti definirani, nerijetko se kod izvođenja zahtjevnijih konstrukcija primjenjuje eksperimentalno ispitivanje i detaljna numerička analiza. Jedno takvo ispitivanje je provedeno za elemente fasade *Karla Tower-a (Karlatornet)* u Gothenburgu. U ovom radu pokazan je utjecaj točkastog pridržanja na stanje naprezanja i deformacija u staklenim elementima fasade. Eksperimentalno ispitivanje je provedeno u laboratoriju Građevinskog fakulteta Sveučilišta u Coimbri. U ovom radu su navedena ispitivanja modelirana u računalnom programu ABAQUS, analizirani različiti utjecaji te pokazana usporedba dobivenih rezultata. Analiza je pokazala da ekscentričnost točke opterećenja i nesavršenosti uzrokovane postupkom laminiranja imaju značajan utjecaj na ponašanje uzorka i raspodjelu naprezanja.

Ključne riječi: *konstrukcijsko staklo, laminirano staklo, točkasto pričvršćeni stakleni elementi, vijčani spojevi sa staklom, eksperimentalno ispitivanje, numeričko modeliranje MKE*

Structural bahaviour of point fixed connections in structural glass

Abstract

Glass has great potential and has become a frequently used material in civil engineering practice over time. Through technological development (heat treatment and lamination), it has been transformed into a structural material and has a wide range of applications in construction, especially in facades, but also in striking architectural elements. Since the regulations for the design of structural glass elements are not fully defined, experimental testing and detailed numerical analysis are often used when implementing more demanding structures. One such test was conducted for the facade elements of the Karla Tower (Karlatornet) in Gothenburg. This thesis shows the influence of point-fixed connections on stress and strain distribution in glass elements of the facade. The experimental test was conducted in the laboratory of the Faculty of Civil Engineering, University of Coimbra. In this thesis, the experimental tests are modeled in the ABAQUS computer program, analyzing different influences and presenting a comparison of the obtained results. The analysis showed that the eccentricity of the load point and imperfections caused by the lamination process have a significant impact on the behavior of the sample and the stress distribution.

TABLE OF CONTENT

1 INTRODUCTION

1.1 Framework

Glass is a unique material. When used in the building facade it allows for a dematerialised contour. The light flows in and the visual horizon becomes unobstructed. Additionally, glass has the potential for significative energy savings with building operation throughout its lifetime. Glass also has high aesthetic and architectural potential. It is selected many times for striking architectural landmarks in our cities.

Interesting though it may be, glass represents an engineering challenge, due to its brittle nature, and has been long used only for non-structural elements in the building. However, technological developments like tempering or lamination rendered it able for use in construction as a structural material. Nevertheless, the design codes are not yet sufficiently comprehensive to cover design of unconventional geometries and structures. In such cases, design must still be validated by means of full-scale tests and corresponding advanced numerical models.

Yuanda Europe, Lda recently designed and constructed the glass facade of the Karla tower in Gothenburg, Sweden (Figure 1.1), which is the highest building in the Nordic countries, reaching 247m. The project includes an all-glass cube box sticking out of the facade, 230m above ground level. Yuanda Europe commissioned the experimental testing of the bolted connections to the Civil Engineering Department of the University of Coimbra. The objective was to characterize the mechanical behaviour of the connections and obtain the characteristic resistance to validate the design calculations, and, thus, guaranty a high safety level, for such a critical structure [S. Jordão and E. Inca, 2024].

The building's architecture firm is Skidmore, Owings and Merrill (SOM) and it is being built by Serneke Group AB with several subcontracts for specialised tasks. Yuanda Europe is in charge of the glass façade (design and construction). The construction started in 2019 and is expected to be finished in 2024.

Figure 1.1 Karla tower in Gothenburg, Sweden [6]

1.2 Aim and objectives

The first aim of the present thesis is to report the experimental tests in terms of preparation, execution and results. The second aim is to prepare accurate numerical models corresponding to the experimental tests on the bolted connections of Karla Tower (Abaqus software), and confront the numerical and experimental results, in view of the structural behaviour of the connections.

1.3 Organisation of thesis

Thesis organisation is explained in Table 1.1.

CHAPTER	DESCRIPTION
1. Introduction	General description of the thesis with objectives and methodology of work.
2. State of art appraisal	Introduction of point fixing in structural glass with design guidance. Numerical and experimental works of other researchers. Infill material introduction.
3. Experimental campaign	Detailed explanation of experimental work in laboratory. Introduction of the properties of testing samples, results of each sample and their comparison.
4. Numerical analysis	Detailed explanation of numerical analysis. Introduction of model geometry and mesh. Comparison of numerical results with experimental ones. Discussion about results.
5. Conclusions and future work	Final words about work and suggestions for future work.

Table 1.1: Organisation of thesis

2 STATE OF THE ART APPRAISAL

2.1 Glass as structural material

History of the existence of the adapted natural glass goes back in around 3500 years B.C in Egypt which was used for rings, neckless and mostly jewerly, but the significant improvement in glass usage occured in Syria with the development of the "glass blowing" tehnicque. In that times Roman empire was ruling the Mediterreanean and their new ways of making glass in large dimensions such as the "cylinder" method (Figure 2.1) were spread.
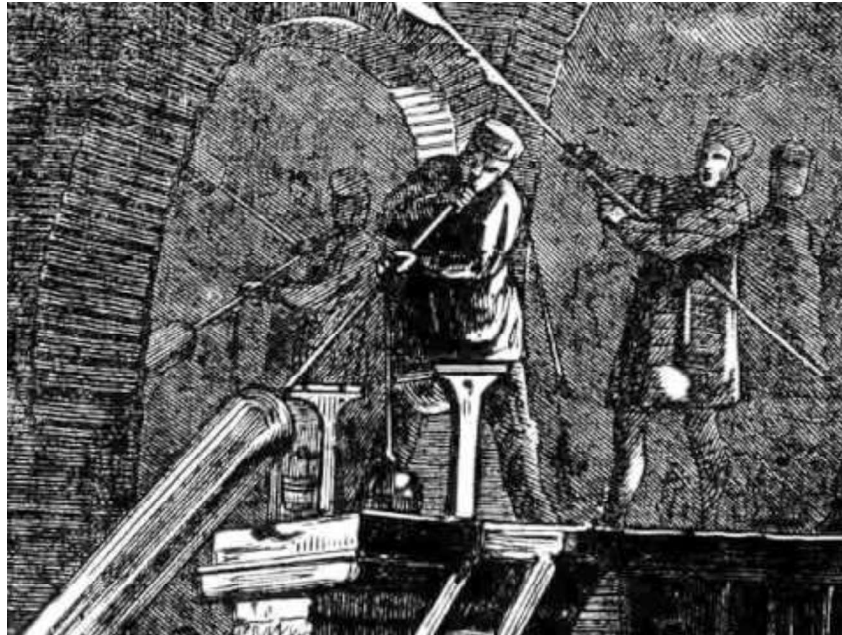

Figure 2.1 – The "cylinder" method of glass making

After the fall of the Roman empire the usage of the glass and its progress slowed down until the first Industrial revolution where the automated machine for the cylinder method was invented. The real mass production of flat glass started after Alistair Pilkington discovered the "float" process (Figure 2.2) back in 1959. Before that glass needed to be polished in order to become fully transaprent and that took a loot of time and work and the opposite of that – the flat glass didn't require to be polished after the float process. This process reduced the price of the flat glass and the industry was able to start a mass production. Until this day, around 90% of the flat glass in the world is made by float proces.
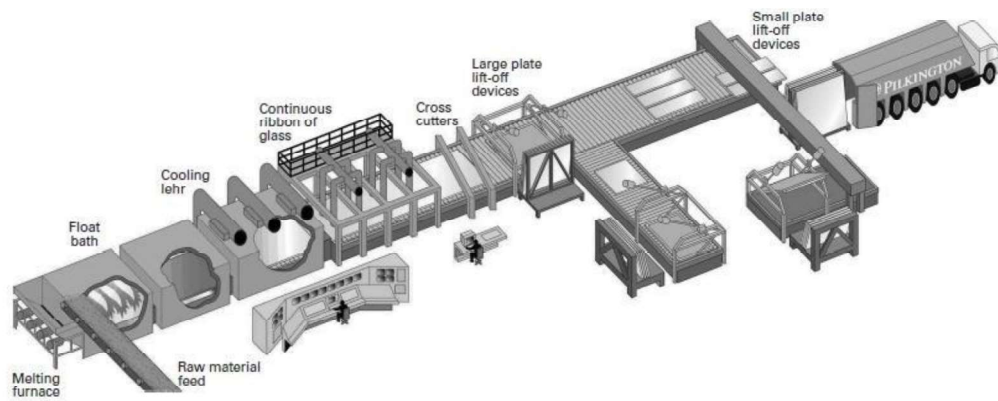
Figure 2.2 – The "float" glass process

Glass can be divided in few groups based on chemical properties:

Silicate glass	The most common type of the glass, main element is silicate dioxide (SiO_2). The other components of the glass are natrium oxide (Na2O), calcium oxide (CaO), mangesium oxide (MgO) and they are used depending on the wanted glass properties. It is used widely in all comercial glasses.
Borosilicate glass	Main element is boron trioxide (B2O3). It's mainly used in laboratory gears due to its high temperature and chemical resistance.
Phosphorate glass	Main element is phosphor pentoxide (P2O5). They are mainly used in special optics.
Aluminosilicate glass	This glass has an addition of aluminum oxide (Al2O3) beside all silicate elements. It has improved mechanical and thermical properties compared to normal silicate glass.
Lead glass	This glass contains significant amounts of lead oxide (PbO). It has high refractive index of light and it's used for making optics lenses and crystal objects.

Table 2.1 – Glass types with different chemical properties

Glass failure is consideres as unsafe way due to lack of material plastic yield, such as steel, which makes is sensitive to stress concentrations. Mechanical properties of glass in stress – strain curves (Figure 2.3) show perfect linear-elastic and isotropic behaviour until sudden failure of the glass steel.
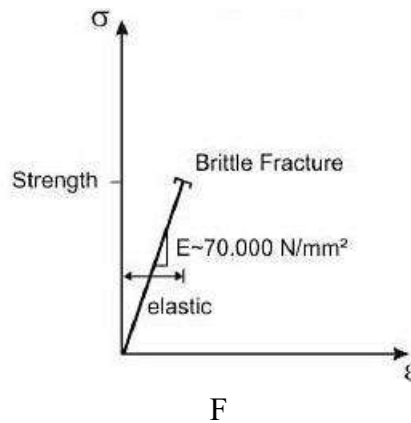
Figure 2.3 – Stress-strain curves of float glass (JRC,2014)

In modern times investors are seeking new designs which are interesting to ordinary people (Figure 2.4) and glass is used to make from colulmns, stairs, walls to bridges, skyscreapers and airports which are load bearing objects.
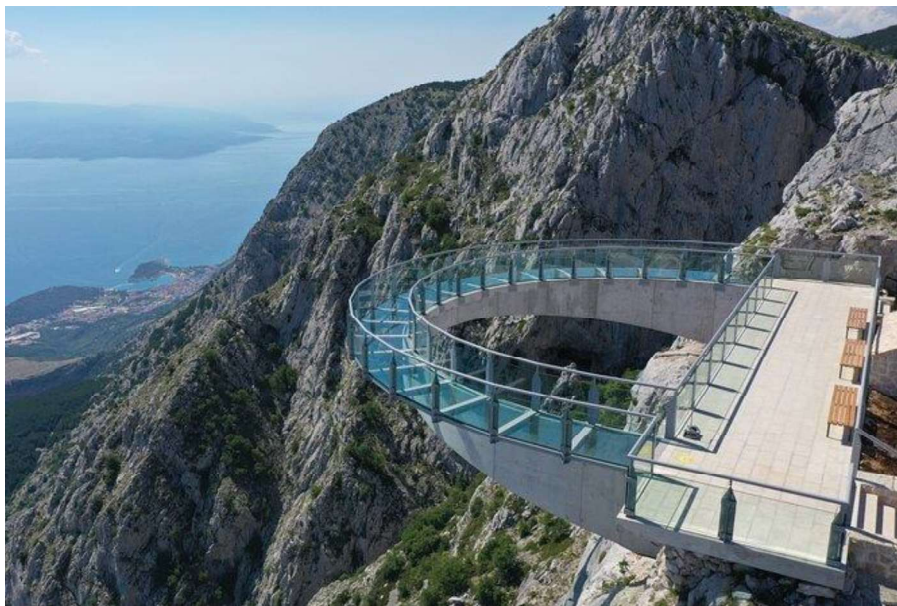

Figure 2.4 – Skywall Biokovo, Croatia [9]

2.2 Point fixing in structural glass

Due to rise,in a recent years, in need of having more efficient architectural desings researchers are using glass as structural material. Due to low capacity of glass – connections between glass and the underlying structural material impose a number of challenges and require careful engineering. These connections are most commonly achived using either and adhesive or various mechanical connections such as clamped, friction-grip or bolted connections. [2] Currently the bolted connections (Figure 2.5) are considered as the primary used method of point-fixing of glass panels.

Figure 2.5 – Bolted connections [1]

Clamped connections (Figure 2.6) are done by metal parts which mechanically clamp the edges of the glass. Stresses are reduced by putting a soft layer plastic material or etylene propylene diene terpolymer (EDPM) due to their hard contact. These are commonly used in facades or in objects such as bathroom shower.
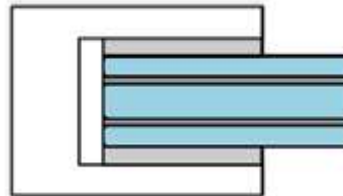

Figure 2.6 – Clamped connection scheme (Bedon and Santarsiero, 2018)

Friction-grip joints are the second option of mechanical connections, which take advantage of initial preload of bolts and they are efficinet for transmission of in-plane loads. Due to that, the distirbution of stress in wide on surface and local peaks are minimized. Having a wide influence surface, these conections can also be subjected to out of plane deformations and their their making should be done with proper care to avoid possible local failure.

The bolted connections (Figure 2.7) are commonly used in modern times, procedure of making bolt connections is done in few steps; first of all hole is drilled trough glass, secondly bolt is placed inside the hole with metal tube and finally infill material is added between metal bush and glass itself for many reasons. Responses of the structure is different whether tensile or compressive loads are applied. Due to their high stiffness,the glass panels can sustain high

amounts of in-plane actions as a lateral loading of the structure. This can cause tensile and compressive loads in glass panels which act as a brace in the facade of the building. [2] There is a limited knowledge and informations about compressive response of the glass elements defined by connection characteristics such as drilled hole size or used infill material.
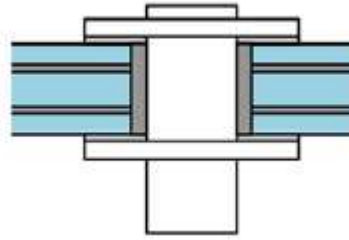
Figure 2.7 – Bolted connection scheme (Bedon and Santarsiero, 2018)

Adhesive connections are mainly done by bonding glass components to metal part or to other glass by adhesive material. There are 3 different failure modes which can describe resistance of adhesive connections; adherends' failure - failure of the bonded components (glass or metal parts), cohesive failure - failure of the adhesive within the thickness which is the less favorable because it does not allow to exploit the maximum loadl capacity and adhesive failure - failure at the interface between adhesive and adherend. There are 3 types of adhesive connections; surface-like connections.which are realized by UV curing interlayers, the forces are transmitted over a large surface, linear connections where forces are transmitted in long linear surface and punctual connections where forces are transmitted over a small bonded area. There are several benefits of using adhesive connections compared to bolted ones: they can transfer the incoming forces over a distributed region, their production stage is much cheaper compared to bolted joints, distribution of stresses is not valid around the hole since there is no drilling in process, and it's better for architectural designs because connector is not passing throught glass. Finally, by considering all reasons from above, the adhesive connections are very likely to be used in near future instead of bolted connections.

Laminated adhesive connections (Figure 2.8) are made as the adhesive material is placed between metal connector and the LG panel. After the autoclave process the object becomes assembly of metal part bonded fully to glass with adhesive layer. The main reasons of laminated connections are simple preparation and application processes compared to other bonding technologies, fully transparency of the adhesive and semi – automatic glass manufacturing process which is known by most of glass manufactures.
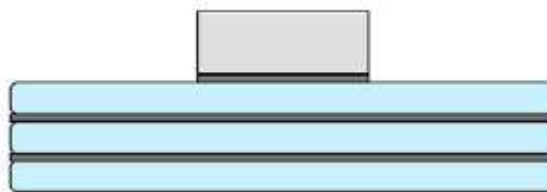
Figure 2.8– Laminated adhesive connection (Bedon and Santarsiero, 2018)

2.3 Structural behaviour of lap-pinned connections

The behaviour of a lap-pinned connection in glass refers to how it responds to applied load and external forces on to the glass panels. Firstly, the type of load is defined such as: tensile load which occures if tensile stress exceeds the tensile strenght of the glass or bolts and shear load which occures if shear stress exceeds the shear strenght of the bolts or the glass in shear. Tensile stress (σ_t) is calculated by dividing applied tensile load (F) and cross section of glass panel (A_g). However, there is existing analytical formulation based on classical theories and in which local effect are considered by glass thickness, hole diameter, position of the hole from the glass edges and others (Figure 2.9).

$$\sigma_{max} = \frac{PKt}{t*(2c-d)}$$

$$K_t = 12.882 - 52.714*(d/2c) + 89.762*(d/2c)^2 - 51.667*(d/2c)^3$$

d – diameter of hole (mm)

c – length from edges of the glass to center of the hole (mm)

t – thickness of the glass (mm)
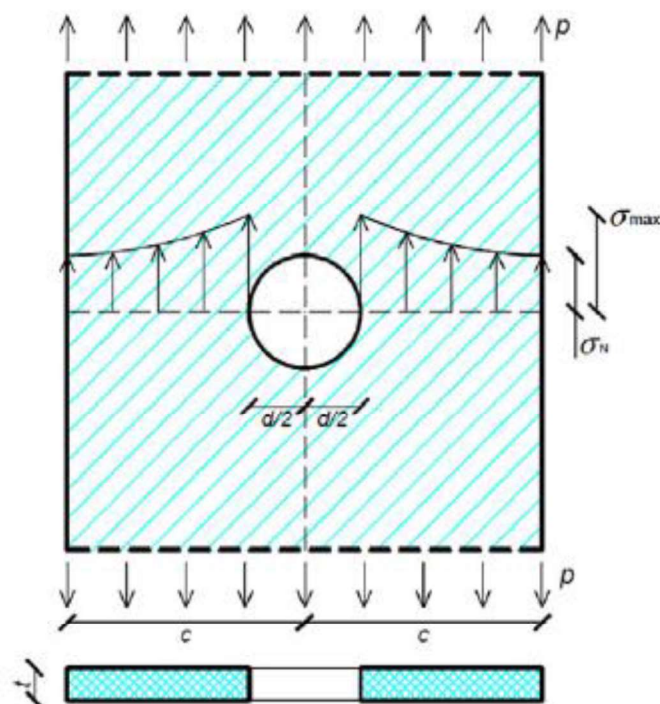
Figure 2.9 – Distribution of stresses in cross section (Bedon and Amadio, 2016)

To make proper calculations it should be considered to use appropriate material properties (such as modulus of elasticity, ultimate tensile strenght), ensure proper edge distance to minimize stress concetrations at the edges and around the pins and to distribute applied load evenly across the connection to avoid local stress concetrations that could lead to failure.

2.4 Design guidance

To get better qualities of glass itself, laminated glass is used commonly. It's made of at least two plies of glass which are bonded with the interlayer in between. Interlayer's job is to keep the strenght of glasses and to keep uniformed layer if it gets broken. Laminated glass can be made of various glass types and different thickness which depends on usage. It's great alternative for traditional glass in: glass floors, glass stairs, skylights, glass roofs (Figure 2.10), aquariums, windows where there is a chance of high risk of breaks in or for the buildings where is high risk of natural loads such as wind.
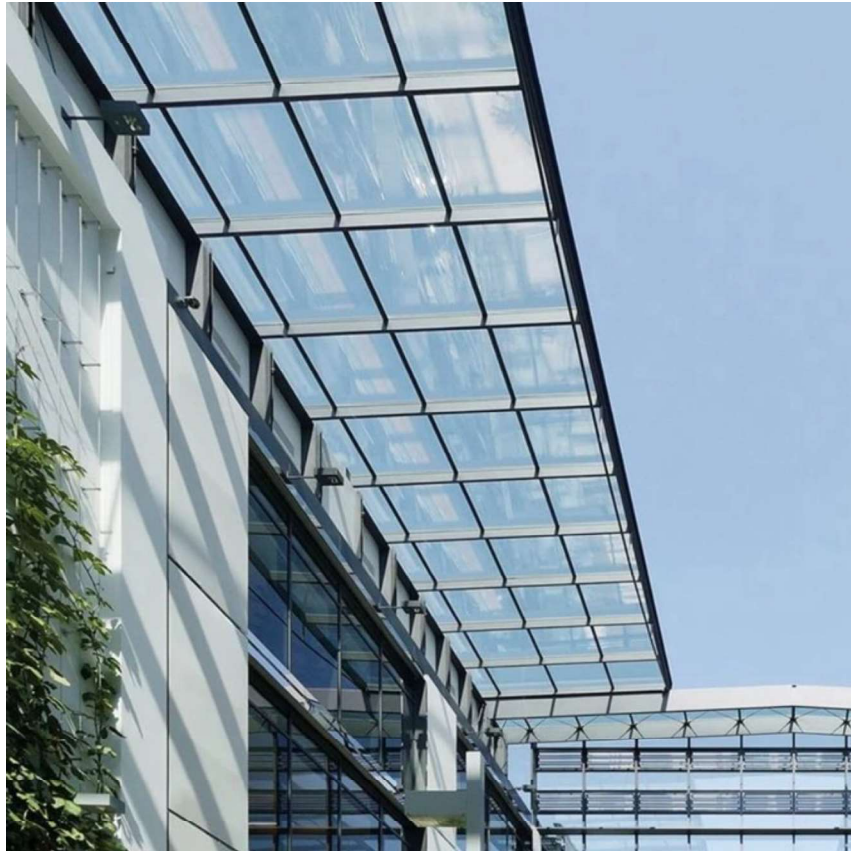
Figure 2.10 – Glass roof [2]

Benefits of using laminated glass instead of traditional are many;firstly low-emissivity glass can help to reduce heat gained from the sun,which allows air conditioning to be used less frequently and emissions to be reduced, secondly, laminated glass doesn't shatter when it breaks, so there is a reduced risk of someone getting injured or cut by shards of glass and thirdly, laminated glass is available in many colours or tones and can be manufactured straight or curved for greater design choice.

2.5 Experimental research

The experimental work [2] which was done by Mirko Pejatović, Roman Wan-Wendner, Sartipi Sahand and Jan Belis in Ghent University, Department of Structural Engineering and

Building Materials was focused on performance of point-fixed connections in structural glass panels.

There were 40 tested specimens which were subdivided in ten groups of four specimens each. Each group had different properties which are presented in Figure 2.11; hole diameter (32/42 mm), glass thickness (6/8 mm), number of glass plies (1/2) and mortar type. Samples with dimensions of 670 x 200 mm were made of either monolithic or laminated heat strengthened glass (HSG). Geometry and detailed view of the sample is presented in Figure 2.12.

Specimen series	Number of specimens	Injection mortar type	Number of glass plies	Interlayer type	Nominal glass thickness [mm]	Hole diameter [mm]
F-1 × 6-42	4	fischer FIS V Plus	1	PVB	6	42
F-2 × 6-42	4		2		6	
F-2 × 8-42	4		2		8	
F-2 × 6-32	4		2		6	32
F-2 × 8-32	4		2		8	
H-1 × 6-42	4	Hilti Hit HY270	1	PVB	6	42
H-2 × 6-42	4		2		6	
H-2 × 8-42	4		2		8	
H-2 × 6-32	4		2		6	32
H-2 × 8-32	4		2		8	

Figure 2.11: Overview of samples [3]
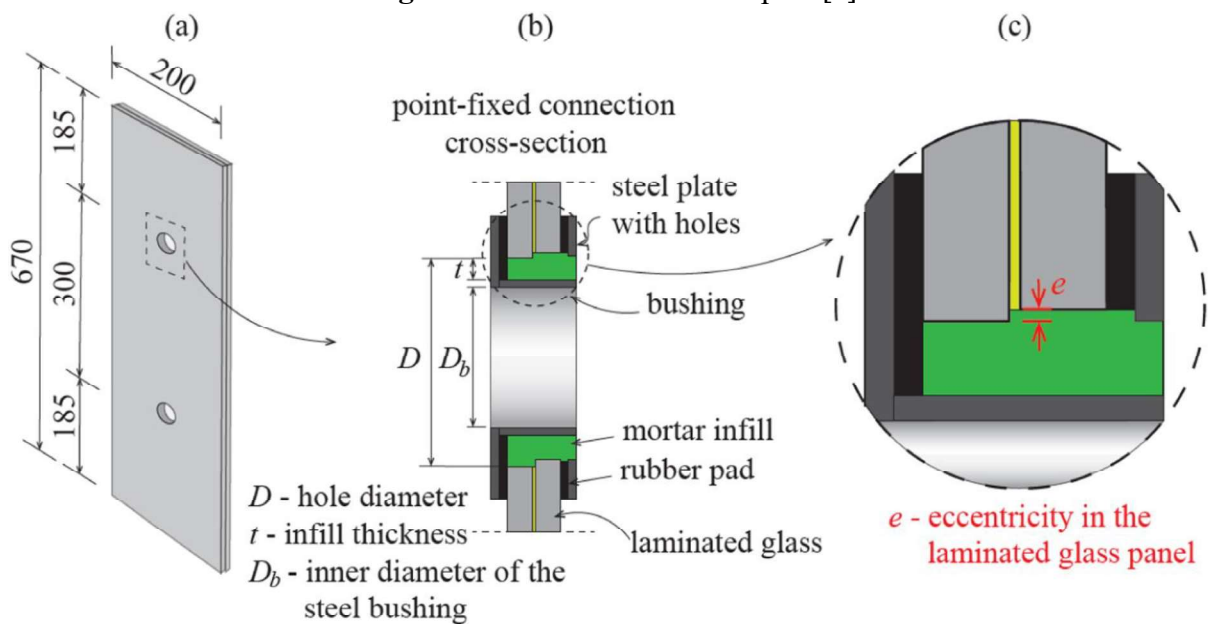
Figure 2.12: (a) dimensions of sample in mm, (b) elements of point-fixed connections, (c) detail of the edge of the hole in the laminated glass panell with eccentricity. [3]

Two different types of infill products were used; fischer FIS V Plus [5] and Hilti hit HY270 [6]. Each sample had two holes which had distance of 300 mm between themselves and diameter of either 32 mm or 42 mm.

Two failure modes were observed: infill failure (IF) and splitting failure in the glass (SF) presented in Figure 2.13.

Figure 2.13: (a) IF F-1 X 6-42-2 and (b) SF F-2 X 6-42-1 [3]

Test results were presented in terms of load-displacement curves and crack patern failure. In terms of failure load there was no noticeable performance difference between both products acording to the calculated statistical values in Table 2.2. Results show that specimens with larger holes perform slightly better in fischer product and Hilti product gives better yields results and based on the standard deviation it gives more consistent results. The tests provided that in case of Hilti hit HY270 the displacements at failure have higher values.

In case of monolithic glass samples, premature IF causes the primary peak in the force-displacement graph where the glass is still intact, furthure incrising of the displacement resulted in failure of the glass and the panel. However in force-displacement curves of laminated panels, only one peak is visible which corresponds to the glass fracture.

Specimen	F_u	Mean StDev 0.05	δ_u	Mean StDev 0.05	Failure mode	Specimen	F_u	Mean StDev 0.05	δ_u	Mean StDev 0.05	Failure mode
	[kN]	[kN]	[mm]	[mm]			[kN]	[kN]	[mm]	[mm]	
F-1 × 6-42-1	15.92	16.54	1.64	1.69	IF	H-1 × 6-42-1	17.44	15.55	2.99	3.06	IF
F-1 × 6-42-2	13.43	2.65	1.50	0.19	IF	H-1 × 6-42-2	14.91	1.38	3.51	0.35	IF
F-1 × 6-42-3	16.99	12.18	1.69	1.39	IF	H-1 × 6-42-3	14.25	13.29	2.66	2.49	IF
F-1 × 6-42-4	19.83		1.95		SF	H-1 × 6-42-4	15.61		3.08		IF
F-2 × 6-42-1	39.52	42.56	2.22	2.72	SF	H-2 × 6-42-1	34.24	41.29	3.65	3.84	SF
F-2 × 6-42-2	38.99	5.69	2.77	0.39	SF	H-2 × 6-42-2	37.02	7.49	3.12	0.60	SF
F-2 × 6-42-3	40.71	33.20	2.72	2.08	SF	H-2 × 6-42-3	42.70	28.97	4.54	2.84	SF
F-2 × 6-42-4	51.03		3.19		SF	H-2 × 6-42-4	51.22		4.05		SF
F-2 × 6-32-1	30.16	37.91	3.70	3.83	SF	H-2 × 6-32-1	29.39	33.85	4.11	4.01	SF
F-2 × 6-32-2	29.45	9.46	2.89	0.73	SF	H-2 × 6-32-2	35.43	3.07	3.80	0.18	SF
F-2 × 6-32-3	47.66	22.35	4.09	2.63	SF	H-2 × 6-32-3	34.32	28.79	3.93	3.71	SF
F-2 × 6-32-4	44.37		4.63		SF	H-2 × 6-32-4	36.26		4.21		SF
F-2 × 8-42-1	57.69	65.10	2.71	3.20	SF	H-2 × 8-42-1	55.25	54.33	4.69	4.27	SF
F-2 × 8-42-2	56.23	9.57	3.27	0.36	SF	H-2 × 8-42-2	51.75	2.93	5.29	0.86	SF
F-2 × 8-42-3	75.29	49.36	3.26	2.61	SF	H-2 × 8-42-3	58.07	49.51	3.61	2.86	SF
F-2 × 8-42-4	71.20		3.58		SF	H-2 × 8-42-4	52.26		3.51		SF
F-2 × 8-32-1	48.45	47.05	4.80	4.83	SF	H-2 × 8-32-1	50.89	49.86	4.61	4.50	SF
F-2 × 8-32-2	39.02	5.55	4.17	0.58	SF	H-2 × 8-32-2	52.93	4.35	5.22	0.58	SF
F-2 × 8-32-3	48.97	37.93	4.78	3.87	SF	H-2 × 8-32-3	43.45	42.70	3.82	3.55	SF
F-2 × 8-32-4	51.76		5.59		SF	H-2 × 8-32-4	52.14		4.36		SF

Table 2.2: Experimental results table [3]
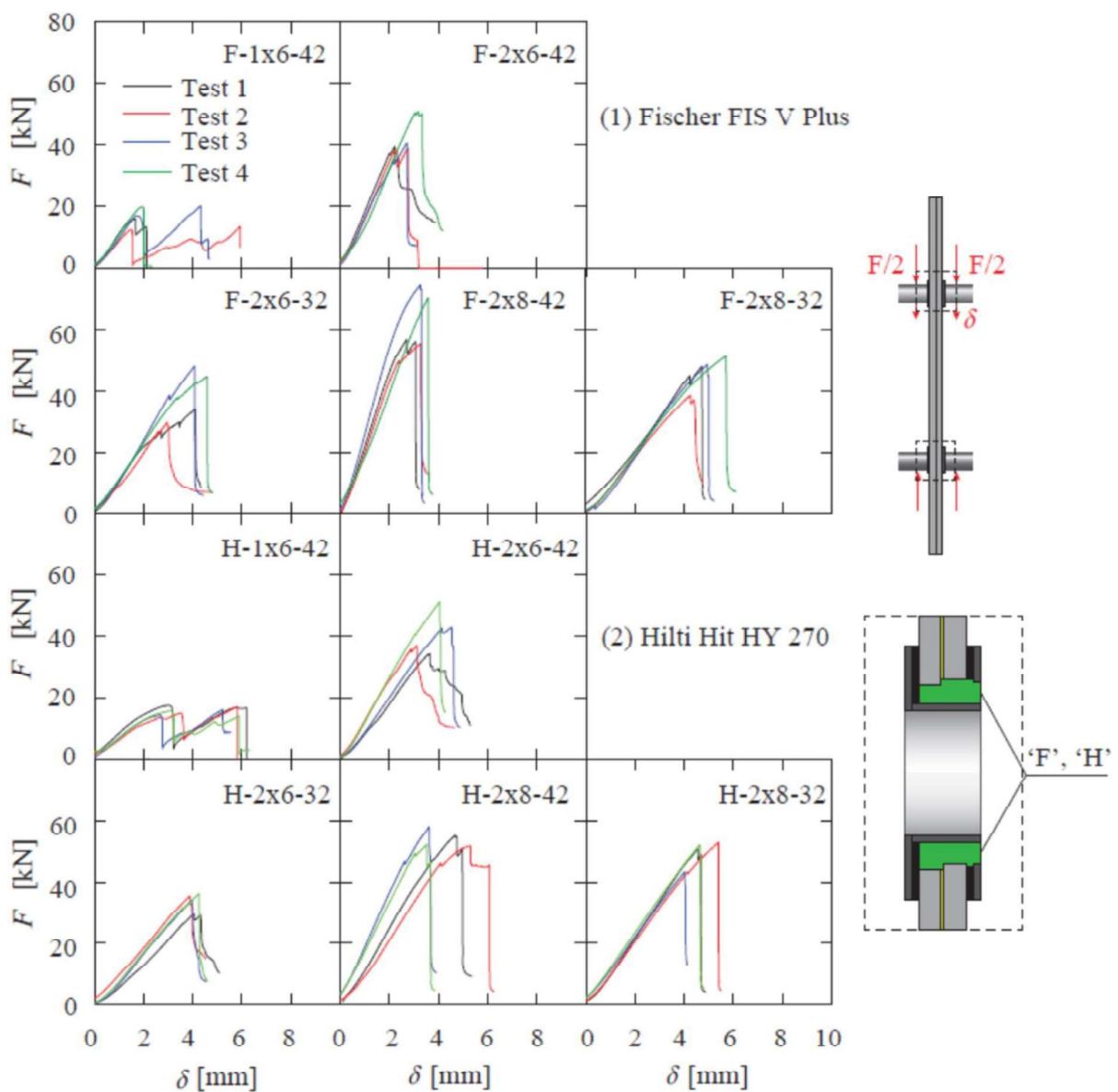
Figure 2.14: Force-displacement curves for all specimens [3]

Simmilar things was done by Danijel Mocibob and Jan Belis back in 2008. [7] They were making test on glass panels subjected to a locally introduced axial compressive load.

13

Furthuremore uniaxial tensile test were also executed on identical test samples to allow a comparison of both loading cases.

They used nine heat-strengthened glass specimens with dimensions of 200 x 500 mm. Specimens were devided in three groups with a different glass thickness and composition presented in Table 2.3.

GROUP	GLASS THICKNESS (mm)	NUMBER OF PANELS
1	6	1
2	6	2
3	8	2

Table 2.3: Specimens properties

Every specimen had a hole with diameter of 42 mm in which axially rigid bolted connection devices had been placed to introduce loads[8]. Connection devices were made of a steel M20 bolt, a steel tube and a steel cylinder presented in Figure 2.8c. Between glass and steel was injected mortar Hilti HIT HY 50 [9] to fill up the free space.

An axial compressive load (F_c) was applied as shown is Figure 2.15. Test results were presented in Figure 2.16 with first breakage load ($F_{c,b}$), the failure load ($F_{c,u}$) and the correspoding elongation at the failure ($d_{c,u}$) of the specimens subjected to compressive load. In Figure 2.17 are presented curves of longitudinal displacements-in plane compressive load.
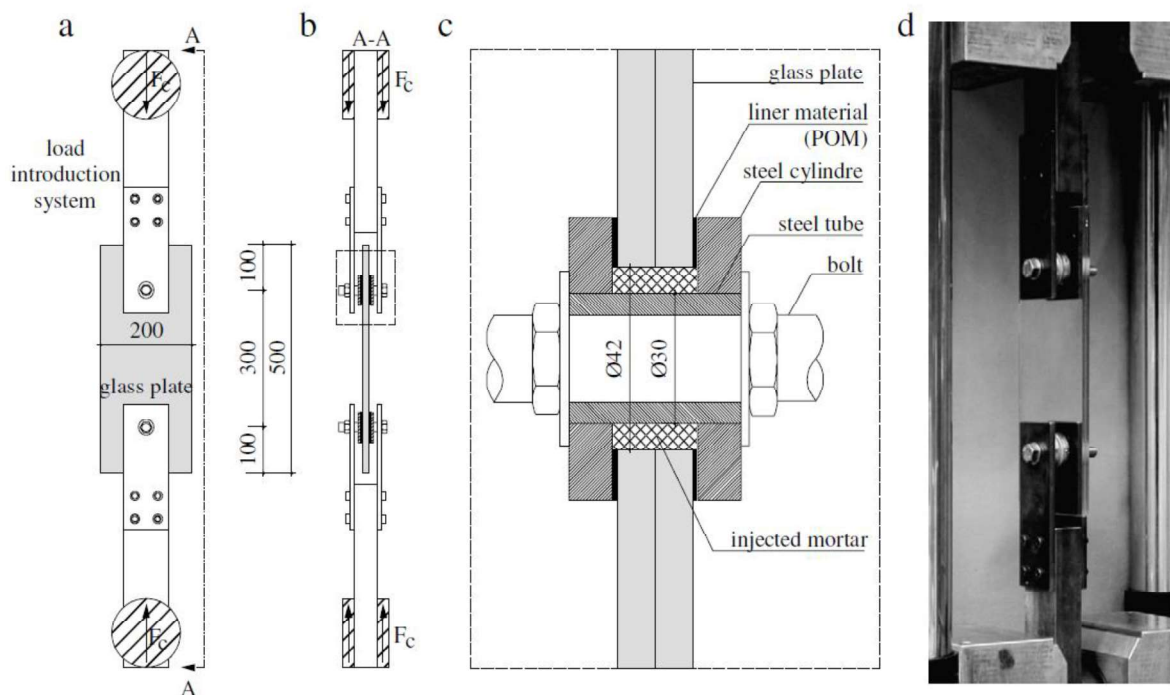
Figure 2.15: (a) Front view, (b) Side view, (c) connection detail; (d) test speciment in laboratory [4]

Specimen name	First compressive breakage load $F_{c,b}$ (kN)	Ultimate compressive failure load $F_{c,u}$ (kN)	Elongation at failure $\delta_{c,u}$ (compression case) (mm)	First tensile breakage load $F_{t,b}$ (kN)	Ultimate tensile failure load $F_{t,u}$ (kN)
1 × 6-1	19.12	17.64	6.97	12.00	14.25
1 × 6-2	16.32	18.92	5.70	13.26	15.08
1 × 6-3	15.80	19.48	7.55	14.60	21.56
2 × 6-1	33.68	23.20	3.74	24.56	17.96
2 × 6-2	30.44	28.76	2.55	20.04	18.72
2 × 6-3	23.52	21.24	3.43	32.60	32.60
2 × 8-1	48.88	41.24	2.44	38.92	38.92
2 × 8-2	46.04	36.88	3.61	39.48	39.48
2 × 8-3	51.12	35.28	4.35	49.80	49.80

Figure 2.16: Experimental results for in plane load [4]

Failure of the (1 x 6) specimens (Fig. 2.17a) happend by chrushing mortar due to high compressive loads and that happend before breakage of the glass plates. Chrush of the mortar led to crack of the glass due to contra pressure of the steel tube and the glas.

Failure of the (2 x 6) specimens (Fig. 2.17b) happend with smaller displacements and higher initial breakage loads but the latter never reached twice the level of the (1 x 6) failure loads which was expected due to the laminations. Secondly both of the glass plates failed separately and had two local maximums.

Failure of the (2 x 8) specimens (Fig. 2.17c) showed the smallest displacements and the highest failure loads. However, in spite of the significant residual resistance after initial glass breakage, the level of the latter was never reached again.
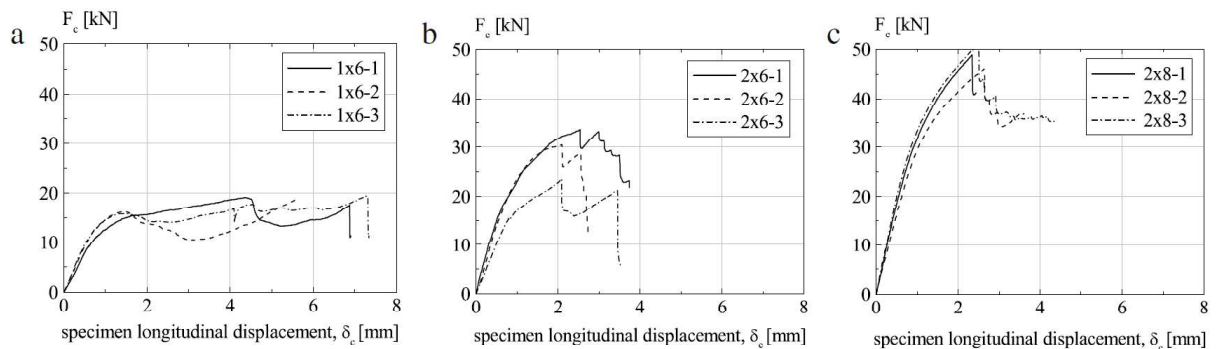
Figure 2.17: (a) 6 mm monolithic glass 1 x 6 ; (b) 6 mm laminated glass 2 x 6; (c) 8 mm laminated glass 2 x 8 [4]

The final crack configuration of the glass panell is presented in Figure 2.18 due to in-plane compressive loads. The position of splitting tension crack initiation is at 0° while crack initiation of the fan-shape took place at 180°
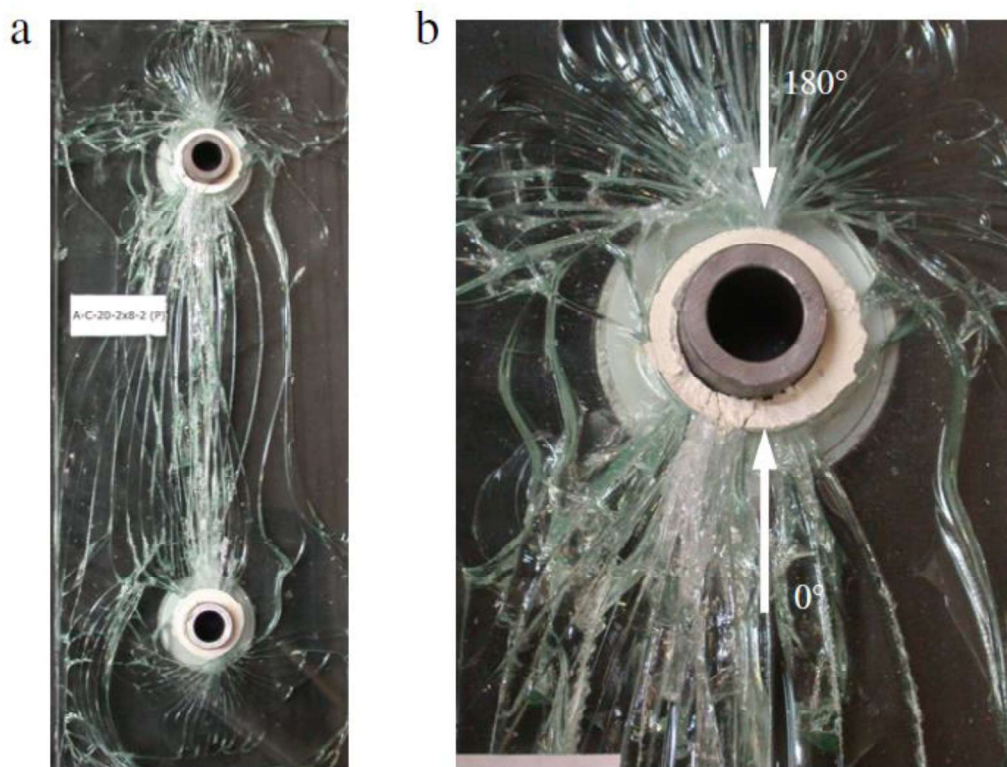
Figure 2.18: Experimental splitting tension crack pattern: (a) final crack pattern; (b) detail of crack initiation at the borehole [4]

In conclusion there were few important things: the initial compressive glass breakage load increased with a glass area, high stress concentrations appeared at the borehole perimeter and by moving from the borehole stress values and stress peaks decreased quickly, crack initiated at different locations – due to the tensile loading case initiated at +/- 90° and propagadet perpendiculary to teh direction of the applied load. Finally the most important geometrical parameter (apart from the thickness) was the borehole diameter – smaller diameters led to higher stress concentrations by applying compressive load. However by applying the tensile load resistance increased priparily due to an increasing panel width.

2.6 Numerical research

By having experimental results, both of those works had numerical analysis for the model.

In Pejatović's work [2] the 3D finite element (FE) model was created in ABAQUS [4] focusing on the linear-elastic stress analysis. The assambled sample is shown in Figure 2.20b and the linear hexahedral elements of tpye C3D8 were adopted for all materials in Figure 2.20c.
Forces were transferred from surface to surface by normal and tangential stresses. Normal contact is modeled as a hard contact whereas the tangential contact was modeled using penalty condition.
Material properties used in FE model are shown in Figure 2.19.

Material	E [MPa]	v [-]
Glass	70,000	0.23
Infill mortar	1500	0.2
Steel	210,000	0.3

Figure 2.19: Material properties [3]
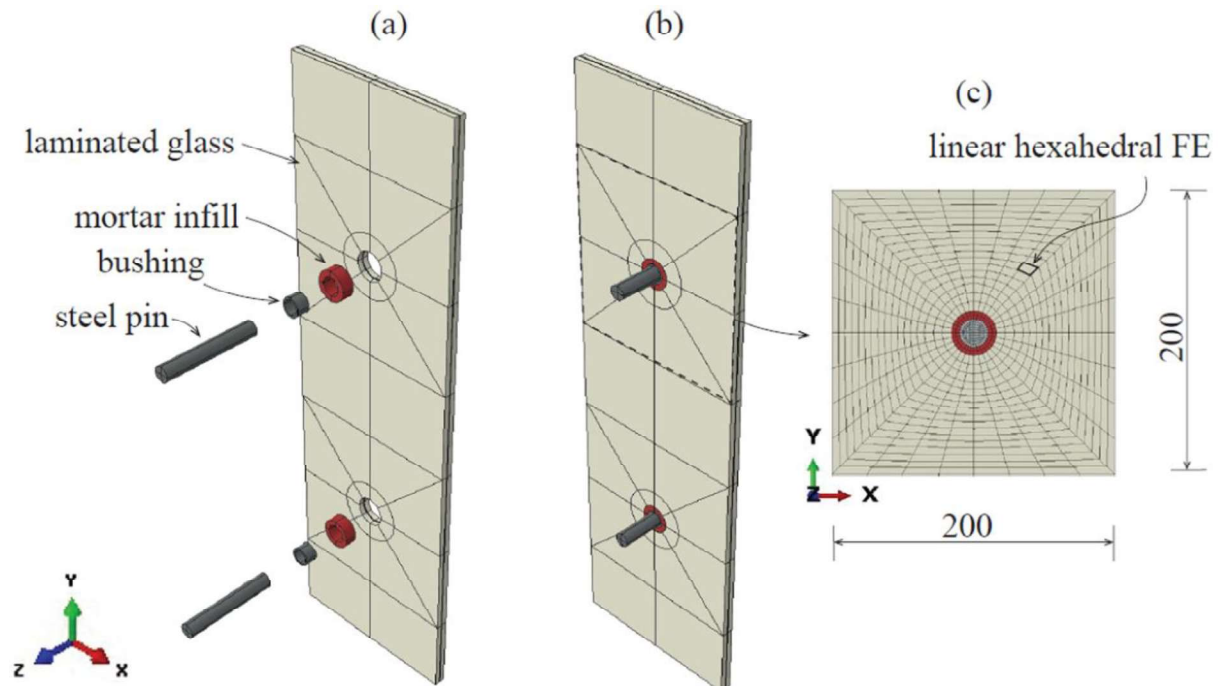
Figure 2.20: (a) Axonometry of 3D FE model - exploded; (b) axonometry of 3D FE model – assembled; (c) mesh around the hole [3]

The eccentricity which accured due to the lamination proces was shown in Figure 2.21. Therefore the numerical analysis had adopted the values of the eccentricity of e= 0mm, 1mm and 2mm. These values were chosen since they were likely to occur in practice.
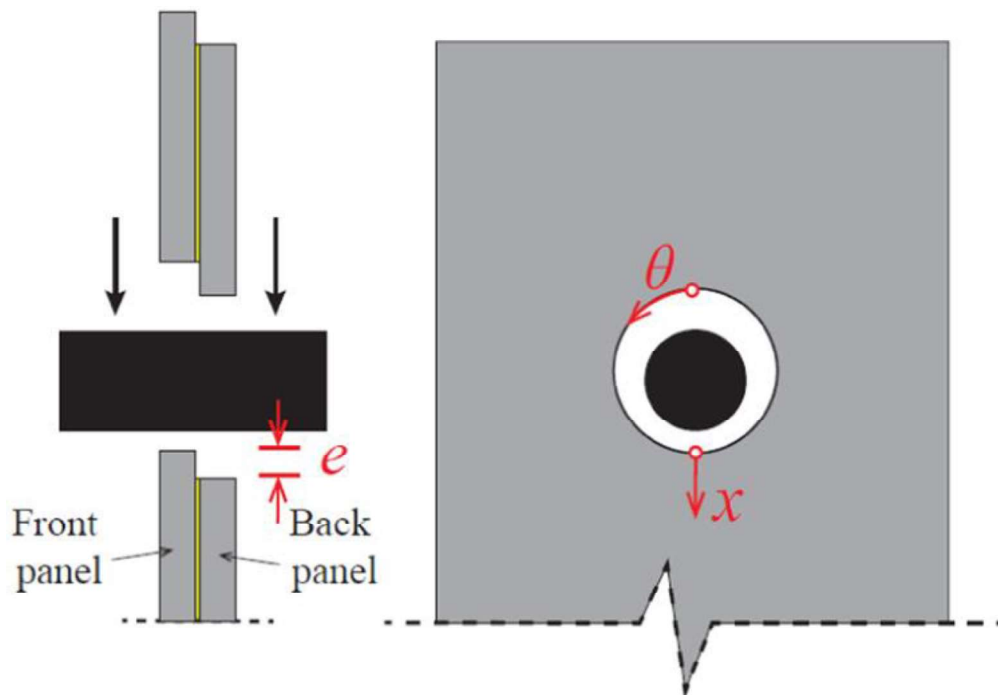
Figure 2.21: Eccentricity due to lamination process [3]

In the Figure 2.22 and Figure 2.23 the effects of the eccentricity e on the princial tensile and compressive stresses are visualised for diameter of 32 mm and 42 mm. The results indicate that both the maximum and the minimum values of principal stresses increase at the perimeter of the hole as eccentricity grows and that occurs because the front panel becomes more elevated compared to the back panel.
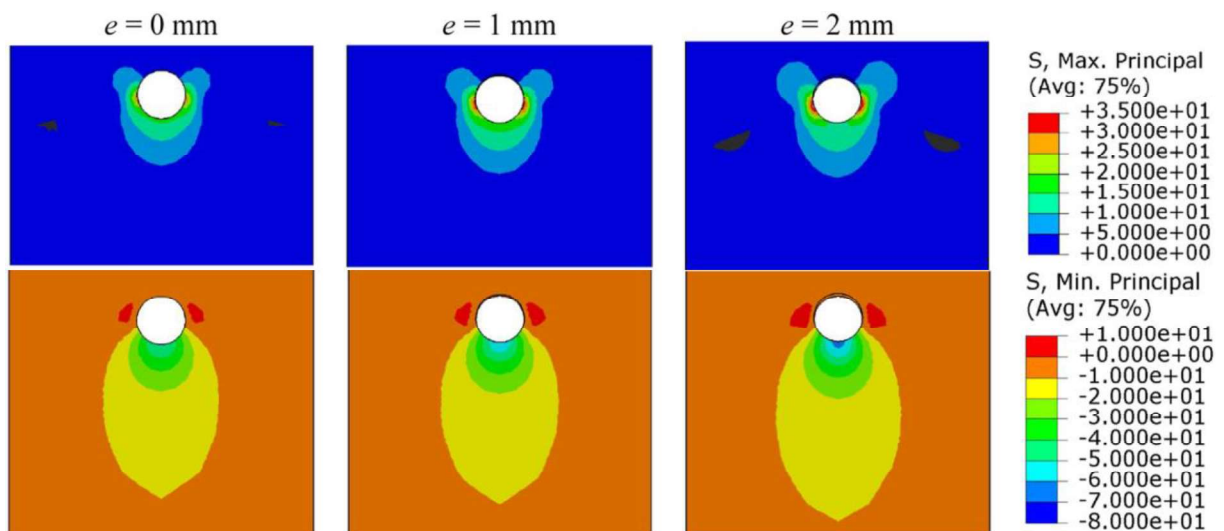
Figure 2.22: Effect of the excentricity e on the principal tensile and compressive stresses in the front panel with the hole diameter equal to 32 mm and friction coeff. of 0,9. [3]
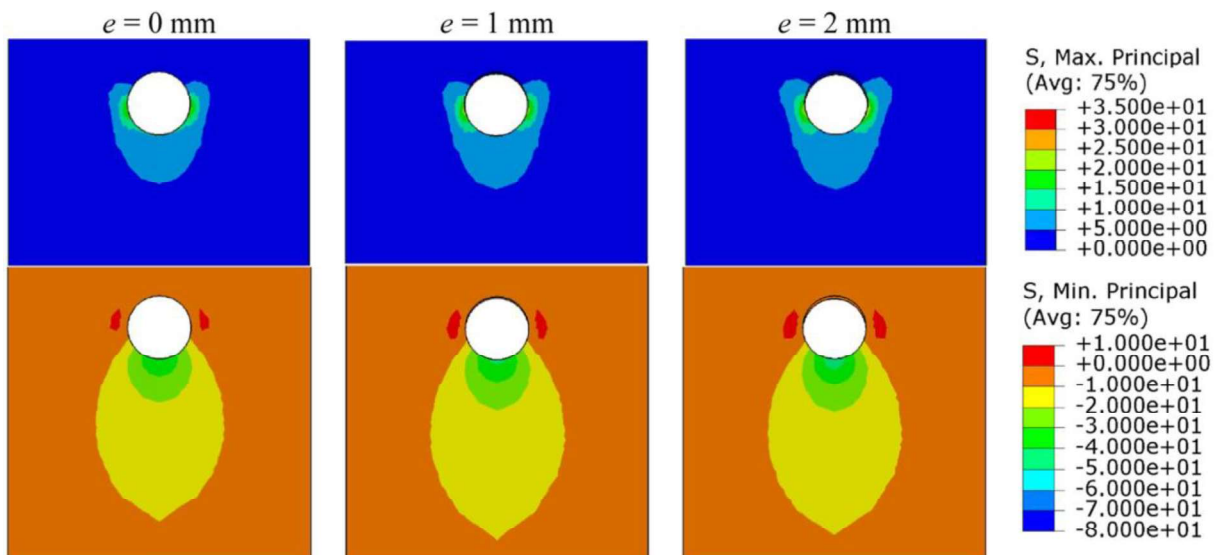
Figure 2.23: Effect of the excentricity e on the principal tensile and compressive stresses in the front panel with the hole diameter equal to 42 mm and friction coeff. of 0,9.[3]

In conclusion authors said that numerical study demonstrates a load eccentricity in the laminated panels had a significant influence on the stress amplification which was larger in the case of a smaller hole diameter. Furthermore it was found out that the friction coefficient can substainally change the distribution of the principal stressses around the hole – higher values of the friction coefficient yield higher values of the maximum principal tensiel stresses around the hole.

In Mocibob and Belis work [3] the numerical analysis was done similar. They made numerical model by using the Finite Element (FE) package Ansys [10]. Due to the symmetry only the upper half of the tested specimen was numerically modelled which is shown in Figure 2.24.
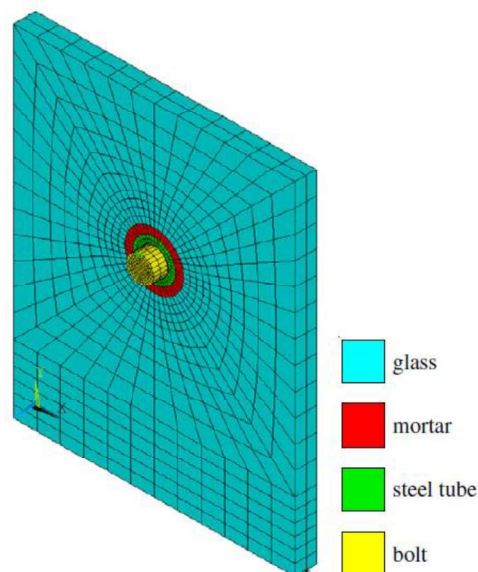
Figure 2.24: Numerical model of half glass panel [4]

In Figure 2.25a is shown the in-plane deformation of the numerical model subjected to a compressive load. The hole was streched to an oval shape in loading direction. Figure 2.25b

shows the principal compressive stresses while Figure 2.25c shows the rincipal tensile stresses in the glass panel. Maximal principal compressive stresses occured at the contact area of connection devices and glass panel and at the same time the maximal tensile stresses in the glass panel occured at the same contact area. In addition, the maximal principal and tensile stresses have only local influence around the glass hole.
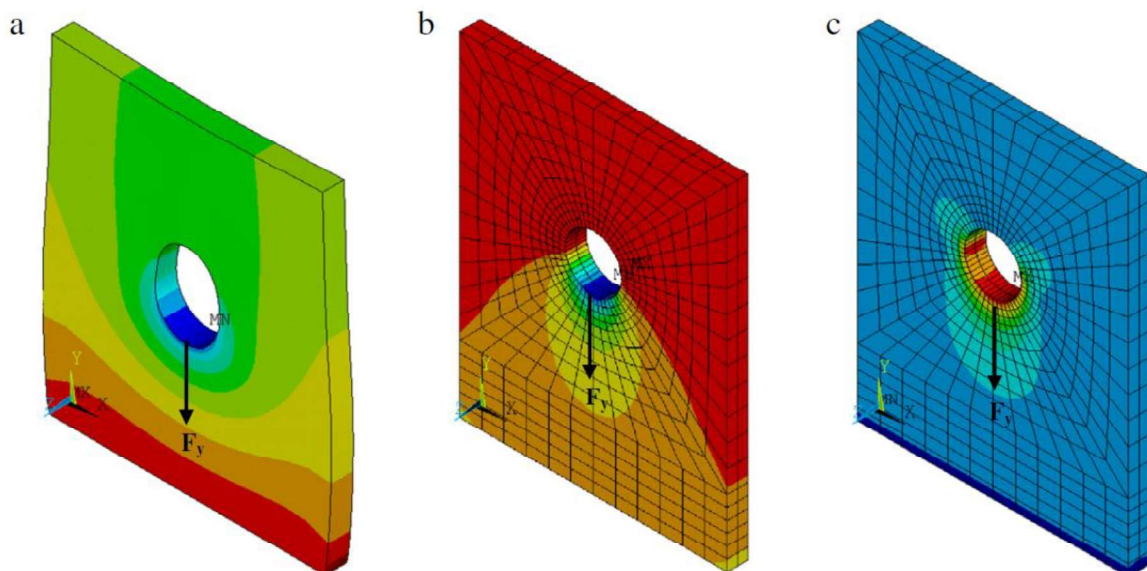
Figure 2.25: (a) borehole deformation; (b) principal compressive stresses distribution; (c) principal tensile stresses distribution [4]

By doing the analysis of different parameters the borehole diameter was found to have highest impact so a stress concentration factor (K_c) was introduced.

In conclusion, while comparing the parametric influence on maximal tensile stresses on glass panels subjected to tensile loads [8,11,12] the follwing differences were found: while keeping the borehole diameter constant and changing the panel width has no influence on the maximal tensile stresses for a glass panels subjected to compressive load,but it has significant influence on glass panels subjected to tensile loads; changing the borehole diameter and keeping the panel width constant does influence maximal tensile stresses for both compressive and tensile load cases; changing the borehole diameter and panel width while keeping the radio d/H constant will influence the maximal tensile stresses in the glass panel when subjected to a compressive load but not when subjected to a tensile load.

2.7 Infill materials

Infill materials are being used in zone between glass and steel tube for several important reason. At the beggining to avoid direct contact between glass and steel which can lead to local stress concetrations, furthermore in point of fixings of laminated glass panels, each glass pane has to be drilled before lamination process. This misalignment could result in uneven loading of glass panes inside a laminated panel; the infill materials is especially needed to account for tolerances and make sure both glass panes are loaded more or less uniformly [2]. Last but not the least important infill material is helping to accomodade the effects of thermal

fluctuations. In conclusion it's important to chose infill material with proper care because it reflects a lot on behaviour of the structure itself.

Tests and examinations on infill materials can be divided in long-term and short-time strenghts in which are taken informations about one of the most imporant properties - elastic modulus and coefficient of thermal expansion.
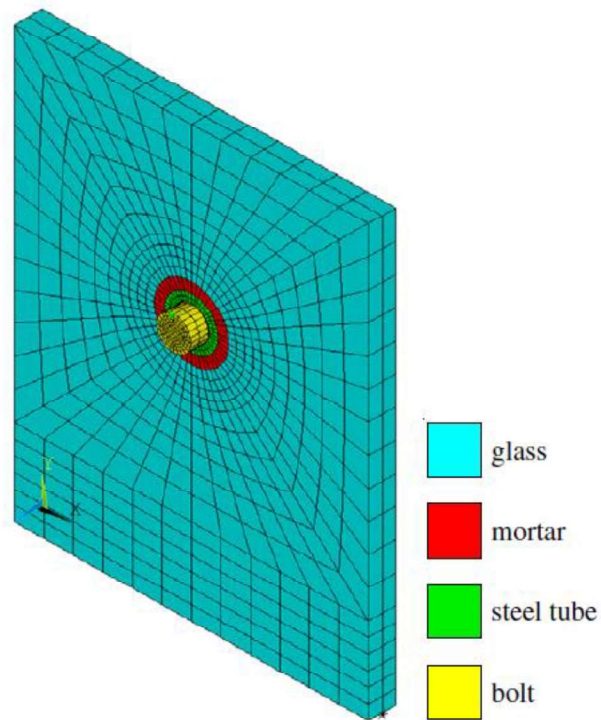
Figure 2.26 – Positioning of the infill material (mortar) between glass and steel tube [4]

Figure 2.27 – Applying of HILTI ,HY-270 [5]

3 EXPERIMENTAL CAMPAIGN

3.1 Introduction

The goal of experimental campaign was to characterise the structural behaviour of the point fixed connections in the all-glass box (Figure 3.1) at Karla tower, particularly the damage accumulation, failure mode, first crack load and ultimate load.
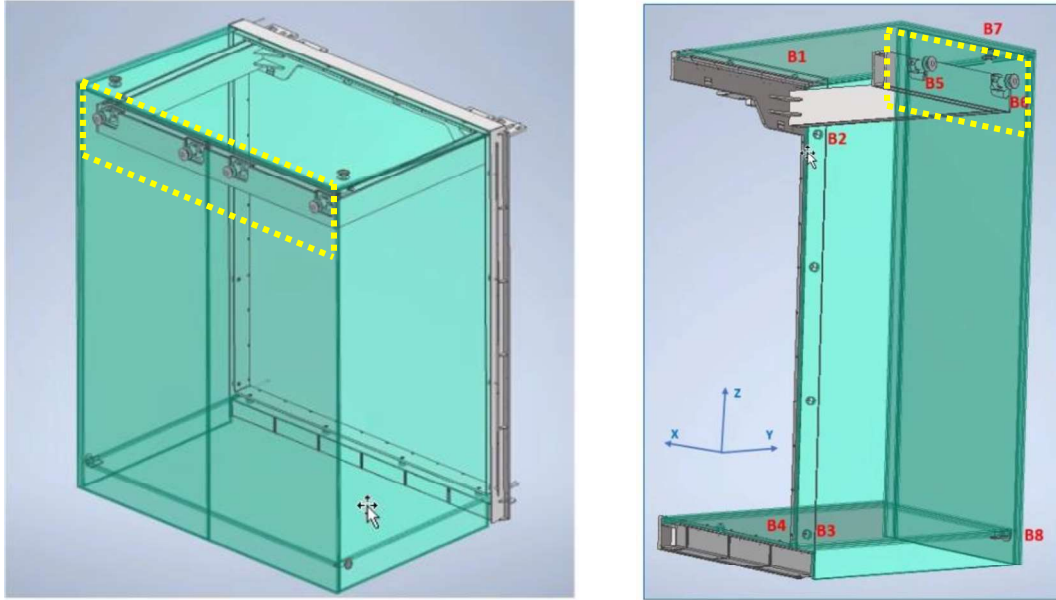
Figure 3.1 - All-glass box at Karla tower | schematic representation (Yanda, Europe)

Five samples (figure 3.2) were used, to have a reasonable level of statistical validation, given the random nature of glass fracture. The characteristic resistance was calculated according to Annex D of EN1990 [1].

Figure 3.2 - Five samples in Laboratory [7]

The experimental campaign took a place in October 2023, at the Laboratory of Structures, Construction and Structural Mechanics (LEMEC) of the Civil Engineering Department (DEC) of University of Coimbra. The tests were performed by Sandra Jordão and Eliana Inca with assistance of a laboratory technician and an engineer from Hilti.

The tests were conducted in a universal testing machine with an 80 Ton capacity load cell, type SERVOSIS (Figure 3.3).

Figure 3.3 – Universal Testing Machine SERVOSIS 80ton [7]

The samples, infill grout, shims and auxiliary parts were provided by Yuanda, Europe. The auxiliary parts correspond to the steel forks, which transfer the load from the universal machine to the bolts (Figure 3.4), stainless steel inserts (Figure 3.6a), grout (Figure 3.6b) and laminated glass specimens (Figure 3.9).

3.2 Geometry and layout

The layout for the test was selected in a way it would correspond to the load transfer and bearing in the region of connection in the actual all-glass box. Thus, a uniaxial layout was foreseen where the sample is pulled in tension (Figure 3.4). The upper bolt corresponds to the one used in the all-glass box (M20, countersank head), and the bottom bolt is stronger and is used to secure the glass and transfer the load (M24, hexagonal head)
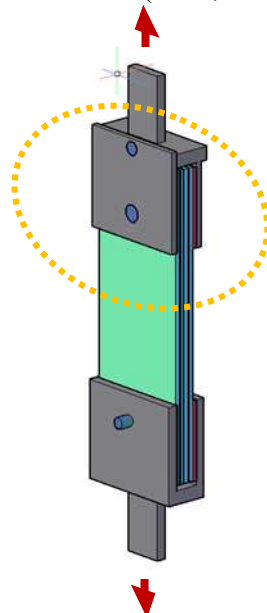
Figure 3.4 – Structural scheme for the experimental tests

The characteristics and geometry of all elements corresponds to those actually used in the real structure. The glass samples are rectangular (700mm by 240mm), and feature 2 boreholes of 80mm diameter, at 120mm from the edges (Figure 3.5). A stainless-steel part, corresponding

to a hollow cylinder sleeve, is used to protect and align the bolt (Fig. 3.7 a)). A specialised grout fills in the remainder space in the borehole, which helps to secure the bolt in place and prevent harsh contact between the metal parts and the glass (Fig. 3.7 b)).
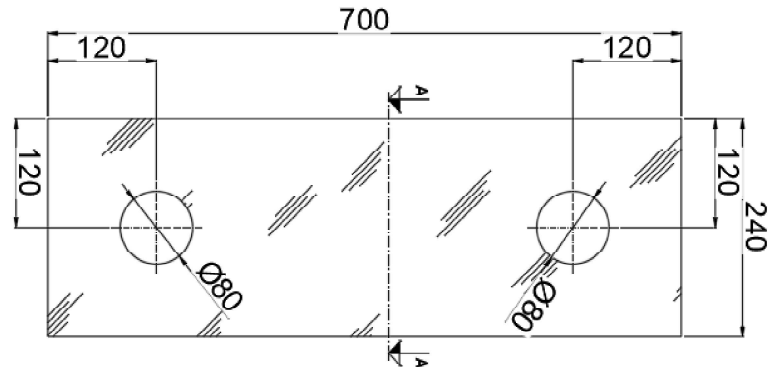
Figure 3.5 – Geometry of the glass samples

    a) Bolts and stainless steel sleeves   b) Grout

Figure 3.6 – Elements fit in the borehole

The samples are connected to two steel parts (forks) which are secured to the universal machine. The upper fork features a detachable plate to assist placing and alignment operations. The plate is then secured to the fork with a bolt. A polymeric material is used as shim to help alignment and avoid harsh contact during mounting operations.

    a) Upper fork with detachable plate   b) Lower fork with shims
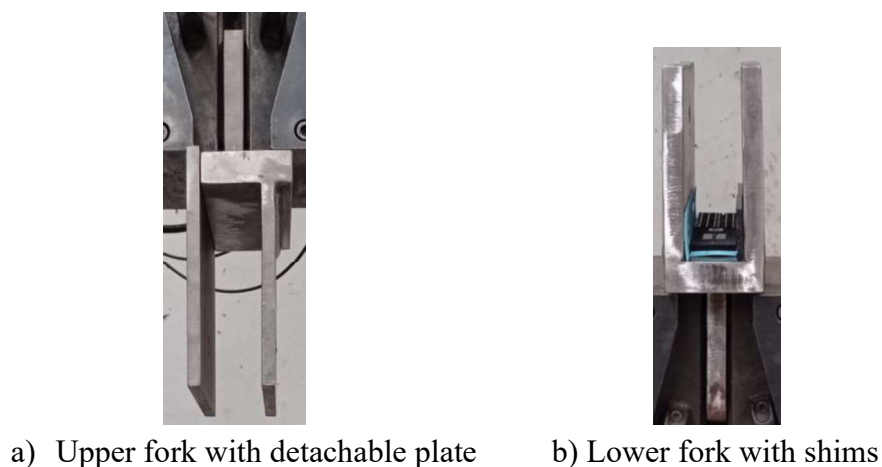
Figure 3.7 – Steel parts for load transfer and shims

The detailed layout of the sample, auxiliary parts and universal machine fitting is represented in Figure 3.8.
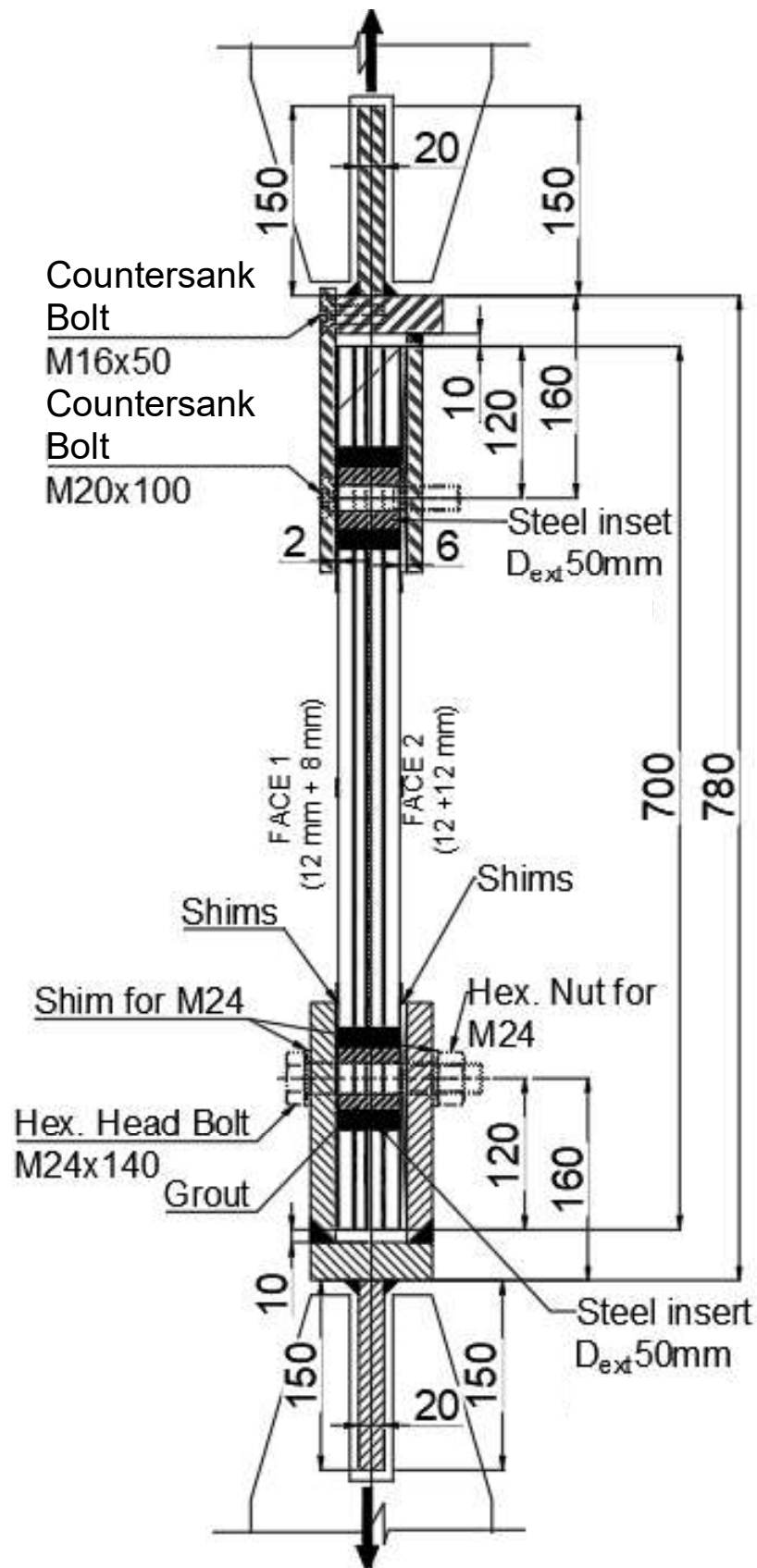
Figure 3.8 – Uniaxial tensile test – Test layout configuration [7]

The samples are composed of 4-ply of Heat Strengthened (HS) glass with nominal thickness of 48.56 mm (Figure 3.9). The choice of HS glass is due to the fact that the glass was drilled, which damages the border. HS enforces a favourable compression stress field which compensates the damage, up to some extent. The lamination material is SentryGlass Xtra (1.52 mm). It was selected because of its improved resistance and stiffness.
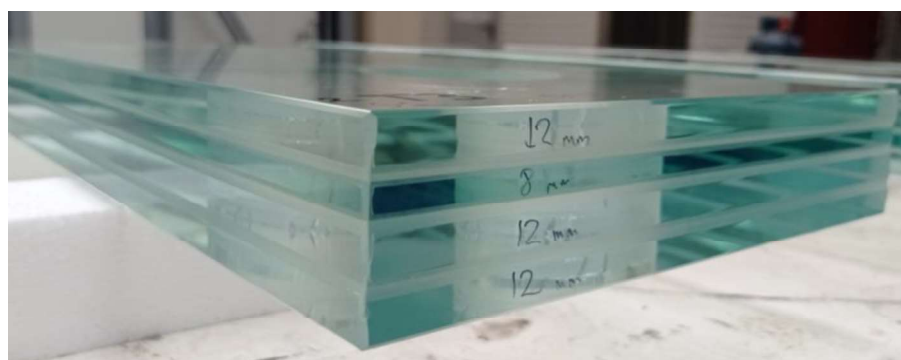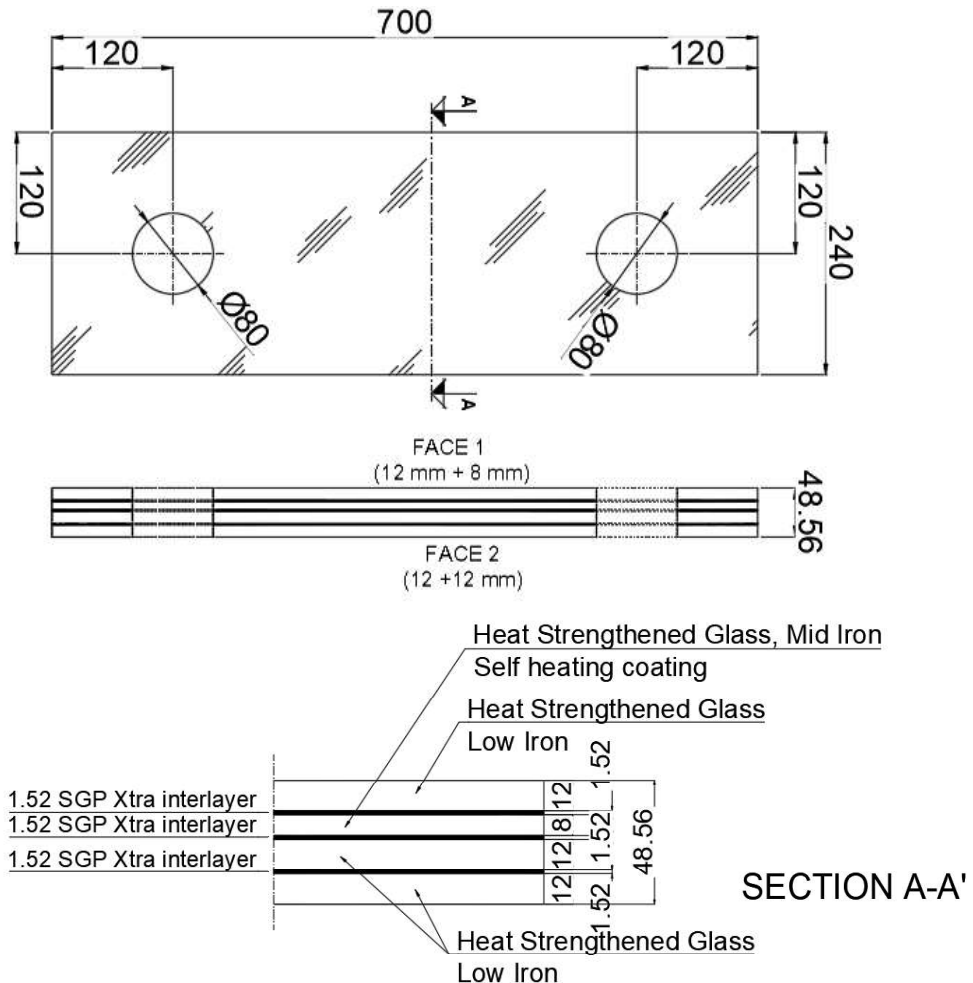
Figure 3.9 – Cross section and composition of the samples [7]

All the specimens were measured on arrival. The nominal measurements regarding the rectangular section and the position of the boreholes were confirmed. The thickness was assessed in several locations throughout the sample and showed some variations. These variations are usual in laminated elements and are related with minor non-uniformities of pressure and temperature, interlayer confinement and moisture and air migration. The locations and values are represented in Figure 3.10.
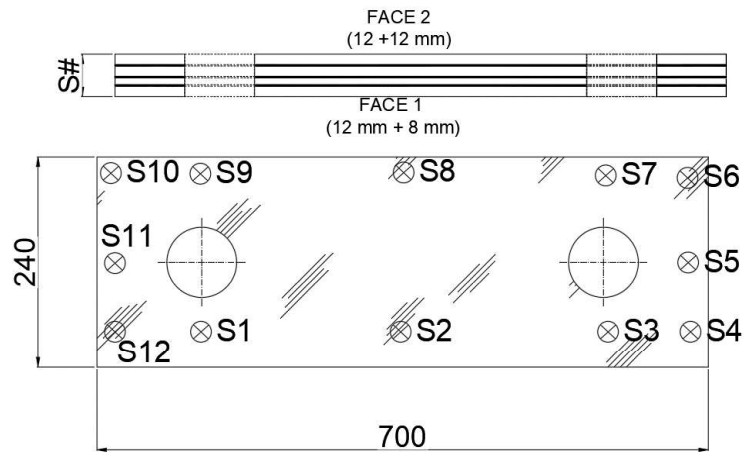
Specimen	S1 [mm]	S2 [mm]	S3 [mm]	S4 [mm]	S5 [mm]	S6 [mm]	S7 [mm]	S8 [mm]	S9 [mm]	S10 [mm]	S11 [mm]	S12 [mm]	Average [mm]
T01	47.63	47.74	47.84	47.48	47.58	47.63	47.67	47.84	47.58	47.58	47.64	47.61	47.7
T02	48.42	48.36	48.18	48.18	48.18	48.37	48.2	48.18	48.08	48.21	48.19	48.34	48.2
T03	48.13	48.24	48.18	48.24	48.18	48.26	48.27	48.28	48.19	48.22	48.19	48.15	48.2
T04	48.26	48.28	48.17	48.53	48.26	48.34	48.25	48.34	48.21	48.23	48.26	48.36	48.3
T05	48.26	48.33	48.26	48.38	48.3	48.47	48.25	48.3	48.23	48.3	48.28	48.33	48.3

Figure 3.10: Thickness at different locations [7]

The initial inspection of the samples showed some fabrication defects associated with the lamination and drilling processes. These are reflected in damage to the borehole wall, and air bubbles in the lamination, close to the borehole (Figure 3.11).

a) T01-TH: L   b) T01-BH: L + B

c) T02-TH: L   d) T02-BH: L

e) T03-TH: L + B   f) T03-BH: L + B

g) T04-TH: L   h) T04-BH: L

i) T05-TH: L+B   j) T04-BH: L+B
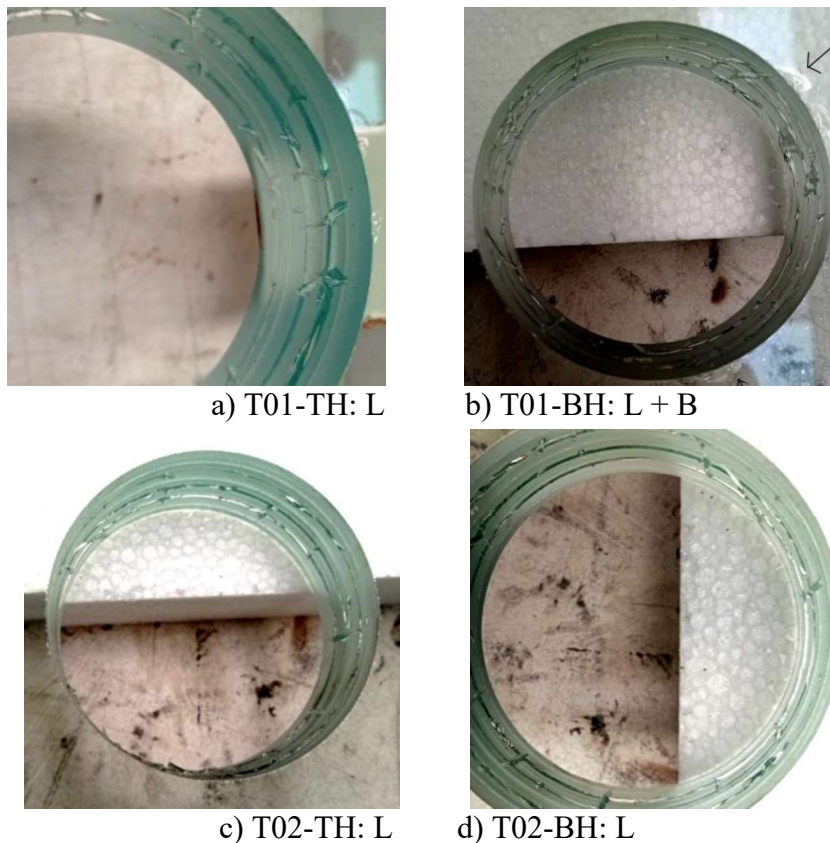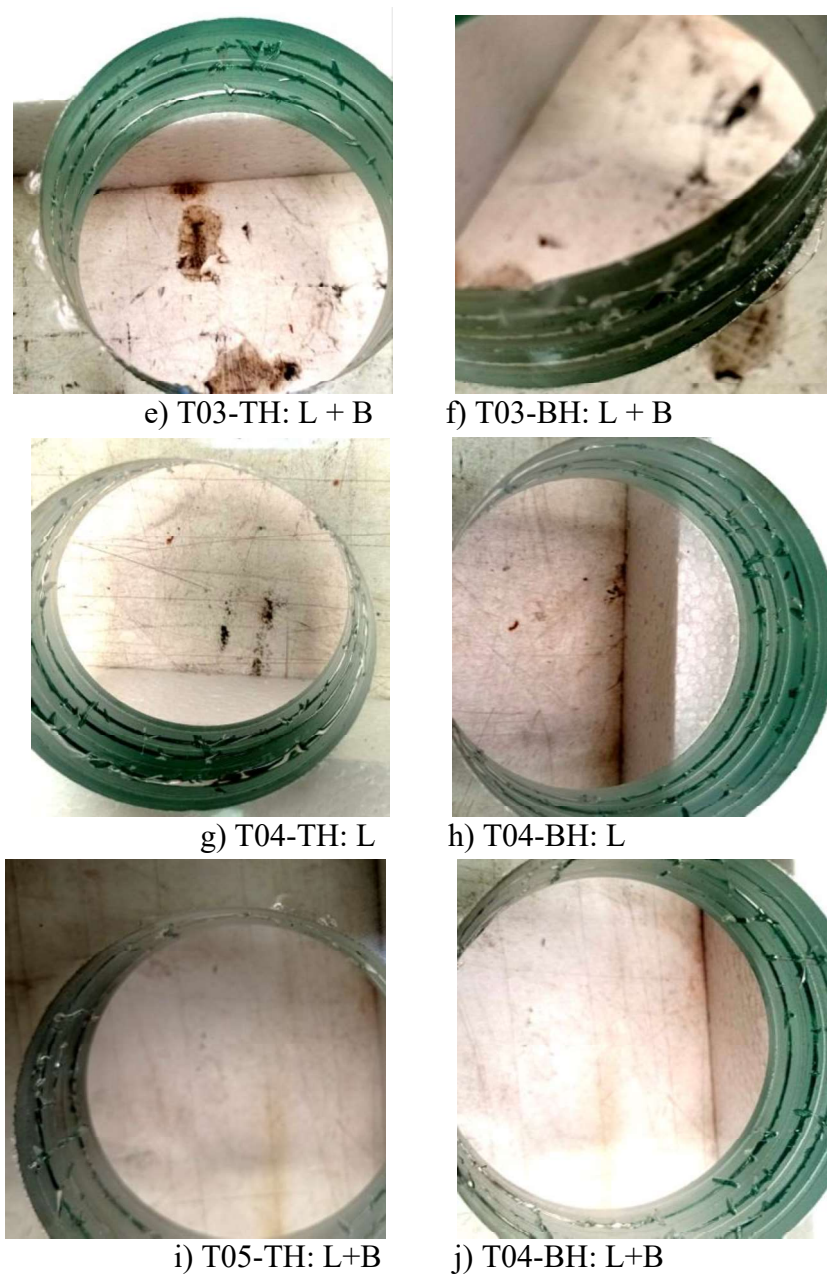
Figure 3.11: Defects of production of the laminated glass samples [7]
TH (Top hole), BH (Bottom hole), L (Lamination defect), B (Border defect)

The preparation of the borehole (Figure 3.12) was finalised with the application of a specialised 2 component grout (HILTI HY270). The grout fills the gap between the stainless bolt sleeve and the glass (15mm), on a total volume of 148,7 cm^3 per cavity. The application followed the instructions of the producer [13] and was overseed by an engineer from HILTY company. The curing time was 45 min at room temperature (approx. 22ºC). The specimens were stored and protected for 7 days before the tests.

Figure 3.12 – Details regarding the grout application [7]

3.3 Instrumentation

The aim of the instrumentation was to characterize the deformability and strain distribution in key locations throughout the samples. This information will assist the characterisation of the structural behaviour of the samples and yield values for comparison with the foreseen numerical model.

The instrumentation with displacement transducers aims to characterize the vertical displacement of the samples, which is mostly related with the deformation at the boreholes. The universal machine measures the vertical displacement; however, these values include the slipping of the forks in the claws, and initial adjustment displacements. For these reasons, two displacement transducers were used to assess the displacement of the samples in the direction of the load (Figure 3.13). The transducer on the right measures the absolute displacement of the sample, and the transducer on the left measures the absolute displacement of the bottom fork. Auxiliary PVC "L" plates were used as stops for the transducers.
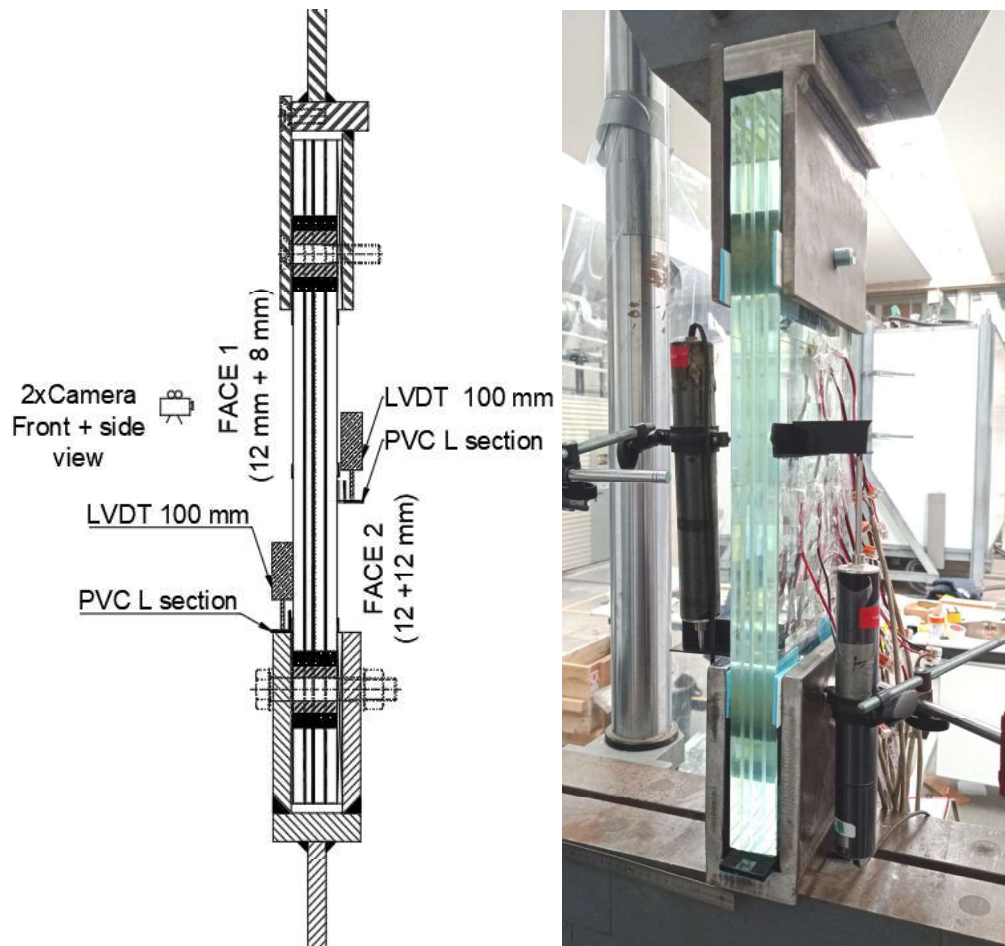
Figure 3.13: Longitudinal transducers layout [7]

The instrumentation with strain gauges (Fig. 3.14 and 3.15) aims to access the strain in the direction of the force, the approximate value of the axial force, provide information in the vicinity of the bolt, and establish whether there is symmetry in the plane of the sample and on the vertical plane orthogonal to the sample.

The longitudinal strains in the direction of the force, are provided by the strain gauges aligned with the bolts.

The approximate value of the axial force in the sample can be calculated from the readings in the vertical strain gauges at mid-hight. These strain gauges also provide information about the shear leg effect.

The strain state in the vicinity of the bolts, is assessed by means of a multidirectional strain gauge (rosette) given the fact that the strain field is disturbed the principal directions are unknown. Ideally a higher number of rosettes should have been foreseen, but this was not possible due to the presence of the fork plates.

To assess symmetry, strain gauges were used in both faces of the samples, and in symmetrical positions at the mid-hight line. The information regarding the eventual asymmetry is particularly important for the correct interpretation of the experimental results and for the calibration of the numerical models.
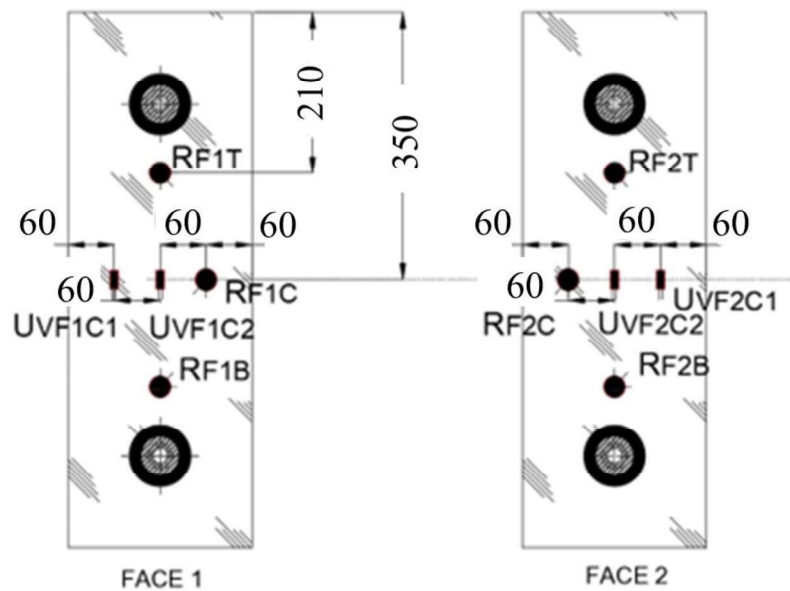
Figure 3.14 – Layout of strain gauges and rosettes [7]
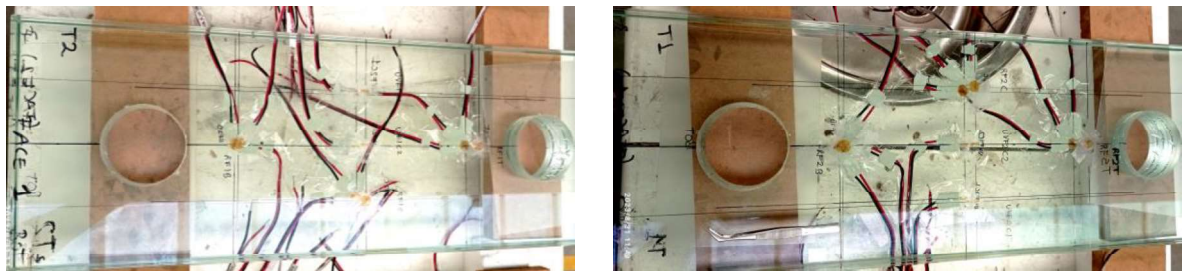
Figure 3.15: Instrumentation with strain gauges and rosettes [7]

3.4 Experimental tests

The first part of the test corresponds to the positioning of the samples in the universal machine. The operation is challenging as the connections of the strain gauges are fragile and the cables are difficult to handle, plus, contact between the glass and metal must be subtle. The detachable part of the upper fork and shims facilitated the operation. After initial positioning, the samples where carefully aligned and held in place with additional shim elements which, on turn, also help preventing harsh contact between the glass and steel. Finally, the cables where connected to the data logger and all the equipment where initialised. Figure 3.16 presents an overview of initial operations and global test apparatus.

Figure 3.16: Positioning of the samples and test apparatus [7]

The load was monotonic, applied in displacement control. The initial displacement rate started as 1 mm/min until at least 2 piles reached failure. After that, the displacement rate was increased to 6 mm/min until the complete separation of the sample. This second part of the test aimed to study the post fracture behavior of the specimens up to complete failure.

3.5 Results

In Figure 3.18 the load *vs* time curves are presented. On the vertical axis is presented the load in [kN] registered on the UTM, and on the horizontal axis the time in minutes of the duration of the test.

Three main performance levels are identified for the first loading phase:

- **1C:** Identifies the first crack during the test. Corresponds to the first crack sound. At this moment there was a small disturbance of the load without load drop. No collapse of any sheet was registered/ observed. The load continued to increase at the initial displacement rate. Identified with a yellow circle.

- **1PF:** Identifies the first breakage of a glass ply during the test. A small disturbance of the load with a drop less than 1.5% was registered. Identified with a yellow rectangle.

- **F:** identifies the fracture of two or all plies on the panel. It identifies the maximum load achieved before a sudden drop of load with more than 5% in relation to the maximum magnitude achieved. After this stage the displacement rate was increase to 6 [mm/min], to study the capacity to sustained load after the sudden breakage of the plies. Identified with a red cross.
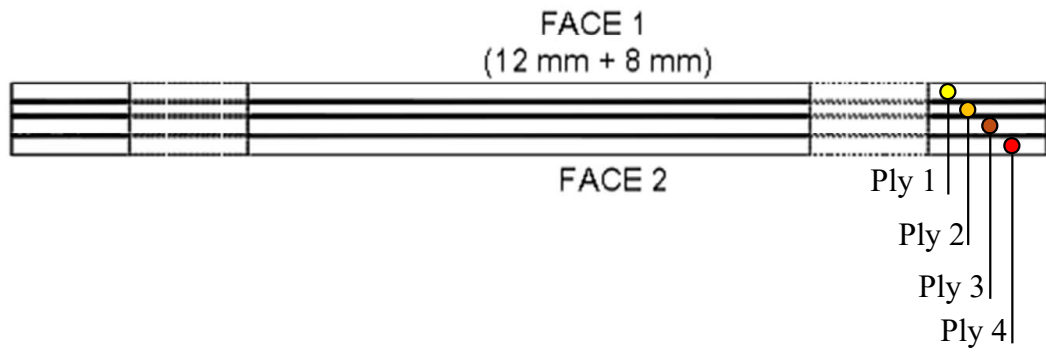
Figure 3.17: Identification of the glass plies in the laminated sample
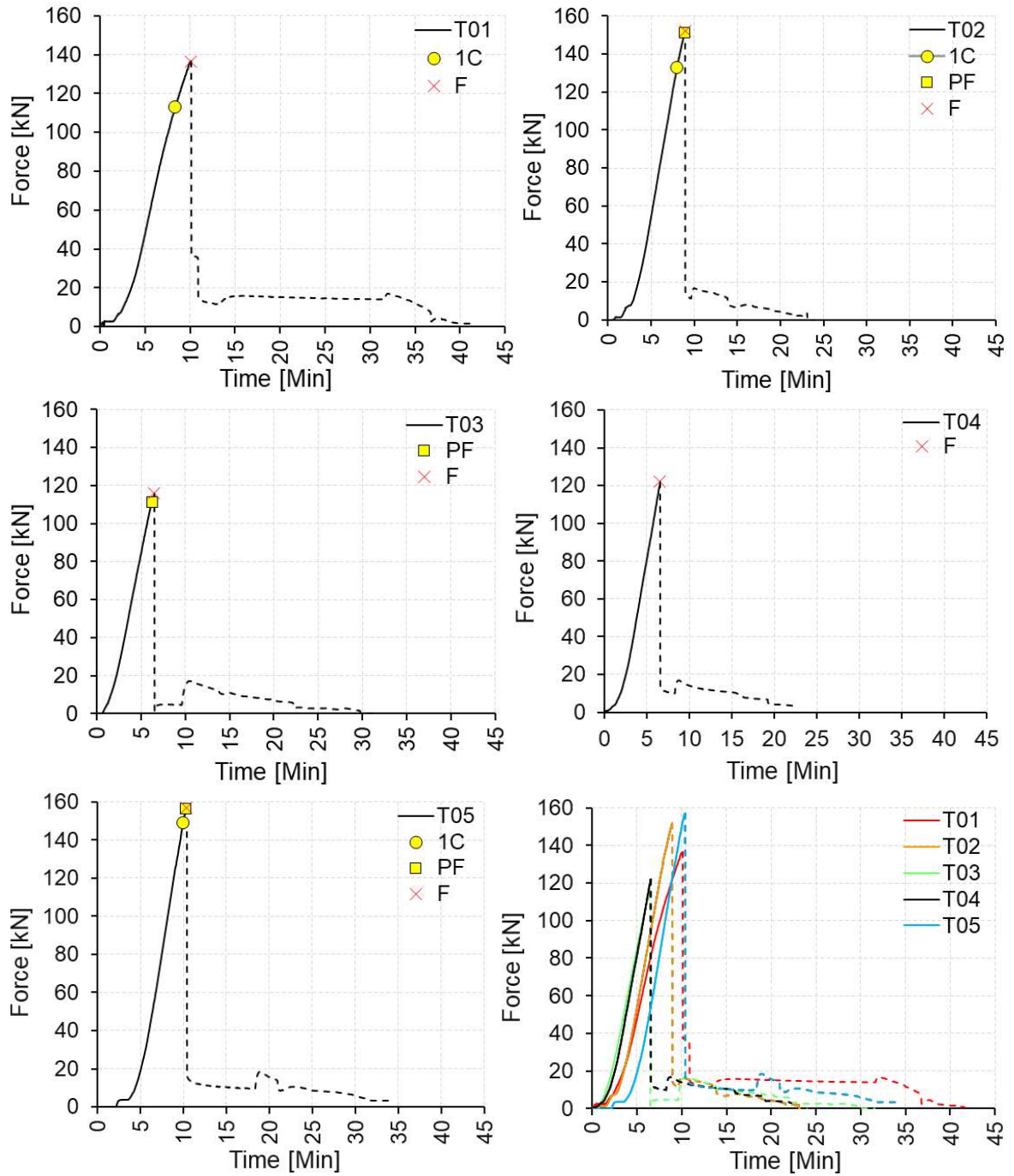
Figure 3.18: Load-time curves

State	Time [min]	Force UTM K[N]	LVDT -Steel [mm]	LVDT-Glass [mm]	Observation
T01-1C	8.35	113.27	6.830	4.390	1st crack
T01-F	10.12	**136.48**	8.290	5.610	Breakage of all plies - top section
T02-1C	7.98	133.10	6.30	-3.43	1st crack
T02-1PF	8.90	151.39	7.07	-3.94	Breakage 3rd ply - top section
T02-F	8.93	**152.01**	7.13	-4.01	Breakage of all plies - top section
T03-1PF	6.28	111.52	4.82	2.87	Breakage 1st ply - bottom section
T03-F	6.48	**115.84**	5.10	1.49	Breakage of all plies - bottom section
T04-F	6.53	**122.00**	5.41	2.67	Breakage of all plies - bottom section
T05-1C	9.97	149.02	6.7	4.11	1st crack
T05-1PF	10.28	156.24	6.97	4.3	Breakage 3rd ply - top section
T05-F	10.38	**157.12**	7.04	4.38	Breakage of all plies -top section

Table 3.2: Description of specimens and test conditions
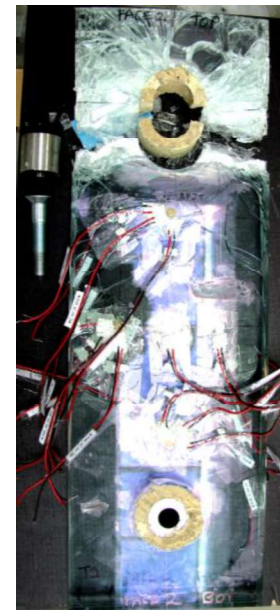
a) Collapse of the 1st ply (top)   b) Collapse three plies (bottom)   c) Specimen after test

Figure 3.19: Progressive failure of the sample (T-01)
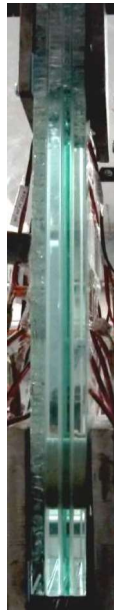
a) Collapse of the 1st ply (top)   b) Collapse three plies (bottom)   c) Specimen after test

Figure 3.20: Progressive failure of the sample (T-02)

a) Collapse of the 1st ply (bottom)   b) Collapse all plies   c) Specimen after test
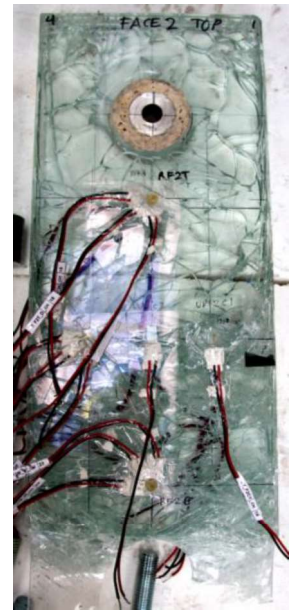
Figure 3.21: Progressive failure of the sample (T-03)

a) Collapse all plies   b) Collapse all plies   c) Specimen after test
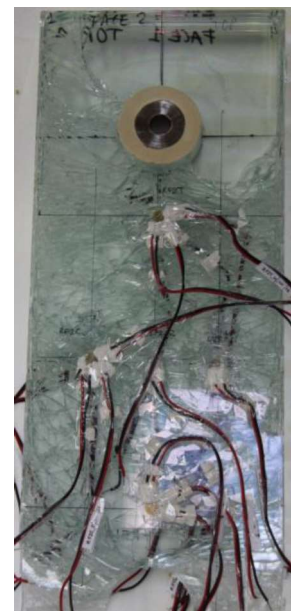
Figure 3.22: Progressive failure of the sample (T-04)
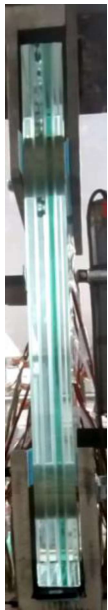
a) Collapse of the 1st ply (top)   b) Collapse 3 plies (top)   c) Specimen after test

Figure 3.23: Progressive failure of the sample (T-05)

In Figure 3.24 the load vs displacement curves are presented. The position of the LVDTs is describe in Figure 3.24. *LVDT Steel*, with red continuous line, registered the vertical displacement on the steel clamps; and *LVDT glass,* with blue continuous line, registered the vertical displacement on the surface of specimen using PVC - L section glued onto the glass surface.
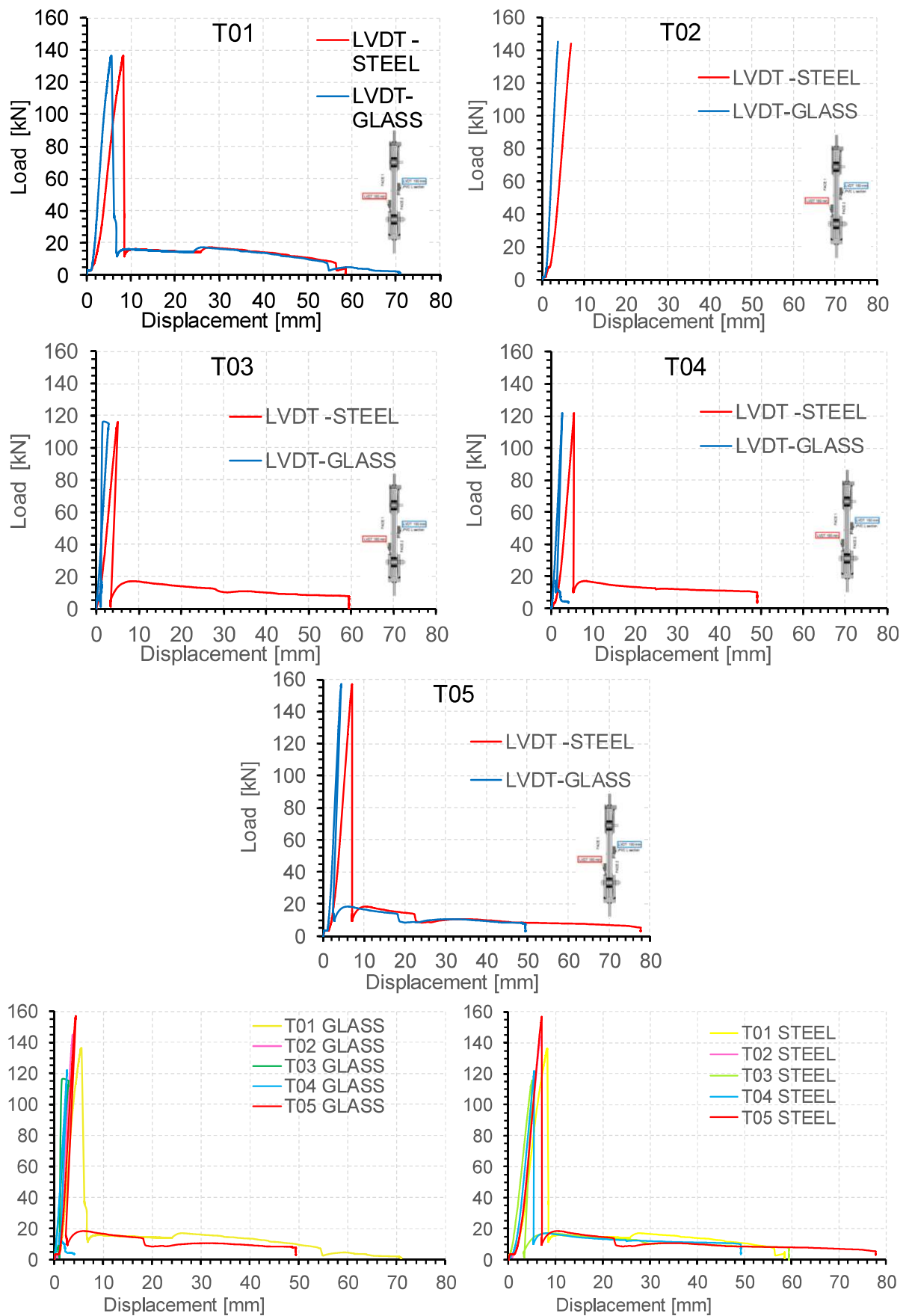
Figure 3.24 Load/Displacement curves T01-T05

The results from LVDT steel represent the displacement that is applied to the sample by the UTM machine, minus the slip at claws. The results from LVDT glass correspond to LVDT steel plus de deformability at the borehole, which is mainly related with the damage to the

grout. Both curves feature an initial irregularity and a small plateau, which are related with expected dislocations until full bearing is established at the boreholes. Once full bearing is reached, both curves exhibit a linear response with identical stiffness, per type.

The nominal strains are presented along lines L1-L1' and L2-L2' in Figure 3.25, at the location of each strain gauge/rosette. The main results are presented for vertical strains ε_y for specific load levels (Fig). In Figures 3.27 to Figure 3.31 the continuous lines correspond to the strain gauges/rosettes for *Face 1* and the dotted lines for strain gauges and rosettes on *Face 2*. The results are presented until the maximum load registered by the UTM, this point was defined before the load drop more than 5%.

The designation for the labels of the rosettes and uni-directional strain gauges depicted in Figure 3.25 is describe in Table 3.3
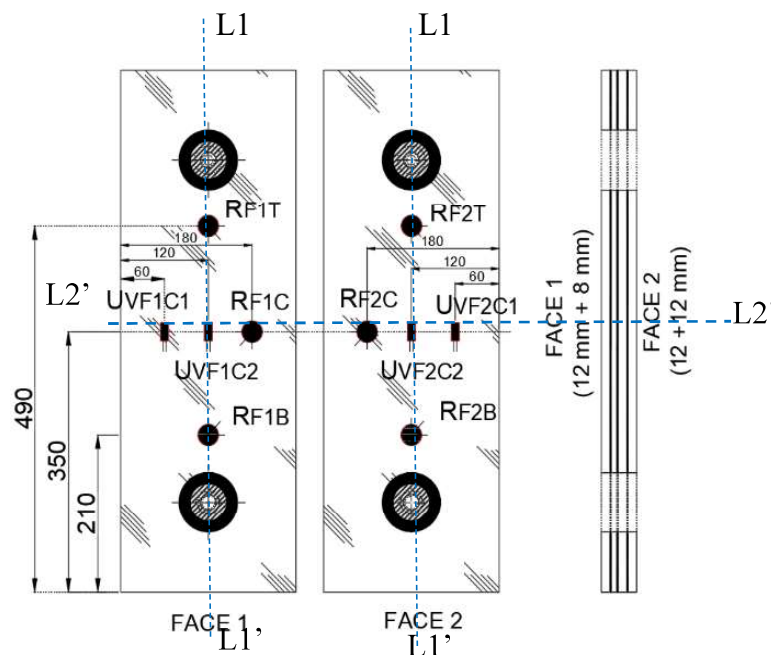
Figure 3.25: Auxiliary lines to establish the vertical strain variations

38
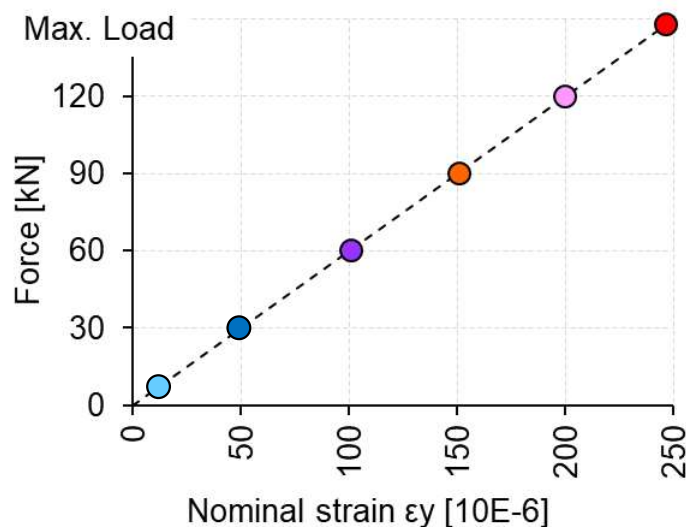
Figure 3.26: Discrete load levels

UV_F#C1:	Unidirectional strain gauge-vertical direction, located at the middle section of the specimen
UV_F#C2:	Unidirectional strain gauge- vertical direction, located at the center of the specimen
RF# Location_Direction:	3-Directional Rosette for: H: Horizontal direction gauge. V: Vertical direction gauge. D: Diagonal direction gauge. Located at T: Top; C: Center: B Bottom

Table 3.3: Description of strain gauge's labels
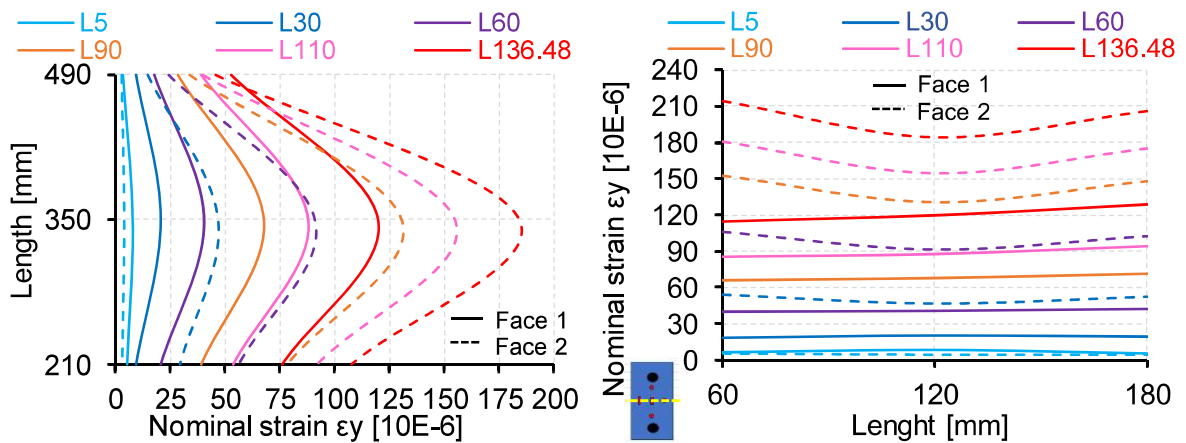
Figure 3.27: T01 Distribution on vertical strain L1-L1' (left) and L2-L2' (right)
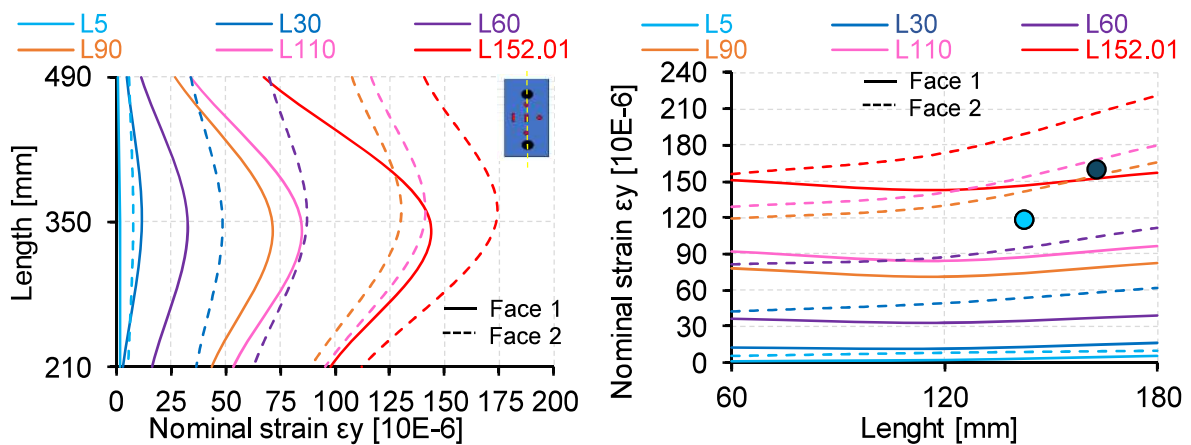
Figure 3.28: T02 Distribution on vertical strain L1-L1' (left) and L2-L2' (right)
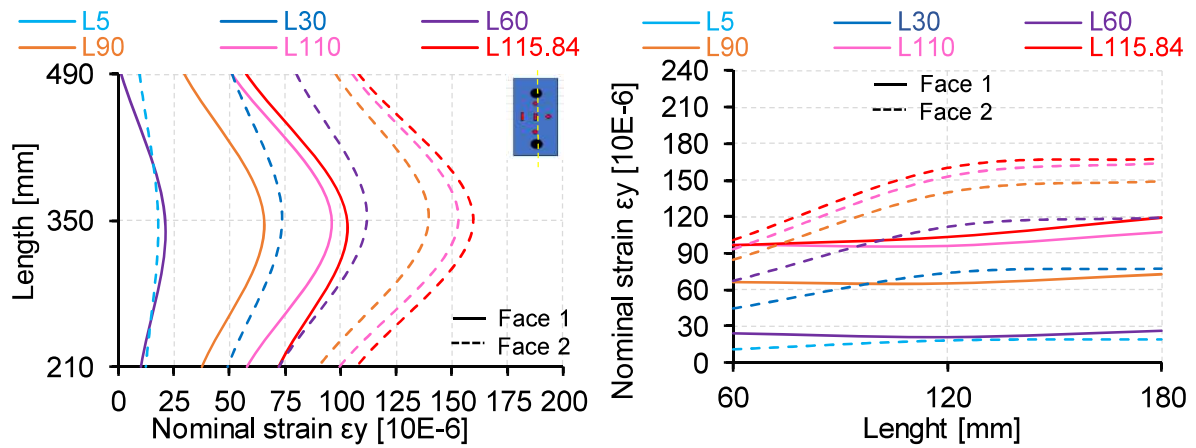
Figure 3.29: T03 Distribution on vertical strain L1-L1' (left) and L2-L2' (right)
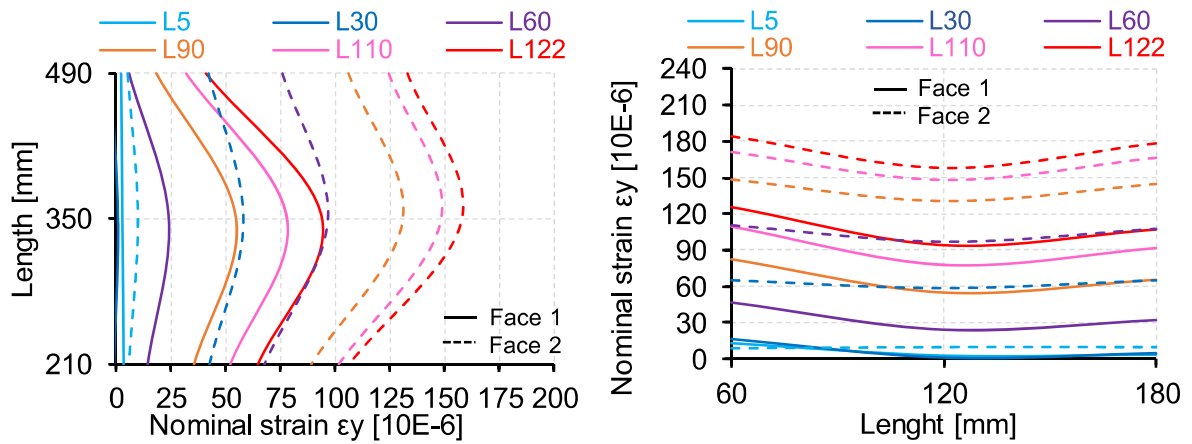
Figure 3.30: T04 Distribution on vertical strain L1-L1' (left) and L2-L2' (right)
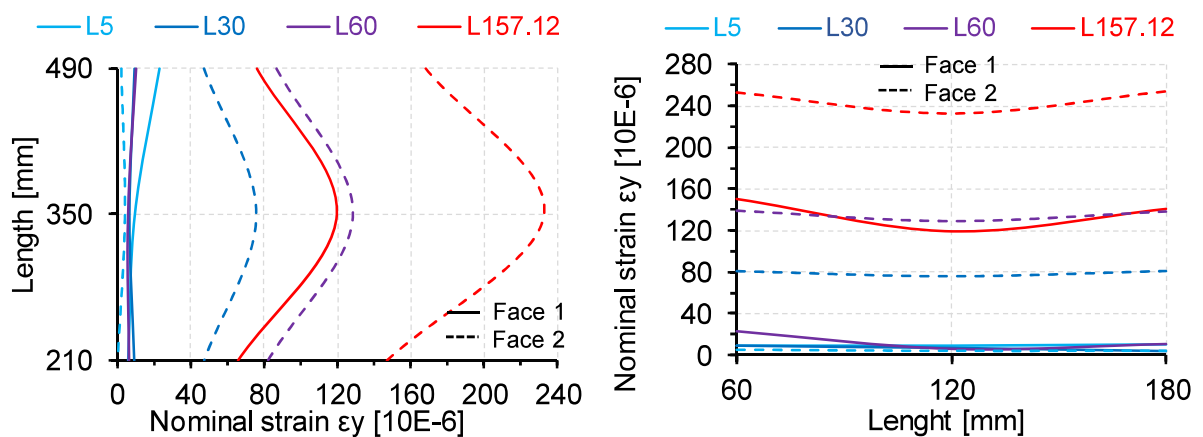
Figure 3.31: T05 Distribution on vertical strain L1-L1' (left) and L2-L2' (right)

The results regarding the vertical strains along the auxiliary vertical line (L1-L1') show higher values at mid high, and lower values close to the bolts. This is as expected, given the distribution of stains close to the vertical diameter of the bolt, which reflects the perturbation of the strain field associated with the bolt hole and the respective bearing stresses (Figure 3.32).
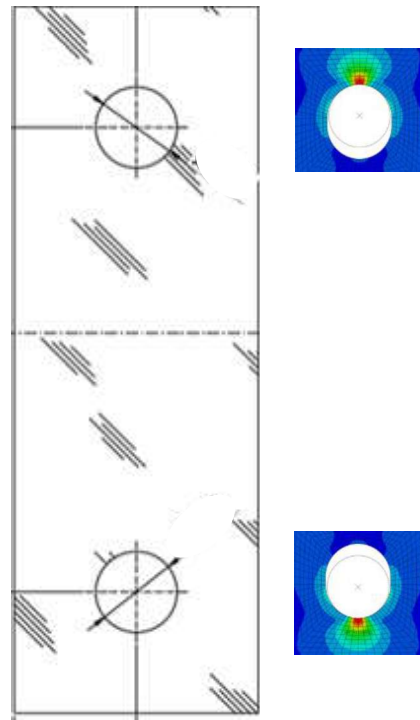
Figure 3.32: Bearing stresses on the glass, in the vicinity of the bolt (top and bottom along the vertical diameter)

The comparison of the vertical strains along the auxiliary vertical line (L1-L1') on Face 1 and Face 2 show significative differences, which increase with the load. This indicates that the samples are subjected to bending along the axes of maximum inertia. This is expected in real structures, and also in tests, due to misalignments of geometry or load. In this particular case, this fact has no bearing on the quality of the results, particularly for the assessment of the design load or for the calibration of the corresponding numerical models.

The results regarding the vertical strains along the auxiliary horizontal line (L2-L2') show higher values at mid width, and lower values close to the vertical edges. This is as expected, given the distribution of stains close to the vertical diameter of the bolt, which reflects the perturbation of the strain field associated with the bolt hole and the respective bearing stresses. Additionally, this may be related with shear lag. Also, in this case, there are differences in the strain values when comparing Face 1 and Face 2, which also indicates a moderate asymmetry.

4 NUMERICAL ANALYSIS

4.1 Introduction

Main part of the master work is numerical analysis of model. First step was 3D model which was made in software AUTOCAD 2022 [14] (Figure 4.1a) based on dimensions taken from experimental samples. Model was made out of single parts (Figure 4.1b): glasses of 12 mm and 8 mm thickness, interlayers of 1,52 mm thickness, steel bolts Ø50 mm and infill material of grout with width of 15mm between end of the glass and bolt to prevent their direct contact. After completing the AUTOCAD step, model was imported in ABAQUS 2021[4] (Figure 4.2) and all parts were formed into one assembly.
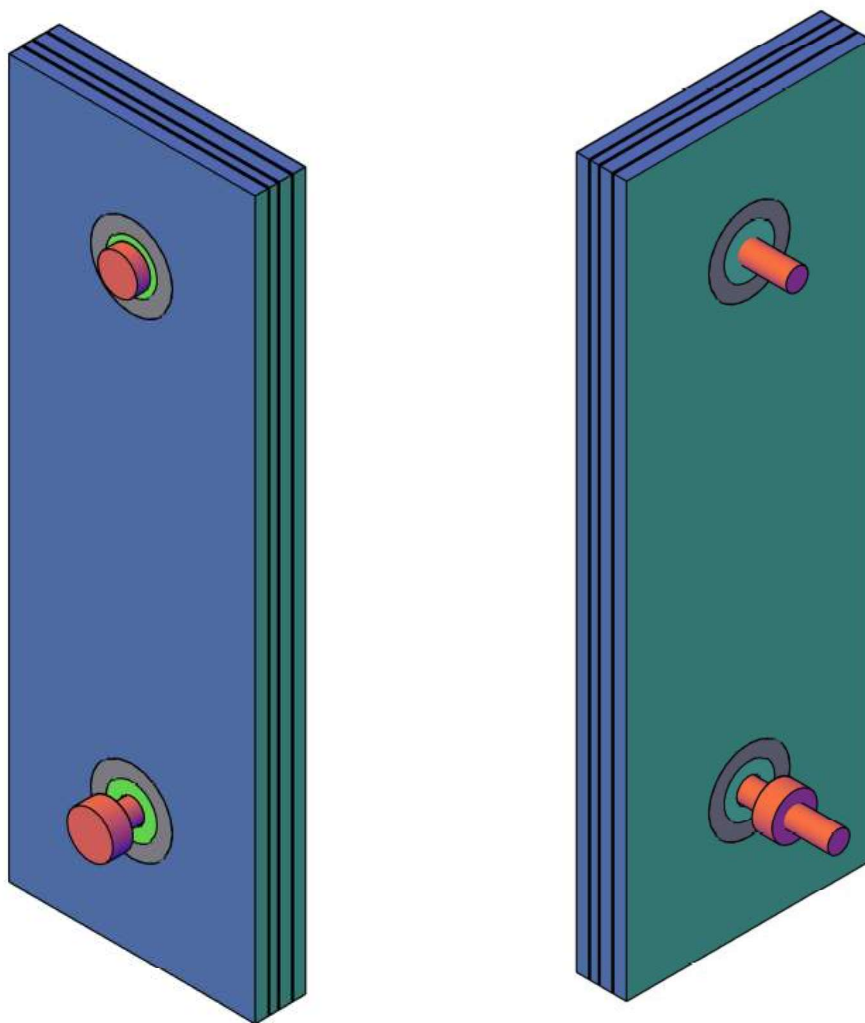
Figure 4.1a: AUTOCAD model Face 1 (left) and Face 2 (right)
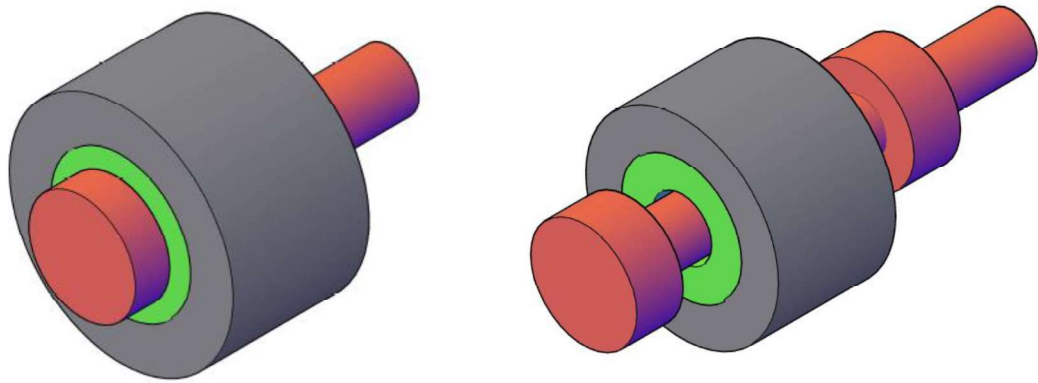
Figure 4.1b – Bolt section top (left) and bottom (right)

Figure 4.2: Model assembly in ABAQUS

4.2 Geometry and mesh

Dimensions of the samples were 240 x 700 x 48,56 mm with two holes - one on top and one on the bottom, of Ø80 mm – centred at 120 mm from each side of the glass end.

Model was meshed as assembly with linear hexahedral elements (Figure 4.3). There were total of 68788 elements with 92847 nodes. Global approximate sizes of the mesh were separated by usage of material:

- Glass and interlayers – 10,0 mm
- Steel and infill material – 2,5 mm
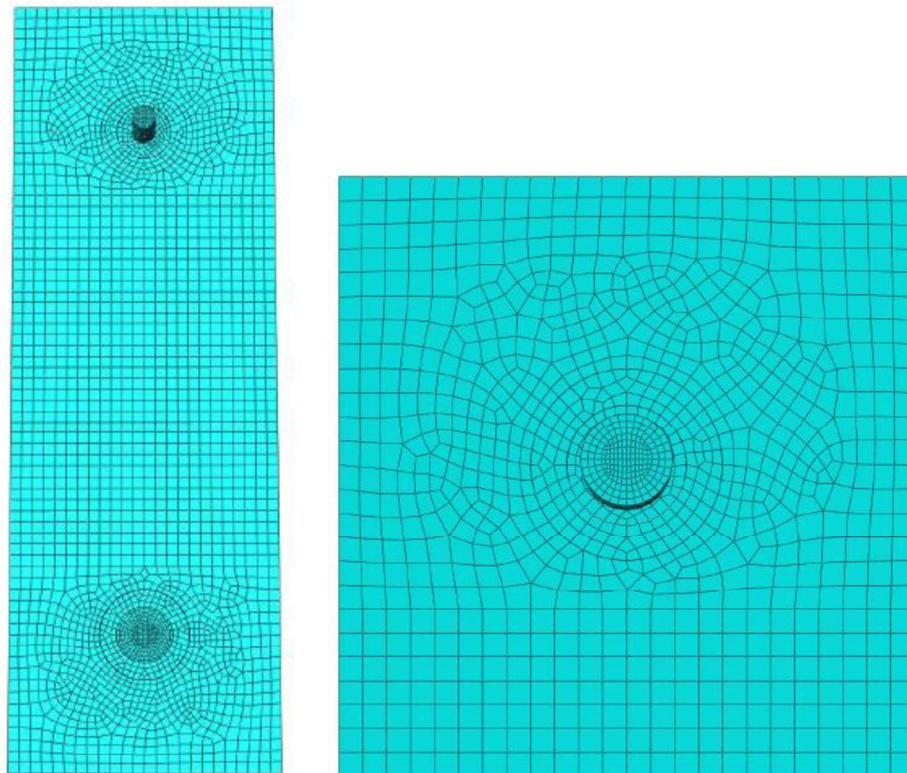
Figure 4.3: Face 2 mesh of the model (left) and top part Face 1 bolted section mesh (right)
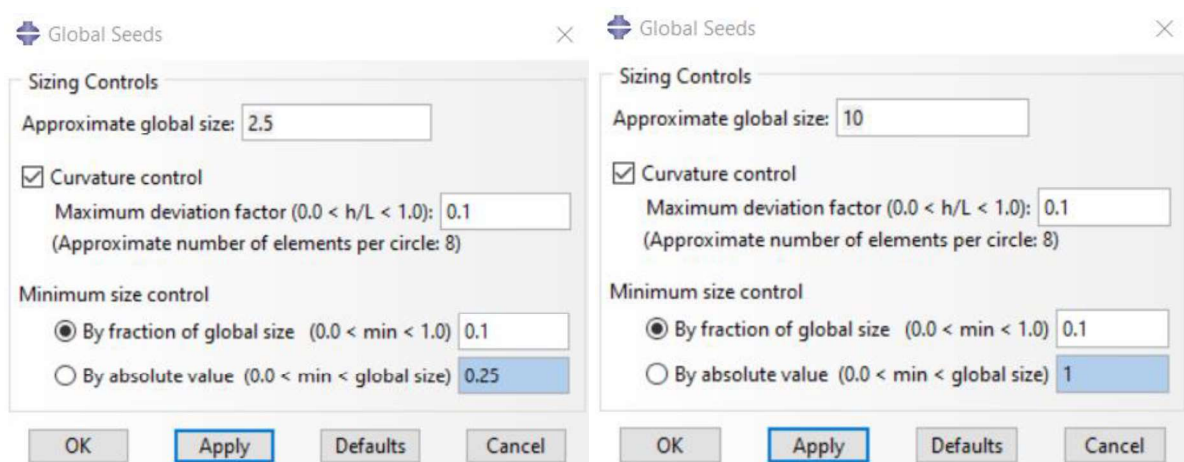
Figure 4.4: Mesh properties of steel/infill material (left) and glass/interlayer (right)

4.3 Material properties

Material properties which were required to identify were: Mass Density, Young's Modulus and Poisson's Ratio. Data of used materials, shown in Table 4.1, came from official product makers: glass [15], interlayer [17], stainless steel [16] and infill grout [13].

MATERIAL	MASS DENSITY	YOUNG'S MODULUS	POISSON'S RATIO
Glass	7,75E-06	70000	0,21
Interlayer	9,50E-07	300	0,45
Infill material	1,66E-06	1700	0,3
Stainless steel	8,00E-07	193000	0,3

Table 4.1: Material properties values

4.4 Analysis settings

After importing parts from AUTOCAD, defining material properties, putting model in assembly and making mesh the next step was to define interaction between surfaces.

Two types of interactions were used: tie contact and surface to surface contact with normal behaviour as "hard" contact and tangential behaviour with friction coefficient of 0,2.
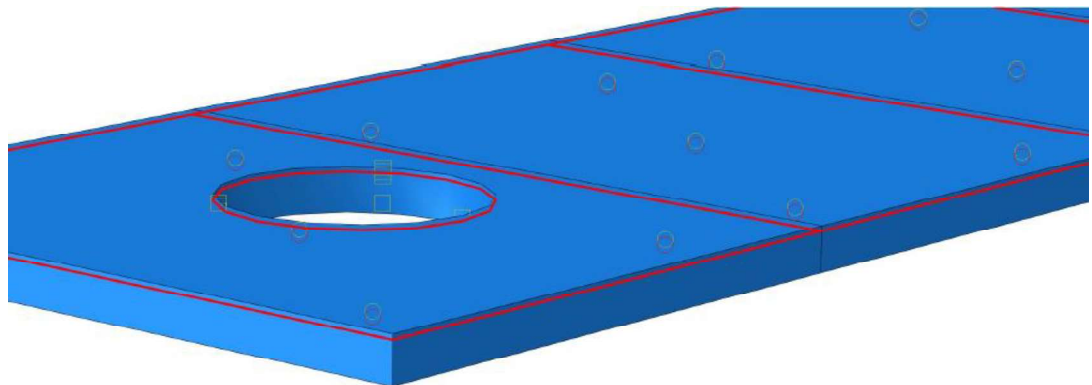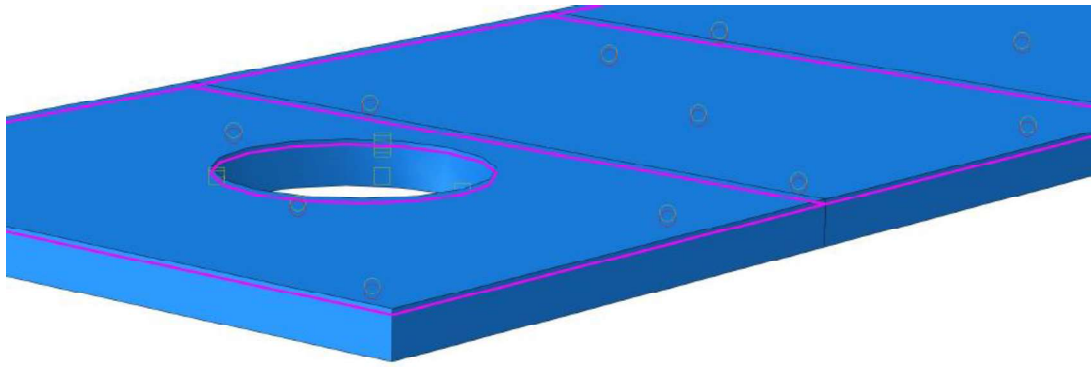
Figure 4.5: Master surface of the glass (top) and slave surface of the interlayer (bot)
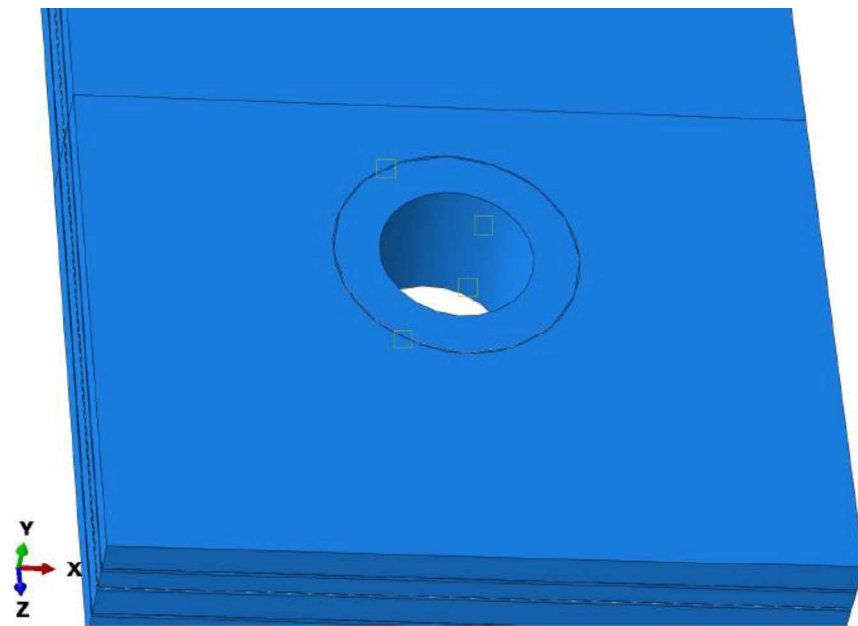
Figure 4.6: Face 1 bottom part
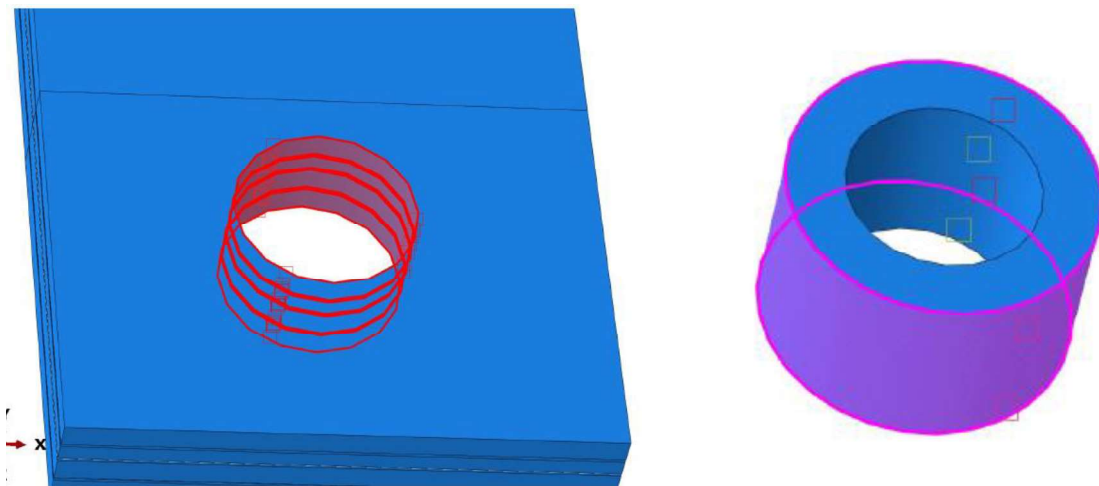
Figure 4.7: Glass/interlayer as master surface (left) and mortar as slave surface (right)
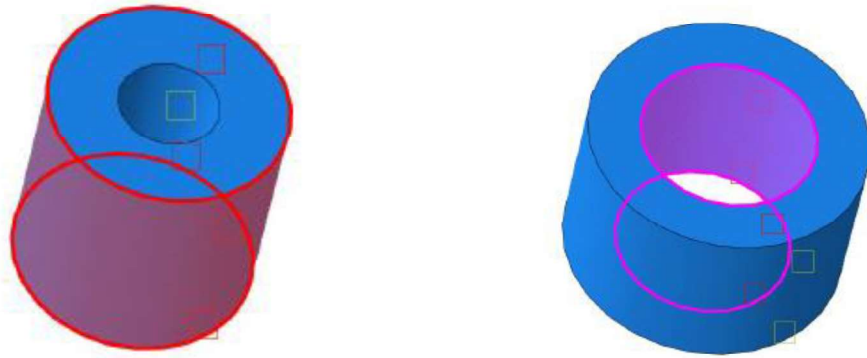
Figure 4.8: Stainless steel as master surface (left) and mortar as slave surface (right)
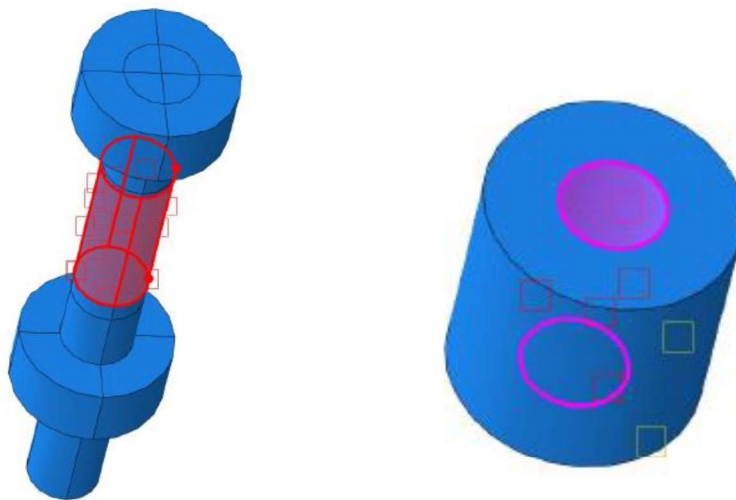
Figure 4.9: Bolt as master surface (left) and stainless steel as slave surface (right)

Second step was to define kinematic coupling surfaces (Figure 4.10) and constrained degrees of freedom in all ways. Reference points were picked in the middle of the glass and offset in Z axis for the distance to the top of the metal clamps in the experiment. Surfaces were chosen on the bolt in thickness of metal clamps; bottom 20mm and top 12mm.
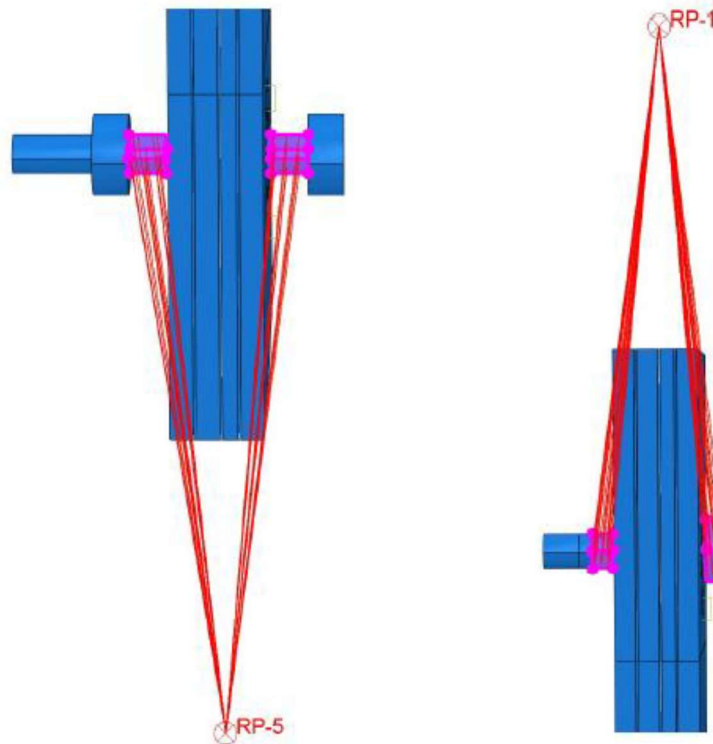
Figure 4.10: Bottom coupling surfaces with reference point (left) and top coupling surfaces with reference point(right)

Third step was to define boundary conditions through reference points. There were two types: initial boundary condition and boundary condition of the load. Load was applied in Z axis and all other rotations and translations were blocked.

Values of degrees of freedom are shown in Table 4.2.

CSYS	BOTTOM INITIAL	BOTTOM LOAD	TOP INITIAL	TOP LOAD
U1	0	0	0	0
U2	0	0	0	0
U3	0	0	-	3
UR1	0	0	0	0
UR2	0	0	0	0
UR3	0	0	0	0

Table 4.2: Boundary condition degree of freedoms values

Last step before running the analysis was to define step manager of load. Analysis was defined as general static. Properties of step are shown below in Table 4.3.

PROCEDURE	TIME PERIOD	INITIAL INCREMENT	MIN. INCREMENT	MAX. INCREMENT
STATIC,GENERAL	10	0,01	1,00E-10	0,1

Table 4.3: Step properties of load

As the numerical model is completely elastic, the onset of failure was set from the nominal resistance of each material and information from the experimental tests. For glass a value of 100-120 kN was used, whereas for the mortar, according to technical data from producer, a maximum compression strength of 65 MPa was used.

4.5 Results

Results were show in 105 increments and step time of 10. The numerical results are presented in following sections.

4.5.1 Load displacement curve

In Figure 4.11 the load vs displacement curve is presented. On the vertical axis is presented the load [kN] and on the horizontal axis the vertical displacement [mm] in the duration of the analysis.
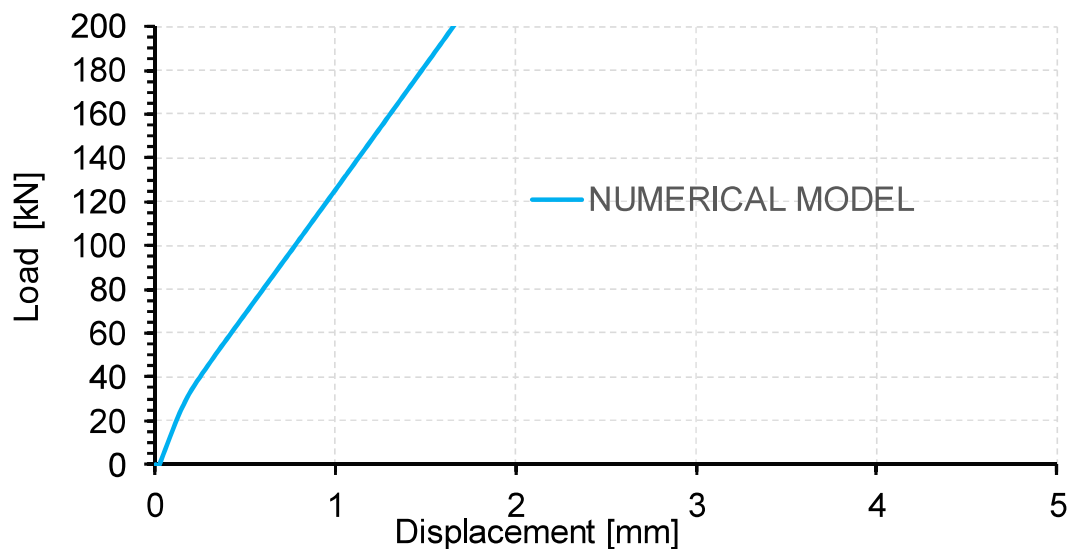
Figure 4.11: Load displacement curve of numerical model

The global behavior curve is mainly elastic, from a load of around 25 kN to failure, where the behavior of the laminated glass governs. In the initial part the stiffness is different as full bearing is still being achieved, due to the presence of the grout.

4.5.2 Nominal strain

The results are presented along lines L1-L1' and L2-L2' in Figure 4.12, at the location of each strain gauge/rosette. The main results are presented for vertical strains εz. For a better understanding of the results, five load rates are studied same as in experimental analysis, corresponding to 5 kN, 30 kN, 60 kN, 90 kN, 110 kN. In Figures 12 to Figure 16 the continuous lines correspond to the strain gauges/rosettes for Face 1 (Figure 4.13), and the dotted lines for strain gauges and rosettes on Face 2 (Figure 4.14).
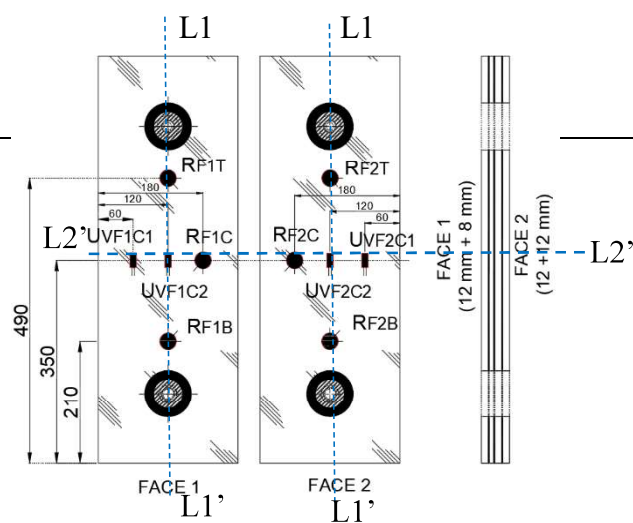
Figure 4.12: Positioning of Lines L1-L1' and L2-L2'
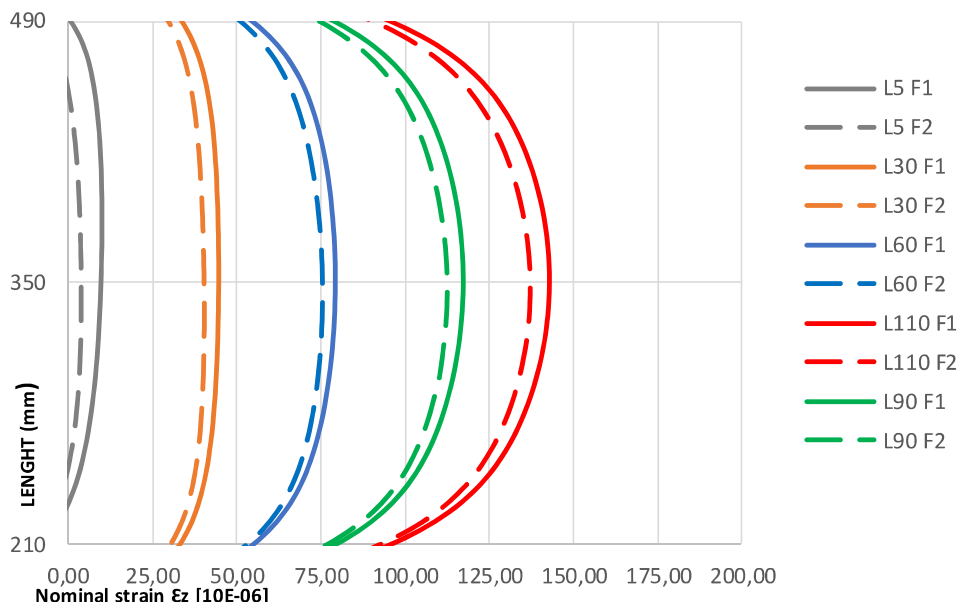
Figure 4.13: Results for numerical analysis L1-L1' line

The plots of the vertical strain along line L1-L1', for the reference load levels, show some small difference between the results for Face 1 and 2, which indicates that there is some asymmetry that causes bending around the major inertia axis. This may be due to the geometry of the bolts and nuts. The results also show some asymmetry between top and bottom sections, which may be due to the same factor or to the differences in the top and bottom meshes around the boreholes. Equivalent effects are visible in the plots of the vertical strain along line L2-L2', in Figure 4.14
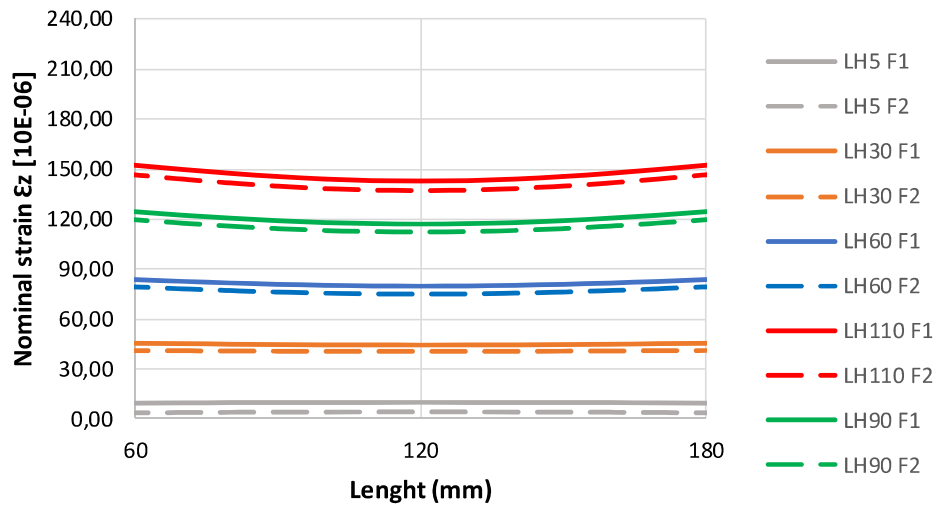
Figure 4.14: Results for numerical analysis L2-L2' line

4.5.3 Mortar and glass behavior

From Figure 4.15 to 4.22 are presented minimal principal stress values for mortar at both top and bottom section through the steps of load value 0 kN, 5 kN, 30 kN, 60 kN, 90 kN, 110 kN and 120 kN.
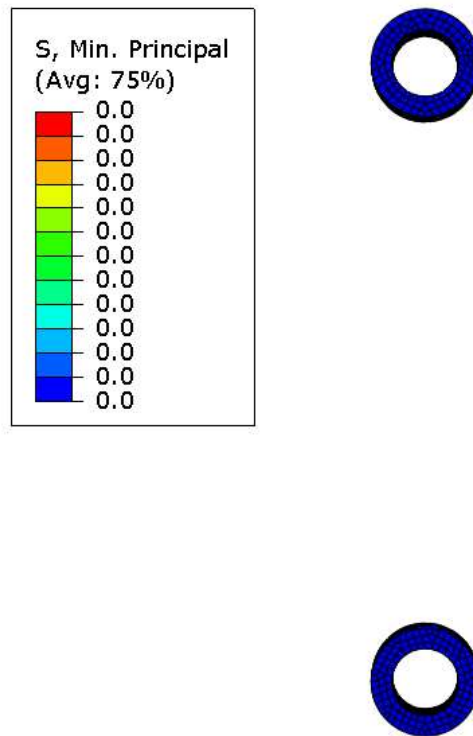
Figure 4.15: Step 0 – applied load of 0 kN
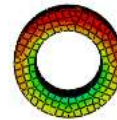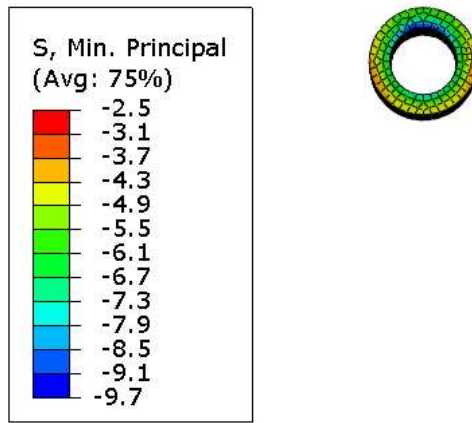
Figure 4.16: Step 6 – applied load of 5 kN
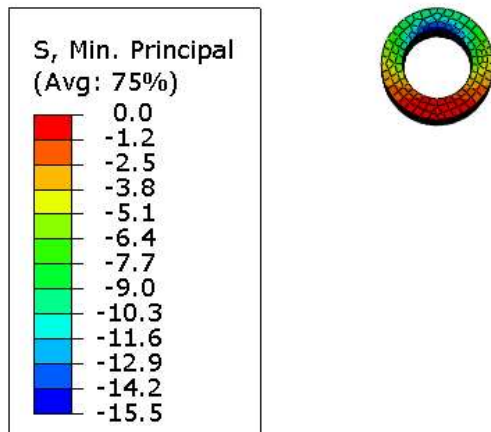
Figure 4.17: Step 11 – applied load of 30 kN
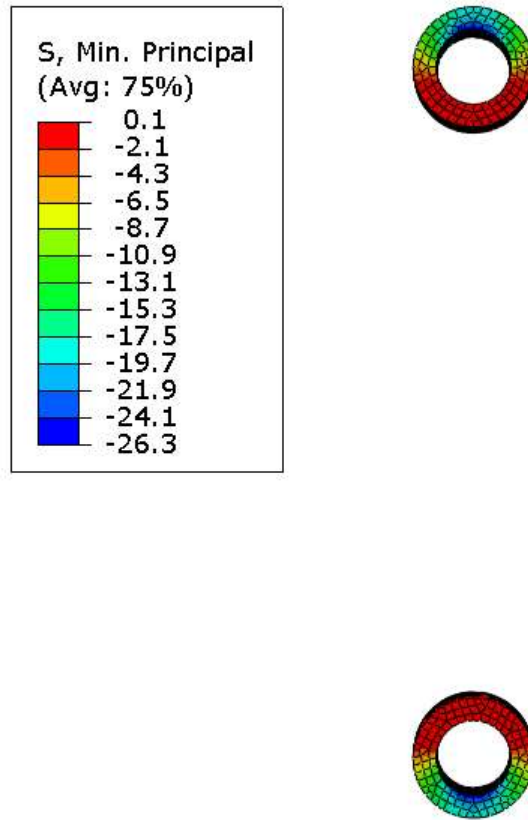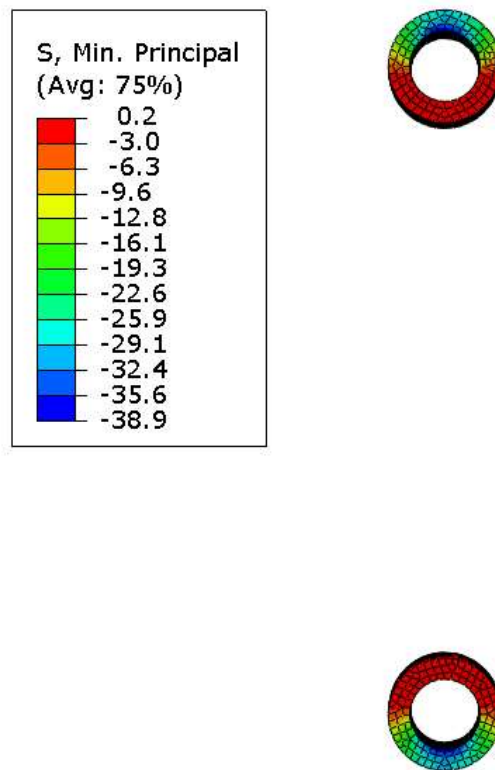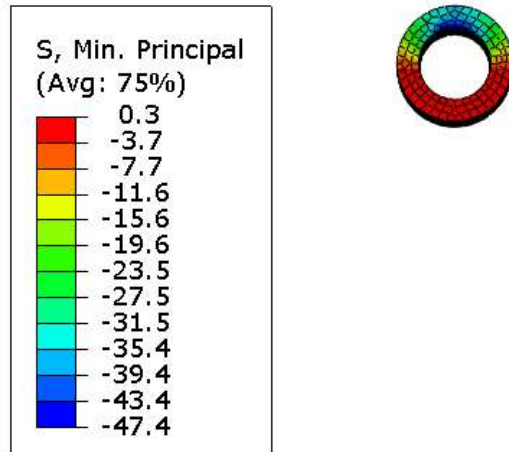
Figure 4.18: Step 19 – applied load of 60 kN

Figure 4.19: Step 28 – applied load of 90 kN
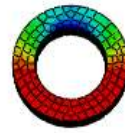
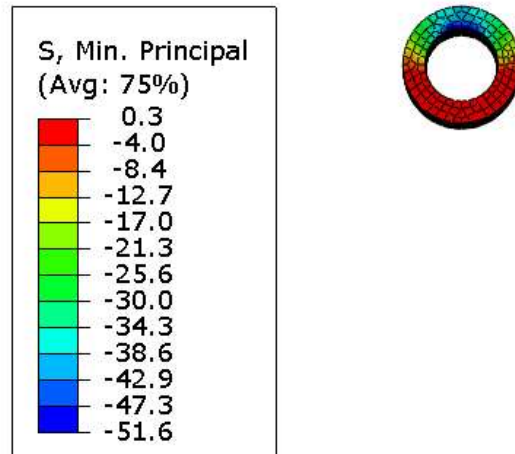**Figure 4.20:** Step 34 – applied load of 110 kN
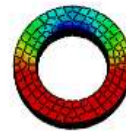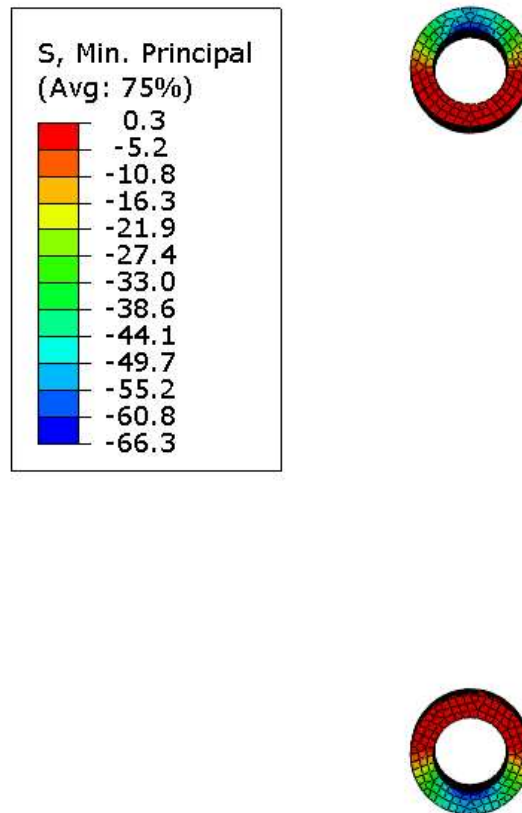

Figure 4.21: Step 37 – applied load of 120 kN

Figure 4.22: Step 47 – applied load of 156 kN

The stress counters are consistent with the load transfer in the samples. Figure 4.22 is established for the time step where the grout reaches its nominal resistance.

From Figure 4.23 to 4.30 are presented minimal principal stress values for glass on Face 1 and Face 2 through the steps of load value 0 kN, 5 kN, 30 kN, 60 kN, 90 kN, 110 kN and 120 kN.
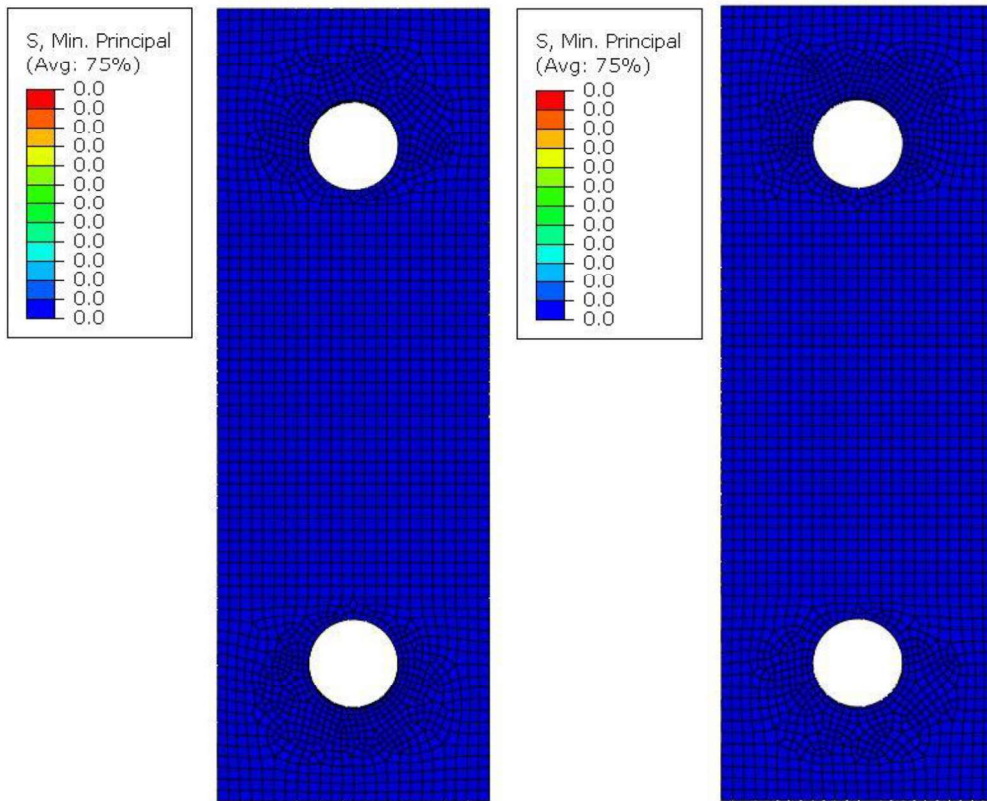
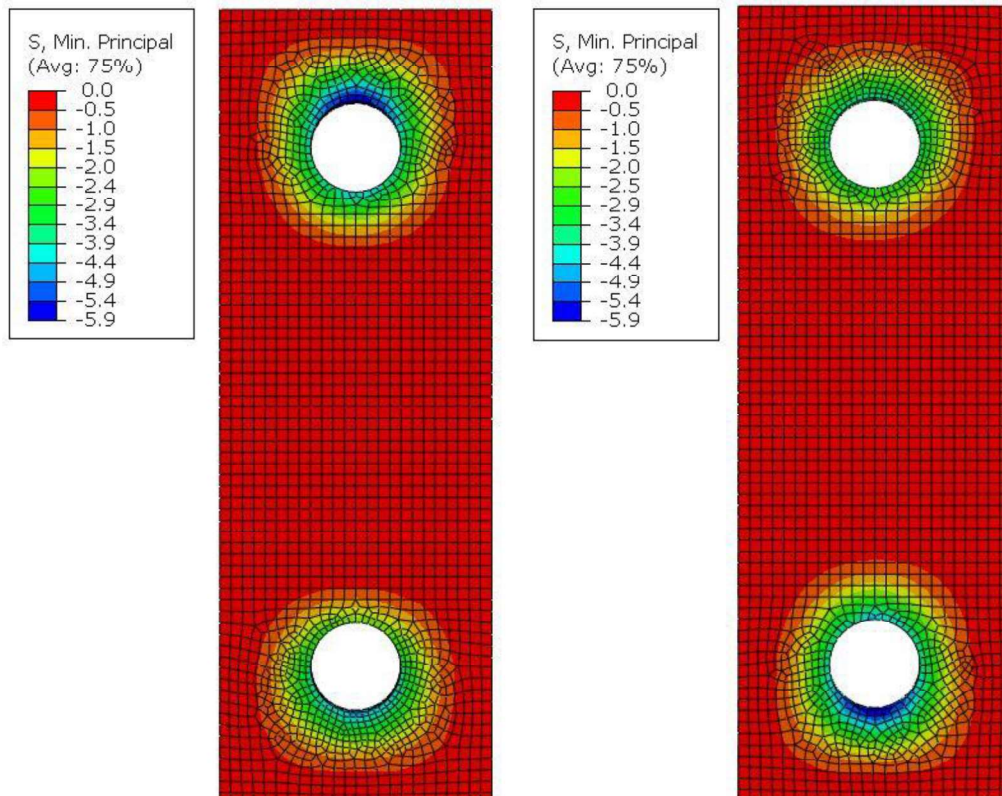**Figure 4.23:** Step 0 – applied load of 0 kN (Face 1 left side, Face 2 right side)

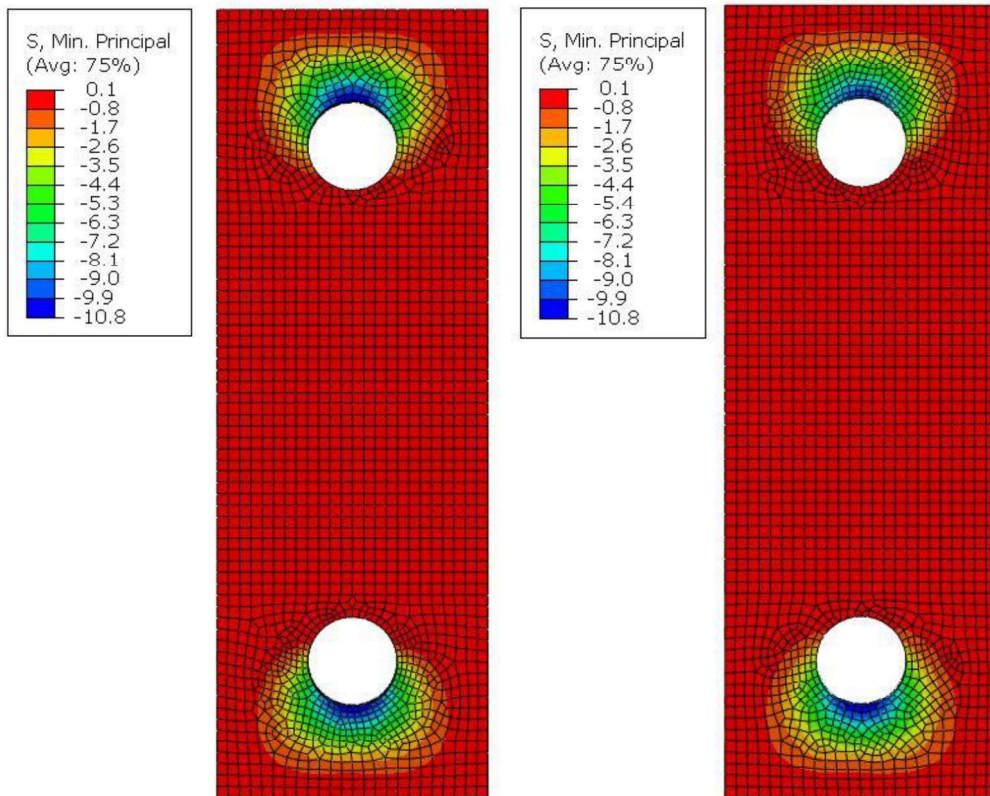**Figure 4.24:** Step 6 – applied load of 5 kN (Face 1 left side, Face 2 right side)

Figure 4.25: Step 11 – applied load of 30 kN (Face 1 left side, Face 2 right side)
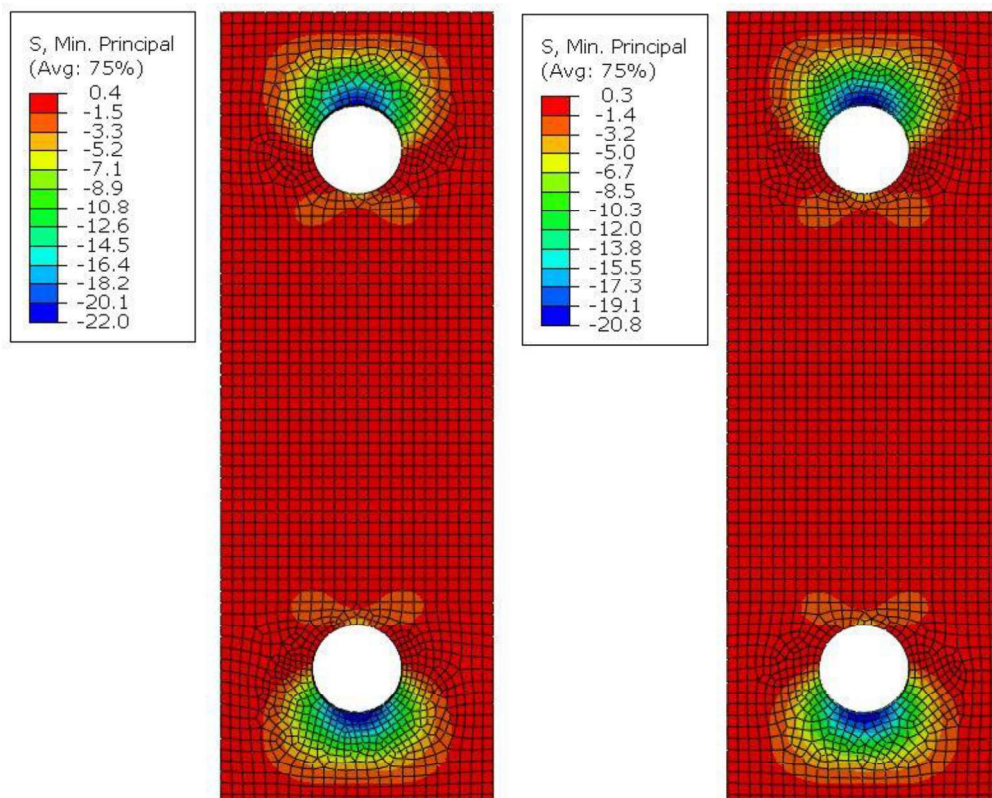

Figure 4.26: Step 19 – applied load of 60 kN (Face 1 left side, Face 2 right side)
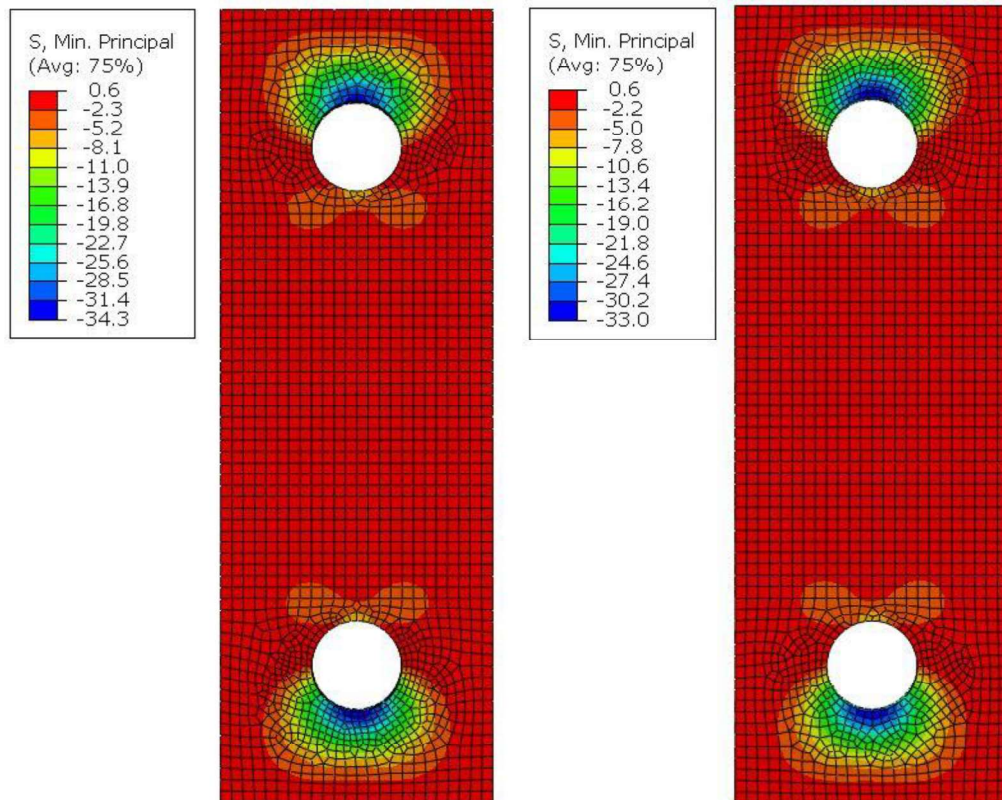
Figure 4.27: Step 28 – applied load of 90 kN (Face 1 left side, Face 2 right side)
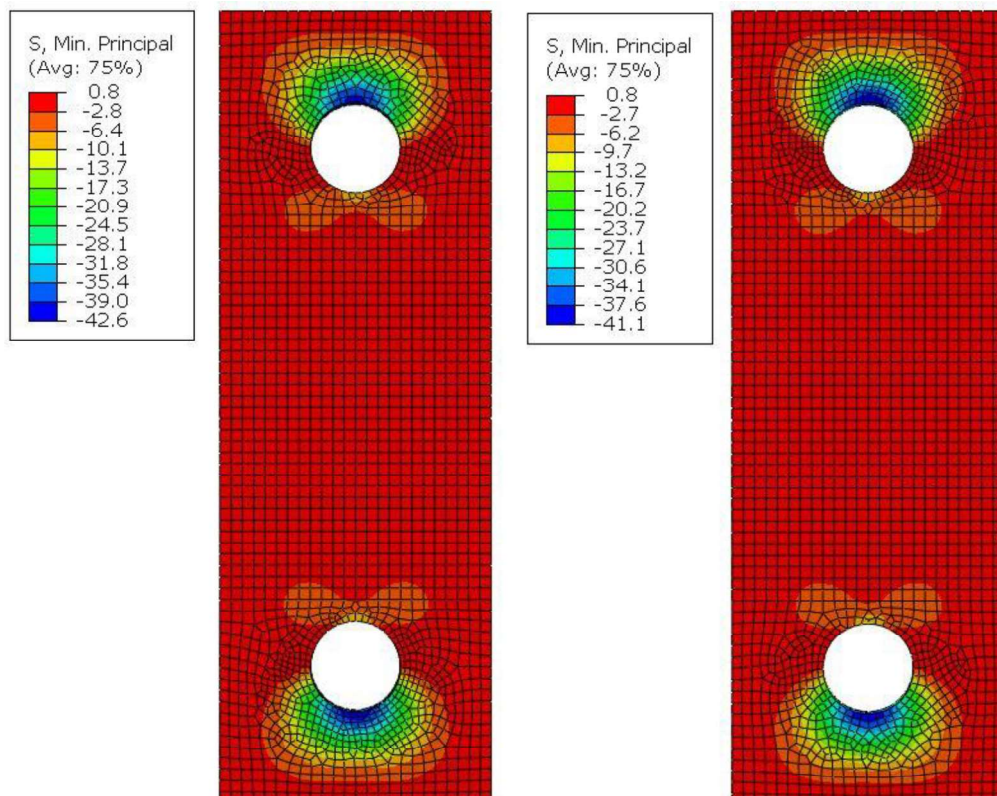

Figure 4.28: Step 34 – applied load of 110 kN (Face 1 left side, Face 2 right side)
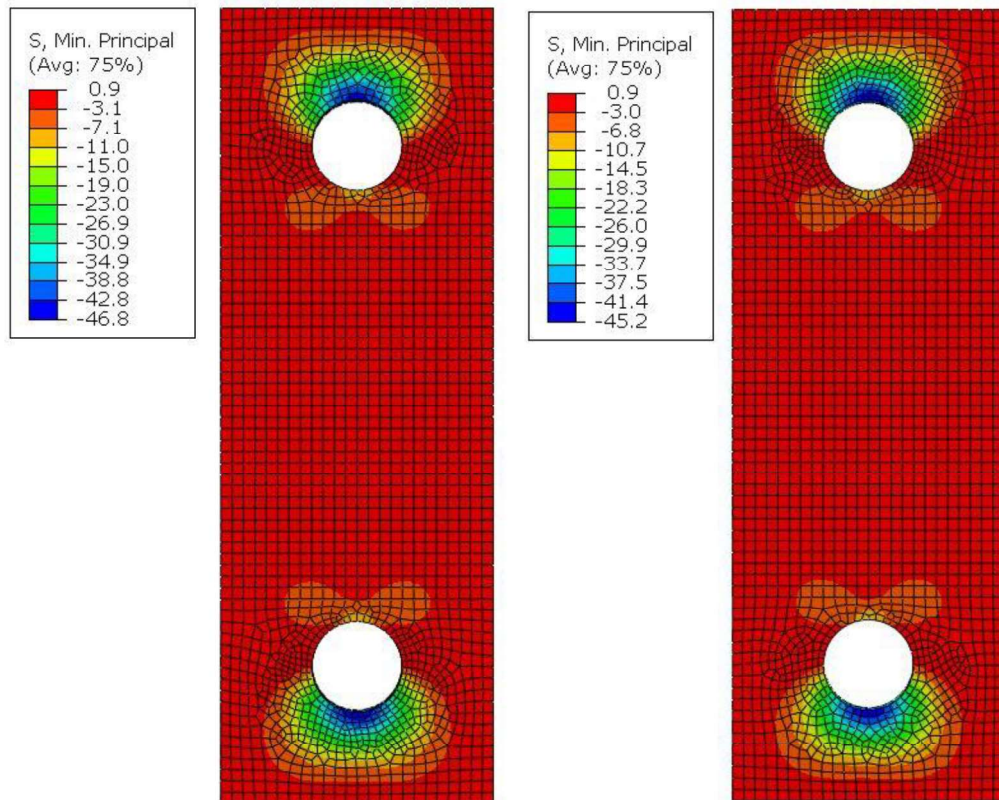
Figure 4.29: Step 37 – applied load of 120 kN (Face 1 left side, Face 2 right side)
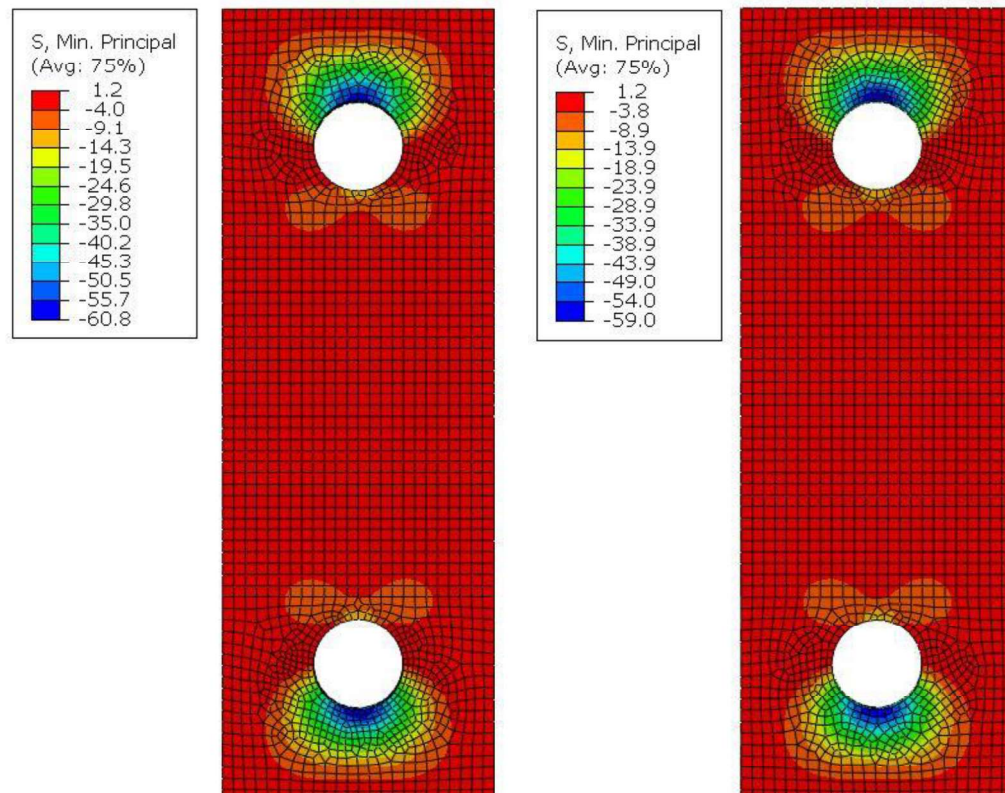

Figure 4.30: Step 47 – applied load of 156 kN (Face 1 left side, Face 2 right side)

4.6 Comparison with the experimental results

4.6.1 Comparation of load displacement curves

Comparison of load displacement curves between numerical model and experimental samples is shown in Figure 4.31.
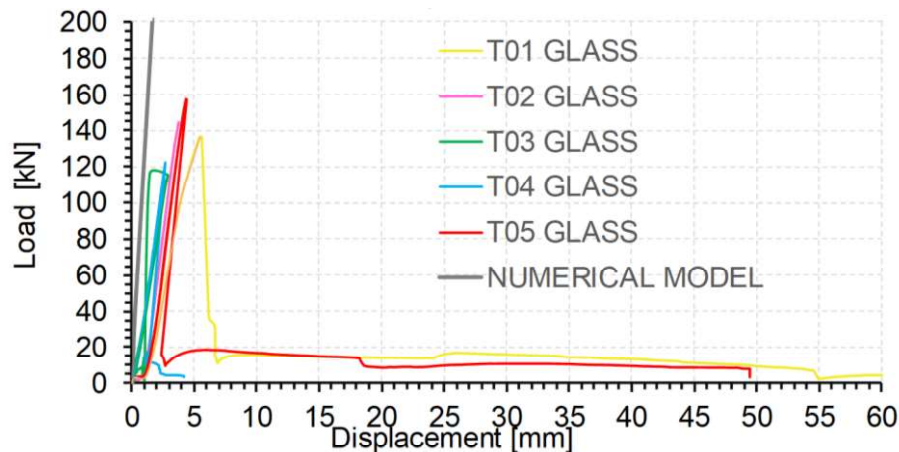

Figure 4.31: Load displacement curves

The comparison between experimental and numerical results in view of the global behaviour shows that the numerical model is more rigid than the experimental one. This is mostly related with the behaviour at the mortar region.

4.6.2 Comparison of Nominal strains

In Figure 4.32 to Figure 4.36 are presented comparisons between nominal strains in vertical line L1-L1' and from Figure 4.37 to Figure 4.41 in horizontal line L2-L2'. Due to lack of experimental results of T05 curves for L90 and L110 are not presented.

SAMPLE	MARK
Numerical model	GREY
T01	RED
T02	BLUE
T03	GREEN
T04	ORANGE
T05	PINK

Table 4.4: Legend of samples

In comparison of vertical line L1-L1' Y axis presents length (mm) from bottom part of the glass toward top part while X axis presents values of nominal strain in Z (vertical) direction of model.

60

COMPARISON OF L5

Figure 4.32: Comparison of nominal strain in line L1-L1' at 5 kN of applied load

COMPARISON OF L30

Figure 4.33: Comparison of nominal strain in line L1-L1' at 30 kN of applied load

COMPARISON OF L60

Figure 4.34: Comparison of nominal strain in line L1-L1' at 60 kN of applied load

COMPARISON OF L90

Figure 4.35: Comparison of nominal strain in line L1-L1' at 90 kN of applied load

COMPARISON OF L110

Figure 4.36: Comparison of nominal strain in line L1-L1' at 110 kN of applied load

In comparison of horizontal line L2-L2' X axis presents length (mm) in the middle of the model from right to the left side and Y axis presents values of nominal strain in Z (vertical) direction of model.
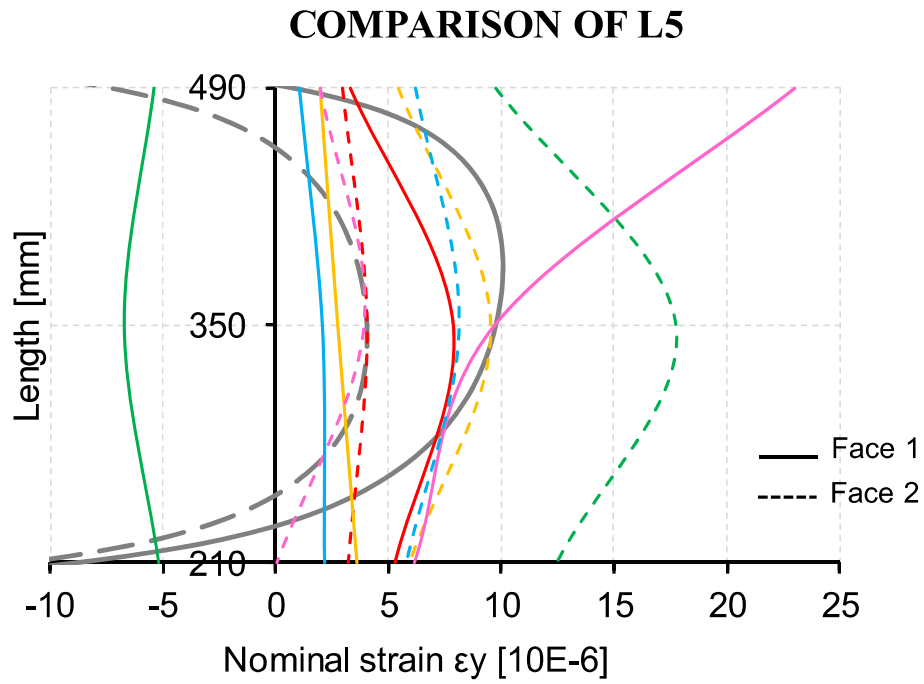
COMPARISON OF L5

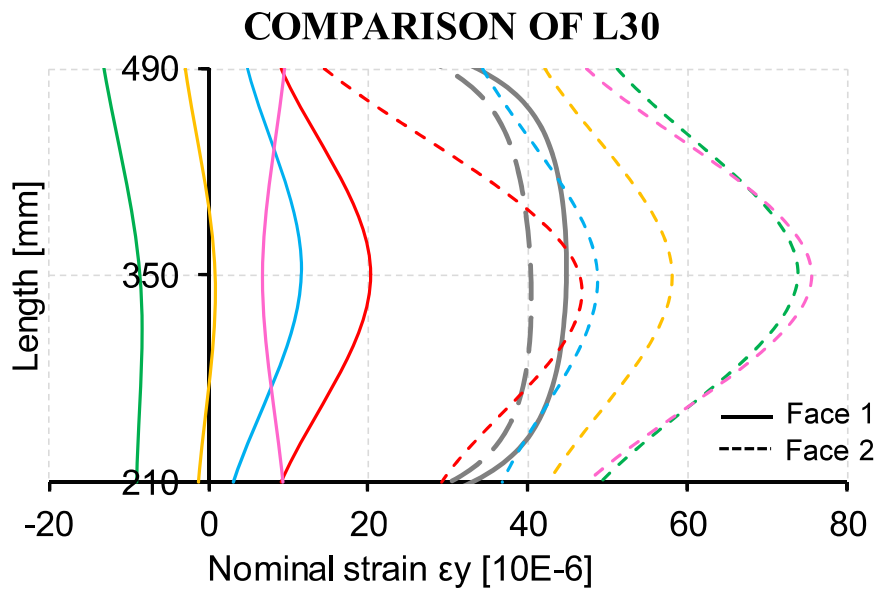**Figure 4.37:** Comparison of nominal strain in line L2-L2' at 5 kN of applied load

Figure 4.38: Comparison of nominal strain in line L2-L2' at 30 kN of applied load
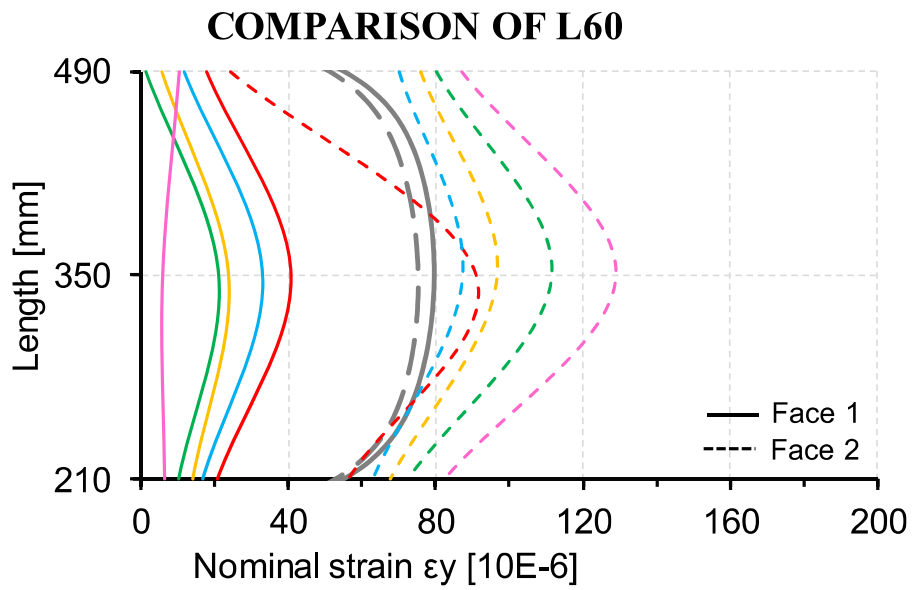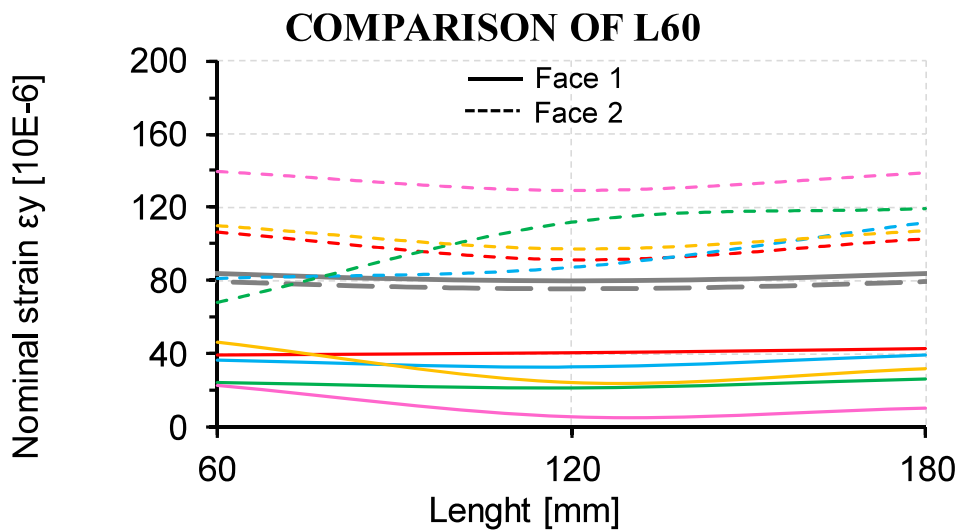

Figure 4.39: Comparison of nominal strain in line L2-L2' at 60 kN of applied load
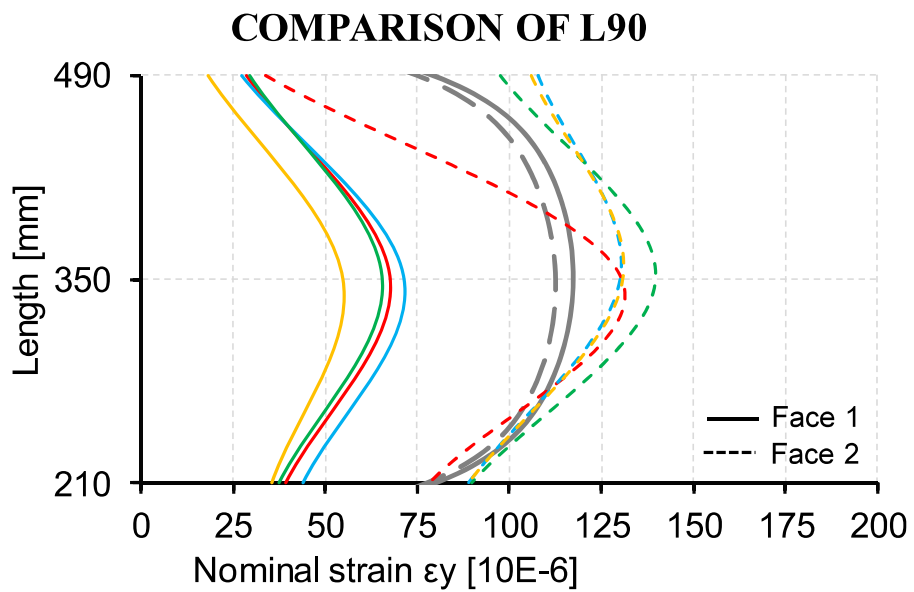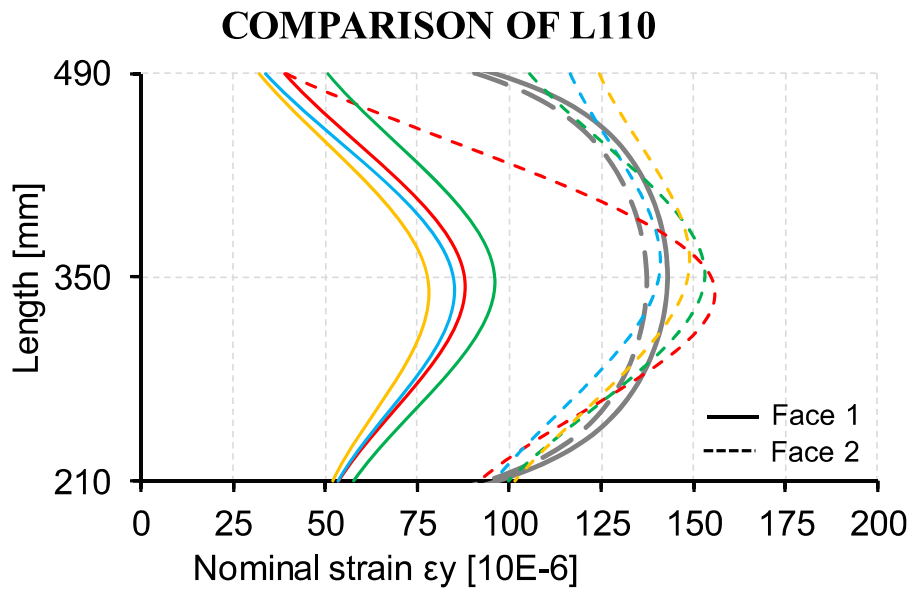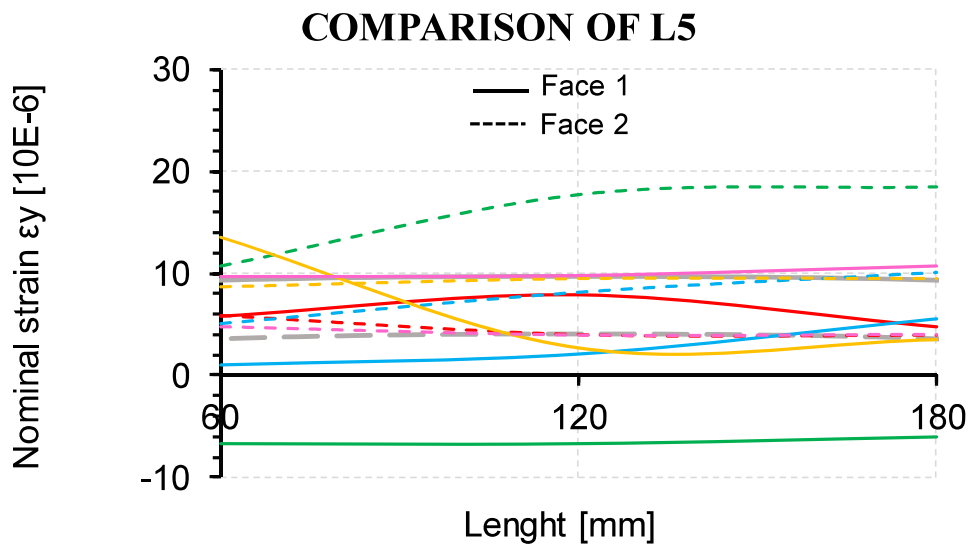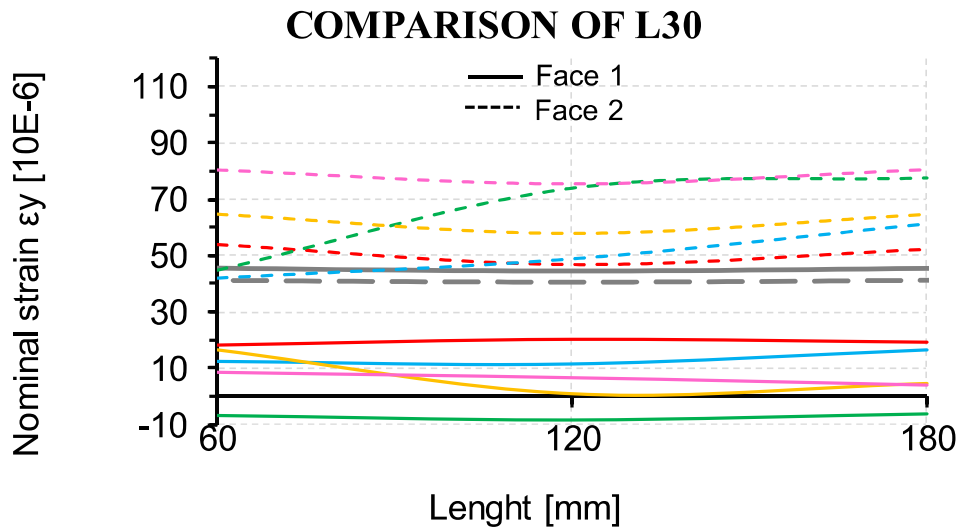
COMPARISON OF L90

Figure showing nominal strain comparison:
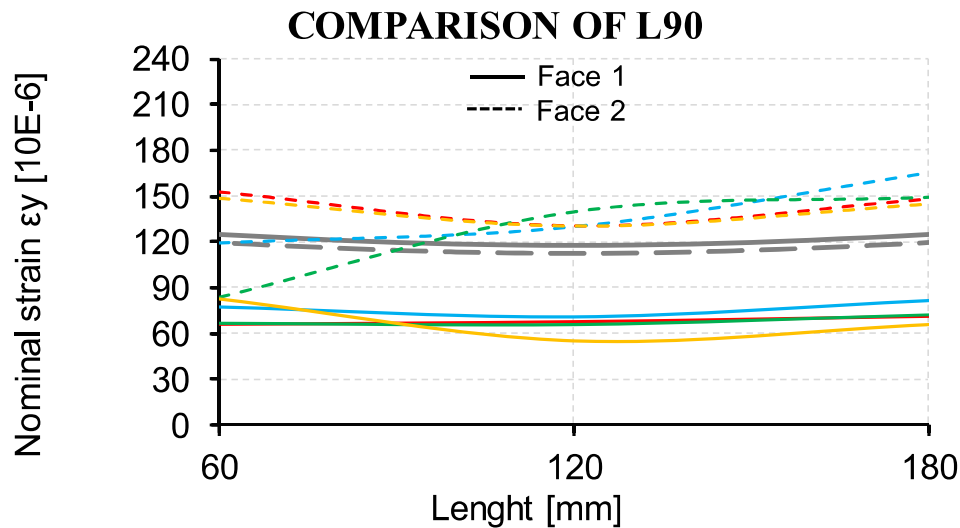
Figure 4.40: Comparison of nominal strain in line L2-L2' at 90 kN of applied load
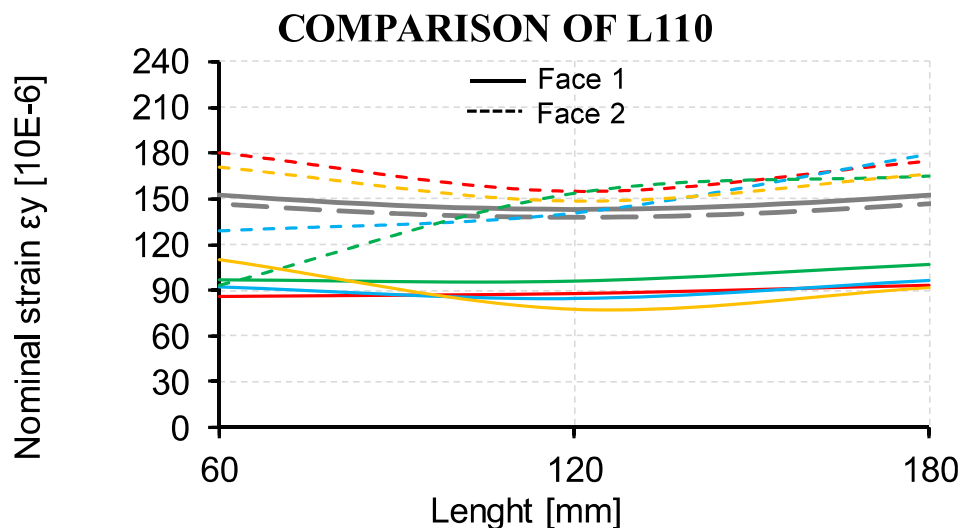
COMPARISON OF L110

Figure 4.41: Comparison of nominal strain in line L2-L2' at 110 kN of applied load

The numerical model features very small asymmetries. Because of that we have close values of nominal strain distribution at lines L1-L1' and L2-L2' for Face 1 and Face 2 of the model. However, if we take a look of the results from experimental samples strain distribution in vertical line L1-L1' and horizontal line L2-L2' we can see that values are different. There is big difference between values of Face 1 and Face 2 due to imperfections of the glass through lamination process and during the process of connecting sample to steel clamps for testing. It was made sure that experimental sample was always aligned by 90 degrees while steel clamps were not. Due to that eccentricity values measured on the Face 1 of the sample were lower than values on the Face 2 which is not the case in numerical model. The numerical model yields a reasonable representation of the global structural behaviour of the model.

5 CONCLUSIONS AND FUTURE WORK

This thesis focuses on numerical analysis of the model which was made to compare its results with the experimental ones from tests made in October 2023. Experimental specimens were exposed to uniaxial tension load until the completly separation. The point-fixed connections were realised by using infill material of HILTI HIT HY-270. An elastic 3D Numerical model was made in Abaqus and it was given the proper material properties. Due to ideal reference point of tension force there was no eccentricity which gave us ideal results of nominal strain values through selected lines in model while in experimental results is seen the difference in values between Face 1 and Face 2 of model.

Future work suggestions starts from introducing plasticity in the material properties specially for the infill material. Seconldy, by doing numerical analysis it's recommended to introduce eccentricity in reference point of the load. Furthermore, making analysis on cycling loads would be recommended to check behaviour of the materials. Finally, by adjusting geometrical properties such as diameter of hole or thickness of glass/infill material it would be good to make comparsion of the obtained results.

Annex D of EN 1990

The assessment of the characteristic resistance of the samples was calculated according to section D7.2, of Annex D of EN 1990 [1]. The variable *Xi,* corresponds to the maximum load prior to a drop of load of more than 5% of the load-displacement and load –time curves presented in Figure 9 and 10. The maximum values are described in table 4, at stage T0#_F, correspondent to maximum load achieved by the samples prior to the breakage of two or more plies.

Samples

n	X_i
	(kN)
1	136.48
2	152.01
3	115.84
4	122
5	157.12

Mean of the n=5 sample results

$$m_x := \frac{X_{i_0}+X_{i_1}+X_{i_2}+X_{i_3}+X_{i_4}}{n_4} = 136.69 \ kN$$

$$sqrs_X := \frac{1}{n_4-1}\cdot\left(\left(X_{i_0}-m_x\right)^2 + \left(X_{i_1}-m_x\right)^2 + \left(X_{i_2}-m_x\right)^2 + \left(X_{i_3}-m_x\right)^2 + \left(X_{i_4}-m_x\right)^2\right)$$

$$sqrs_X = \left(3.257\cdot 10^8\right)N^2$$

Standard deviation

$$s_X := \sqrt{sqrs_X} = 18.046 \ kN$$

Coeficient of variation

$$V_X := \frac{s_X}{m_x} = 0.132$$

Values of kn for 5% characteristic value for n=5 (Table D1-RN1990)

Table D1 : Values of k_n for the 5% characteristic value

n	1	2	3	4	5	6	8	10	20	30	∞
V_X known	2,31	2,01	1,89	1,83	1,80	1,77	1,74	1,72	1,68	1,67	1,64
V_X unknown	-	-	3,37	2,63	2,33	2,18	2,00	1,92	1,76	1,73	1,64

NOTE 1 This table is based on the Normal distribution.
NOTE 2 With a log-normal distribution expression (D.1) becomes :

$k_{n.u} := 2.33$ Vx unknown

Design value of the property X:

$$X_d = \frac{\eta_d}{\gamma_m} \cdot m_x \cdot \left(1 - k_{n.u} \cdot V_X\right)$$

$$X_{d.partial} = \frac{\eta_d}{\gamma_m} \cdot 94.643 \; kN$$

Where:
   η_d: Design value of the conversion factor
   γ_m: Partial factor

The correspondent characteristic value corresponded to the failure load of 5 Heat strengthened 4-ply laminated glass inserts, without consideration of partial factors (η_d / γ_m), corresponds to **94.643 kN.**

REFERENCES

[1] Jordão, S., & Inca, E., (2024). *Karla Tower Development Glass box Yuanda Europe LTD. Structural behaviour of a bolted section*. Laboratory of Structures, Constructions and Structural Mechanics, Department of Civil Engineering, University of Coimbra, ISISE. Commissioned by Yuand Europe LTD

[2] Pejatovic, M., Sartipi, S., Wan-Wendner, R., & Belis, J. (2024). Point-fixed connections in structural glass with injection mortar infill. Experimental investigation and numerical simulations. *Engineering Structures*, *304*, 0141-0296. https://doi.org/10.1016/j.engstruct.2024.117664

[3] CEN/TC 250 N 3672, (2023). 1st WD prEN 19100-1 Eurocode 10 – Design of glass structures

[4] ABAQUS/Standar User's manual, Version 6.14. Dassault Systemes Simulia Corp.

[5] International fischer FIS V Plus S Product Documentation, fischer International; 2020.

[6] Hilti, HIT-HQ 270 Adhesive Product Documentation, Hilti; 2014.

[7] Mocibob, D., & Belis,J., (2008). *Coupled experimental and numerical investigation of structural glass panels with small slenderness subjected to locally introduced axial compression*. Labroatoire de la construction metallique, ICOM, Lausanne,Switzerland and Department of Structural Engineering, Ghent University, Ghent Belgium

[8] Mocibob, D., *Glass panels under shear loading-use of glass envelopes in building stabilization*, Ecole Polytechnique Federale de Lausanne,Lausanne, 2008.

[9] HILTI, HIT-HY-50, Product documentation, HILTI; 2003.

[10] SAS, IP, Inc.Ansys.release 10,SAS IP, Inc,:2005.;2005.

[11] Overend, M., *The appraisal of structural glass assemblies*, Surrey, University of Surrey; 2002.

[12] Maniatis, I., Numerical and experimental investigations on the stress distribution of bolted glass connections under in-plane loads, Munich, Technische Universitat Munchen; 2006.

[13] Hilti, HIT-HY 270 morat for glass constructions, Hilti corporation; 2014.

[14] AutoCAD 2022/Standar User's manual,AUTODESK

[15] Galić M., Grozdanić G., Divić V. Marović, P, Parametric Analyses of the Influence of Temperature, Load Duration, and Interlayer Thickness on a Laminated Glass Structure Exposed to Out-of-Plane Loading; Crystals, 2022.

[16] Stainless Steel 1.4404 (316L) Bar and Section, Aalco, 2020.

[18] Ionoplast interlayer, Specifying and technical data, SentryGlas, 2014.

WEB SITES

[1] IMAGE - https://www.glassonweb.com/news/point-fixing-systems-spider-system

[2] IMAGE - https://www.sggglassmanufacturer.com/products/8.76mm-laminated-glass-for-roof.html

[6] IMAGE - https://www.yuanda-europe.com/projects/karla-tower/

[8] IMAGE - https://www.choosechicago.com/articles/tours-and-attractions/chicagos-observation-decks/

[9] IMAGE - https://www.goadria.com/hr/izleti?turneoExperience=7c715cbf-233e-43d4-877b-1d53a60f1892_Biokovo-Skywalk---tour-guidato

IMMAGE CREDITS

[1] Point fixing of the glass panels; Glass on web

[2]Glass roof; SZG professional glass manufacturer

[3] Pejatovic, M., Sartipi, S., Wan-Wendner, R., & Belis, J. (2024). Point-fixed connections in structural glass with injection mortar infill. Experimental investigation and numerical simulations. *Engineering Structures*, *304*, 0141-0296.

https://doi.org/10.1016/j.engstruct.2024.117664

[4] Mocibob, D., & Belis,J., (2008). *Coupled experimental and numerical investigation of structural glass panels with small slenderness subjected to locally introduced axial compression*. Labroatoire de la construction metallique, ICOM, Lausanne,Switzerland and Department of Structural Engineering, Ghent University, Ghent Belgium

[5] Hilti, HIT-HY 270 morat for glass constructions, Hilti corporation; 2014.

[6] Karla tower, Gothenburg; YUANDA EUROPE LTD

[7] Jordão, S., & Inca, E., (2024). *Karla Tower Development Glass box Yuanda Europe LTD. Structural behaviour of a bolted section*. Laboratory of Structures, Constructions and Structural Mechanics, Department of Civil Engineering, University of Coimbra, ISISE. Commissioned by Yuand Europe LTD

[8] Willis Tower, Chicago, Illinois; Choosechicago

[9] Skywalk Biokovo; Izleti Go Adria